



University of
Stavanger

Faculty of Science and Technology

MASTER'S THESIS

Study program/Specialization: Petroleum Geosciences Engineering	Spring, 2015 Open
Writer: Isabel Rodríguez Gómez	<hr/> (Writer's signature)
Faculty supervisor: Karl Audun Lehne External supervisor(s):	
Title of thesis: Petrophysical characterization of the Lower Cretaceous clastic wedges in the southwestern Barents Sea	
Credits (ECTS): 30	
Keywords: Clastic wedges Knurr Fomration Barents Sea Reservoir Quality Uplift Petrophysical analogues	Pages: 117 +enclosure: CD Stavanger, 15,06,2015

Copyright
by
Isabel Rodríguez Gómez
2015

**PETROPHYSICAL CHARACTERIZATION OF THE LOWER CRETACEOUS
CLASTIC WEDGES IN THE SOUTHWESTERN BARENTS SEA**

BY

Isabel Rodríguez Gómez, B.Sc.

THESIS

Presented to the Faculty of Science and Technology

The University of Stavanger

THE UNIVERSITY OF STAVANGER

JUNE, 2015

ACKNOWLEDGEMENTS

I would like to thank, first of all, my supervisor Karl Audun Lehne for the help and support during these last six months of hard work. I would also like to thank Alejandro Escalona, for giving me the opportunity to work within the LoCra Project, Dora Marin for showing me how the seismic wedges look like, Naomi Matthews for helping me with mineralogy and Lisa Bingham, always there to help with references and any other problem.

A special thanks to my family and my boyfriend, for their unconditional support, love and endless patience. Also, may thanks to my best friend for always cheering me up and listen to me regardless the distance.

Finally, a BIG thanks to all my classmates, because without you I could not have done this!!

ABSTRACT

PETROPHYSICAL CHARACTERIZATION OF THE LOWER CRETACEOUS CLASTIC WEDGES IN THE SOUTHWESTERN BARENTS SEA

Isabel Rodríguez Gómez, B.Sc.

The University of Stavanger, 2015

Supervisor: Karl Audun Lehne

The results of the petrophysical evaluation of four turbidite systems located along the flanks of the Hammerfest Basin, in the southwestern Barents Sea, are presented in this master thesis. These systems are the reservoir of the Lower Cretaceous Clastic Wedges play in this area, which was proven successful in 2012, after drilling the Salina prospect. An environmental analysis, based on the study of cores and logs, shows that sand rich turbidite systems might be expected on the northeastern flanks of the Hammerfest Basin, sourced from the eastern Loppa High. Towards the northwestern and southwestern flanks, sand-mud rich system, sourced from the Loppa High and Finnmark Platform, are expected. This analysis, together with the results from the petrophysical evaluation, suggests a direct dependency of reservoir quality on depositional environment as well as on the type of turbidite system.

A main challenge regarding petrophysical evaluations of these reservoirs is the scarce core data available within the Lower Cretaceous stratigraphic unit. Core data are very important for calibration of the parameters needed for the computation of the reservoir properties. The wells used in this study are among the few with core data available so the results could be calibrated. Therefore, these turbidite systems are proposed as analogues for future petrophysical evaluations of the Lower Cretaceous

sandstone wedges when core data are not available. However, care should be taken in the use of these analogues since differences in the turbidites source area affect some of the petrophysical calculations. The results show that the computing parameters for the calculation of V_{cl} and PHIE/PHIT might be used independently from the reservoir's source area. Yet, for permeability calculations, source area should be taken into consideration.

TABLE OF CONTENTS

List of Tables	xi
List of Figures	xii
1. INTRODUCTION.....	1
2. GEOLOGICAL SETTING	5
2.1. Regional geology	5
2.2. Hammerfest Basin.....	6
2.3. Lower Cretaceous Play	9
2. TURBIDITES BACKGROUND.....	13
3. DATA	18
4. METHODOLOGY	20
4.1. Data quality check and zonation	20
4.2. Lithology identification	20
4.3. Petrographic analysis	20
4.4. Depositional Environment analysis	21
4.5. Petrophysical evaluation	21
4.5.1. Volume of clay.....	22
4.5.2. Porosity	23
4.5.3. Water saturation	26
4.5.4. Permeability	27
4.5.5. Net to gross	27

5.	DATA QUALITY CONTROL AND ZONATION.....	29
6.	LITHOLOGY IDENTIFICATION.....	31
7.	PETROGRAPHIC ANALYSIS.....	34
8.	ENVIRONMENTAL ANALYSIS.....	39
8.1.	Results: Lithofacies, log facies and gamma ray signature.....	39
8.2.	Interpretation of depositional environment.....	45
9.	PETROPHYSICAL EVALUATION.....	57
9.1.	Definition of the Computing Parameters.....	57
9.1.1.	Volume of clay parameters.....	57
9.1.2.	Porosity parameters.....	57
9.1.3.	Water saturation parameters.....	62
9.2.	Results.....	63
9.2.1.	Volume of clay.....	63
9.2.2.	Porosity.....	63
9.2.3.	Mineral model.....	66
9.2.4.	Water saturation.....	66
9.2.5.	Permeability.....	67
9.2.6.	Net to gross.....	69
9.2.7.	Summary of results.....	70

10. FINAL INTERPRETATIONS.....	75
10.1. Estimation of Uplift	75
10.2. Reservoir Quality	78
10.3. Study of Analogues.....	79
11. CONCLUSIONS	84
12. FUTURE WORK	86
<i>APENDIX 1</i>	<i>87</i>
<i>APENDIX 2</i>	<i>92</i>
GLOSSARY.....	99
REFERENCES.....	100

LIST OF TABLES

Table 1 – Average values from literature for the reservoir properties of wells 7120/1-2, 7120/10-2 and 7120/2-1.....	10
Table 2 – Main characteristics from sand-rich fans and mixed mud/sand-rich fans.....	14
Table 3 – Main information of the four study wells.....	19
Table 4 – Thin section analysis.....	36
Table 5 – Heavy mineral assemblage for study wells.....	37
Table 6A – Description of lithofacies.....	41
Table 7 – Description of log facies based on the gamma ray base line, gamma ray shape and neutron-density separation.	44
Table 8 – Description of gamma ray and resistivity signatures.....	45
Table 9 – True mineral densities for the calculation of RHOMA.....	58
Table 10 – Volumes of the two heavy minerals groups for distal and proximal areas	59
Table 11 – Tables with the reference values for the heavy minerals assemblage densities to use in the calculation of RHOMA.	61
Table 12 – Cementation factor, saturation exponent and tortuosity factor values from literature.....	62
Table 13 – Equations representing the porosity-permeability trends.....	68
Table 14 –Computed reservoir properties average values and hypothetical reservoir properties average	74

LIST OF FIGURES

Figure 1 - Map of the southwestern Barents Sea showing the main structural elements as well as the location of the drilled wells.	4
Figure 2 - Geographical and structural map of the Barents Sea.	7
Figure 3 - Chronostratigraphic chart for the southwestern Barents Sea	8
Figure 4–Model of the Lower Cretaceous clastic wedges.....	11
Figure 5–Division of the Lower Cretaceous in stratigraphic sequences... ..	12
Figure 6–Bouma turbidite facies model and environmental model of a submarine fan	15
Figure 7– Gamma ray and resistivity log signatures of the different depositional environments within a sand rich system and a sand-mud rich turbidite system.....	16
Figure 8–Sketch explaining how mineral fractionation function in a turbidite fan.....	17
Figure 9–Knurr Formation zonation.	30
Figure 10– Neutron-density crossplots for lithological identification.....	32
Figure 11– Lithological columns for the study wells.	33
Figure 12– Pettijohn classification of sandstones..	35
Figure 13 –Thin sections.....	38
Figure 14– Neutron-Density crossplot and Neutron-Density-Gamma ray 3D plot displaying the lithofacies and log facies described in the study ...	42
Figure 15A – Summary chart with the observed lithofacies and log facies , the observations in the GR and R logs signature and the final environmental interpretation.	51
Figure 16– Mismatching between computed curves and lab-measurements from point counting.....	65

Figure 17–Porosity-permeability trends.	71
Figure 18– Explicative diagram of the effect that texture has on the porosity-permeability trends.....	72
Figure 19– Analysis of Vcl, PHIE and KH histograms for net to gross cutoff analysis.....	73
Figure 20 –Uplift estimation for the study wells.....	76
Figure 21– Net erosion regional map for the Greater Barents Sea	77
Figure 22– Sketch showing the depth correction applied to the different reservoir zones.	80
Figure 23– Sketch showing the relative variations of reservoir quality between different environments, in a sand-rich system and a mud/sand-rich system.....	81

1. INTRODUCTION

The southwestern Barents Sea was opened for exploration in 1980. Although since that time several discoveries proved the hydrocarbon potential of this petroleum province, it is still considered an immature region with only one field developed (i.e. Snøhvit Field). Until now, exploration has mainly focused on Hammerfest Basin and the western parts of Loppa High, with the Jurassic and Triassic stratigraphic units drawing most attention. The Jurassic sandstones of the Stø Formation are by far, the most prolific reservoir in the province until the moment. Nevertheless, there is growing enthusiasm in expanding hydrocarbon exploration in the area, especially after three recent discoveries with substantial proven reserves: Norvarg (2011), Johan Castberg (2011), Havis (2012) and Alta (2014) (NPD, 2015).

This thesis focuses on the Lower Cretaceous clastic wedges of the Knurr Formation which were seismically defined and mapped along the margins of the Hammerfest Basin. *Figure 1* shows a map of the southwestern Barents Sea, where Hammerfest Basin is located as well as the wells drilled in this area. These wedges were drilled as primary or secondary targets in five wells (7122/2-1, 7120/1-2, 7120/2-2, 7120/10-2, and 7119/1-1) with no success until 2012. That year, the Salina prospect was drilled by Eni (well 7220/10-1), resulting in a gas discovery in the Cretaceous Knurr Formation (NPD, 2015). The other five wells, in spite of being five unsuccessful, have oil shows in the Lower Cretaceous; furthermore, well 7120/1-2 was ranked as a technical discovery and well 7119/1-1 presents a “down to” situation with a gas column of 50 meters (NPD, 2015; Seldal, 2005). Moreover, according to Seldal (2005), almost all the rest of wells drilled through the Lower Cretaceous, also have oil shows. Seldal (2005) explains the play concept of the Lower Cretaceous clastic wedges and aims to demonstrate its undrilled oil potential. This article also provides some interesting porosity and net to gross values indicating that these sandstones have good reservoir quality. Overall, this play seems promising for further exploration. Nevertheless, apart from the publication from Seldal (2005) and the knowledge of the Lower Cretaceous in the Barents Sea from regional studies, there is still little public information about this play, which makes challenging any study about it. Since 2013, the LoCrA Consortium, a project managed by the University of Stavanger and University Centre in Svalbard in cooperation with other universities,

aims for a better understanding of the Lower Cretaceous basins in the Arctic. There are several research studies within this project, one of them being a master thesis by Fjeld (2014), which presents an integrated study of the Lower Cretaceous clastic wedges in the Troms-Finnmark Fault Complex. Another research has defined a sequence stratigraphic framework for the Lower Cretaceous in the southwestern Barents Sea (Marin et al., 2014). Provenance studies in this stratigraphic unit are another branch of research (Matthews et al., 2015), also part of the LoCra Project.

However, a proper petrophysical characterization of these sandstones has not been done yet in any publication. This analysis could be valuable since this is still a play in exploration and the knowledge of the reservoir properties is of primary importance in prospect evaluation. The challenge regarding petrophysical characterization in the Lower Cretaceous of the southwestern Barents Sea area is the limited core data available. Core data are very important in petrophysical analyses for log-calibration purposes. When they are limited or even non-existent, the uncertainty involved in the calculation of porosity, water saturation and permeability becomes a major issue. In order to reduce this uncertainty, assumptions have to be made to define the petrophysical computing parameters used for the calculations, based on analogues in the area for which calibration with core data was possible.

In the southwestern Barents Sea there are only 7 wells with core data from a total of 65 drilled through the Lower Cretaceous. These cored wells could be used as analogues for future petrophysical evaluations of the Lower Cretaceous sandstone wedges. However, the wedges targeted by these wells are sourced from different areas (e.g. Loppa High and Finnmark Platform) and this might influence the calculation of the reservoir properties in the well under study. Thus, it is necessary to understand the possible effects, related to differences in source area, in the calculation of porosity, water saturation and permeability in order to be able to use these wedges as analogues for future projects. Taking this into account, this thesis presents two objectives. First, to perform a petrophysical characterization of the sandstone wedges in Knurr Formation for four of the wells with core data (7122/2-1, 7120/1-2, 7120/2-2 and 7120/10-2) in order to understand their reservoir quality. Second, to analyze the possible differences between the studied wedges in the

calculation of the petrophysical parameters, so that they may be used as analogues in future exploration projects.

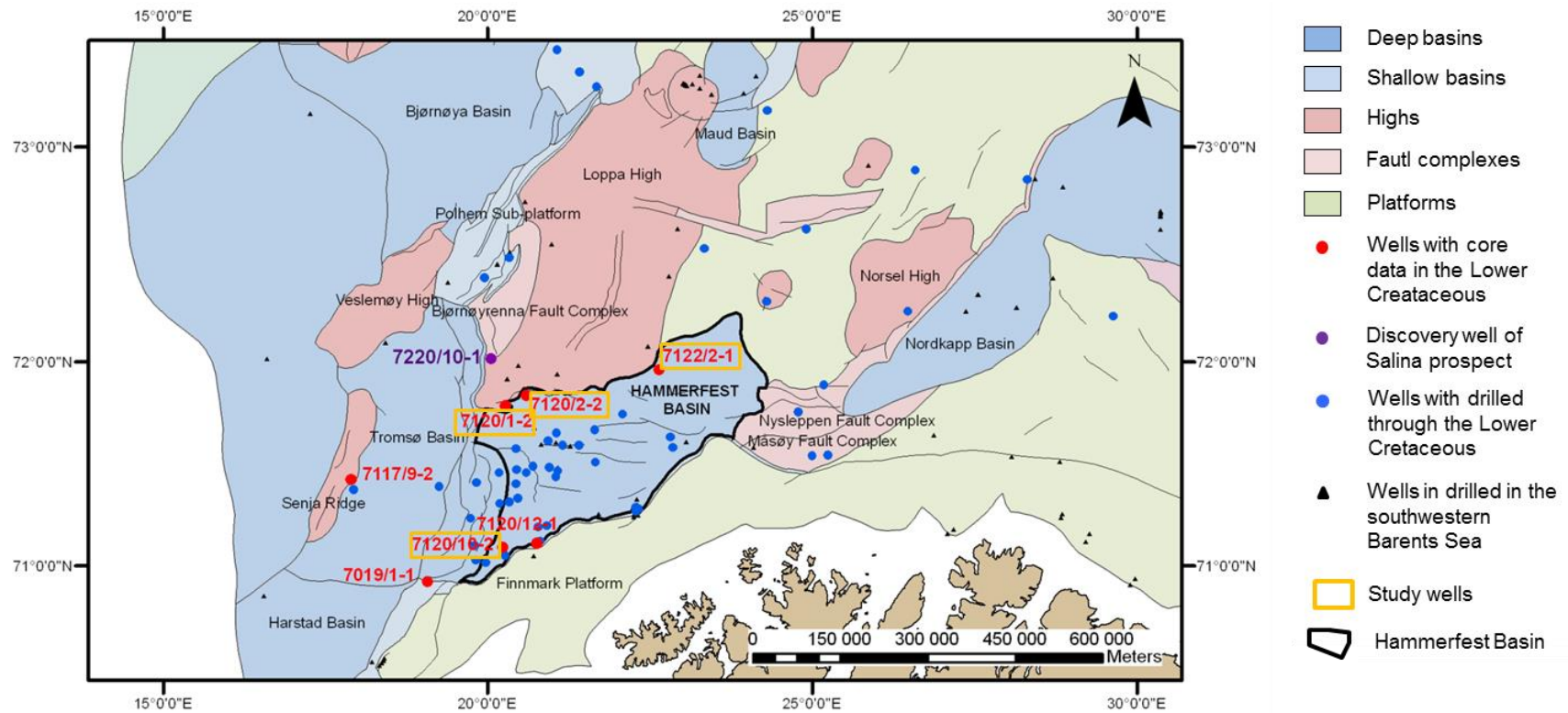


Figure 1 - Map of the southwestern Barents Sea showing the main structural elements in the area as well as the location of the drilled wells.

2. GEOLOGICAL SETTING

2.1. REGIONAL GEOLOGY

The Barents Sea is located in the northwestern corner of the Eurasian Plate, limited by the North Atlantic Ocean and the Svalbard archipelago to the northwest and by Novaya Zemlya to the east (*figure 2A*). It may be divided into two regions with different geological histories: the Eastern Barents Sea, which has been relatively stable since the Late Carboniferous, and the Western Barents Sea, active since the Caledonian Orogeny (Gabrielsen et al., 1990; Smelror et al., 2009). The tectonic history of the Western Barents Sea is mainly controlled by three rift phases –Late Devonian-Carboniferous, Middle Jurassic-Early Cretaceous and Paleocene– that built the complex of basins, platforms and highs visible nowadays (*figure 2B*) (Faleide et al., 2010; Gabrielsen, 1984). Several authors propose that the structural grain of the Caledonian basement, with a NE-SW to ENE-WSW trend, influenced the development of the present structures in the Barents Sea region, where the same trend is observed (Dore, 1995; Faleide et al., 1984; Gabrielsen, 1984).

During Late Paleozoic, crustal extension affected most of the Barents Sea and was responsible for the formation of the major regional fault zones in the region (Faleide et al., 1984; Gabrielsen, 1984). After this first rifting phase, a period of quiescence took place with the development of a regional sag basin filled with carbonates and evaporates of shallow-marine environment (Faleide et al., 2010; Smelror et al., 2009). In the early Triassic, sedimentation changed to a clastic type, with prograding deltaic systems filling the regional basin from the east and southeast, sourced mainly from the Uralides and the Baltic shield respectively (Faleide et al., 2010). During the early - middle Jurassic, coastal marine environments developed leading to the formation of the most prolific reservoirs in the Barents Sea, the sandstones from the Stø Formation (Gabrielsen, 1984; Smelror et al., 2009). The second rifting phase, which affected mostly the southwestern Barents Sea, started in the Late Jurassic and it was characterized by the development of well-defined rift basins (e.g. Hammerfest Basin, Tromsø Basin, Bjørnøya Basin) (Riis et al., 1986). During the Lower Cretaceous, marine environment dominated by distal conditions with periodic

restricted bottom circulation characterized the southwestern area (Faleide et al., 1993). At the same time, the northern Barents Sea experienced widespread magmatism as part of the Arctic Large Igneous Province which resulted in regional uplift and erosion (Døssing et al., 2013; Faleide et al., 2010). Consequently, there was little or no deposition of Upper Cretaceous sediments in the Barents Sea except in the southwestern area (Faleide et al., 2010). The Cenozoic was characterized by sea floor spreading leading to the opening of the North Atlantic Ocean and by major regional uplift from the Miocene to the Middle Pliocene (Dore, 1995; Faleide et al., 2010; Smelror et al., 2009). Due to this uplift, which was especially intense in the northwestern areas, most of the Cenozoic sediments and even older rocks were eroded (Henriksen et al., 2011). This has important implications for the petroleum systems in the area in terms of reservoir quality, maturity and migration. The reservoir quality at a particular depth is, in general, lower than expected, source rock is also found to be more mature than expected and finally, the removal of overburden is thought to have re-activated the migration of hydrocarbons leading in some cases to the emptying of reservoirs (Henriksen et al., 2011).

Figure 3 presents the lithostratigraphic column of the South Western Barents Sea showing the geological formations in the area as well as the main geodynamic events occurring since Devonian.

2.2. HAMMERFEST BASIN

The Hammerfest Basin is located in the southwestern Barents Sea, bounded by the Troms-Finmark Platform to the south, the Loppa High to the north and the Tromsø Basin to the west (*figure 1*). To the east, the basin grades into the Bjarmeland Platform. The Hammerfest Basin was formed during the second rifting phase in the Late Jurassic. This rifting led to faulting in the southwestern Barents Sea and deposition of Upper Jurassic organic rich shales of Hekkingen Formation in restricted basins between tilted fault blocks (Faleide et al., 1993). The rifting event contributed to the uplift and erosion of the present-day Loppa High and the Troms-Finmark Platform leading to the formation of clastic sediments which were transported and deposited in the Hammerfest Basin (Faleide et al., 1993; Gabrielsen et al., 1990; Worsley, 2008). These sediments are found along the basin margins in form of sandstone wedges associated with rotated fault blocks (Seldal, 2005) and constitute

the reservoir of what is known as the Lower Cretaceous Play in the Southwestern Barents Sea.

The end of rifting in the Hammerfest basin was around Aptian times. During Aptian/Albian, major regional subsidence took place in the Tromsø Basin which became the depocenter in the Southwestern Barents Sea through the Late Cretaceous and Cenozoic (Faleide et al., 1993).

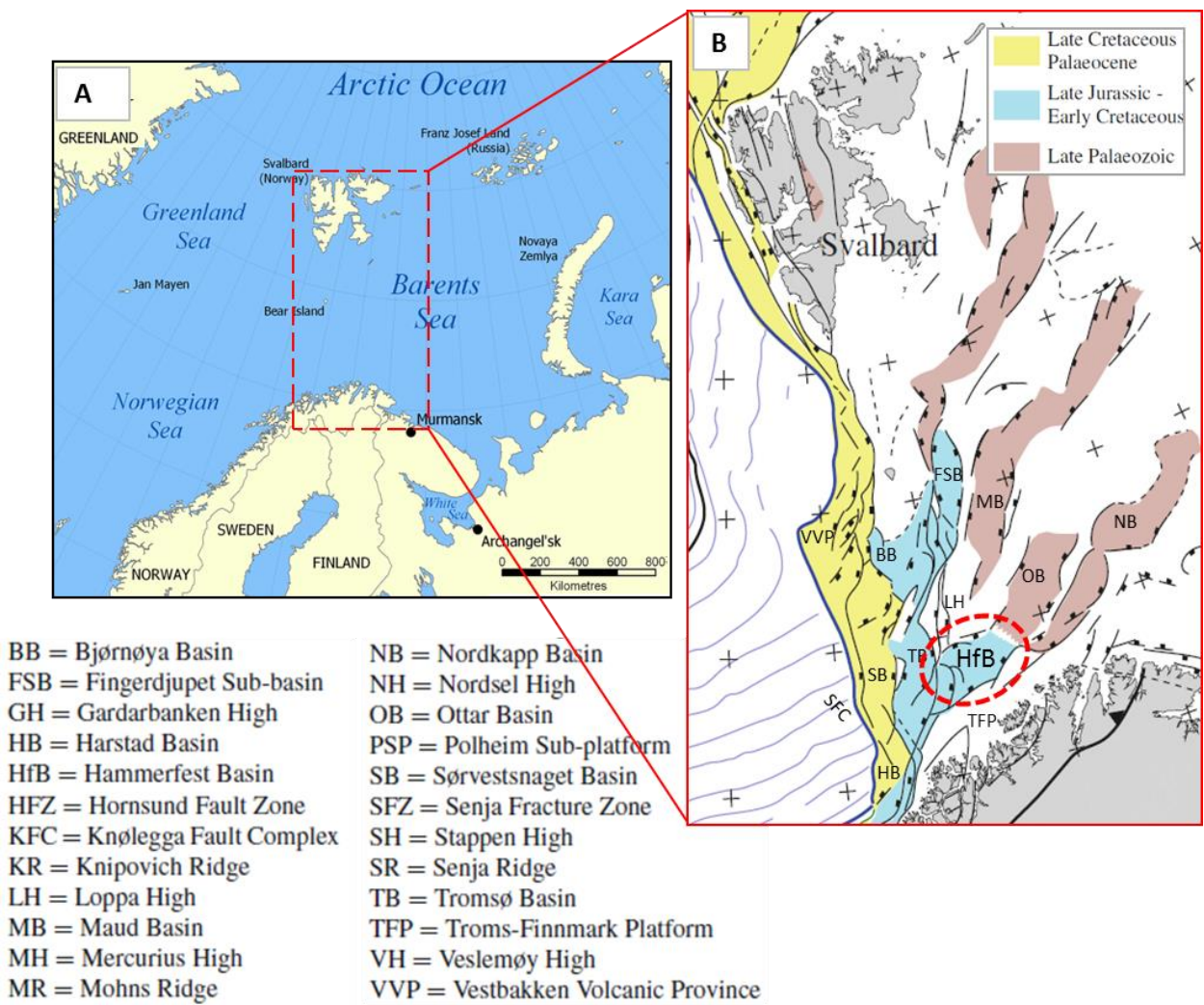


Figure 2 - A) Geographical map of the Barents Sea. B) Structural map of the Western Barents Sea with classification of the main basins according to the rift phase in which they were formed. Hammerfest Basin is highlighted with a red circle (modified from Faleide et al. (2010))

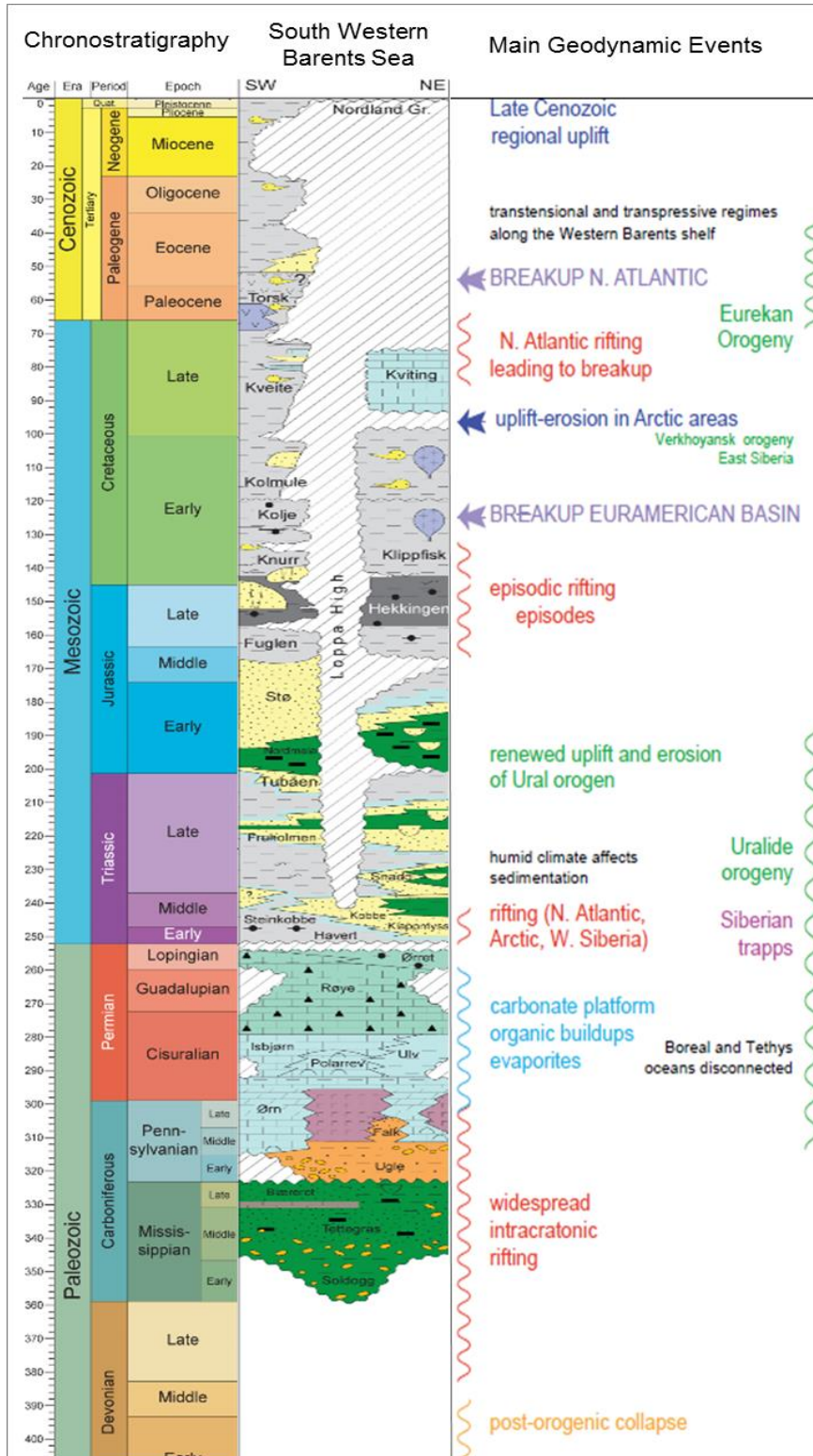


Figure 3 - Chronostratigraphic chart showing the geological formations in the South Western Barents Sea and a summary of the main geodynamic events occurring since the Devonian (Modified from Smelror et al. (2009))

2.3. LOWER CRETACEOUS PLAY

The model of the Lower Cretaceous sandstone wedges play is described by Seldal (2005) as turbiditic sandstones developed along the faulted basin margins of the Hammerfest Basin, consisting of hanging-wall wedge fans and spillover fans (*figure 4A-B*). The term “wedge” refers to the shape that these turbiditic sandstones show in seismic (in this thesis, the term wedge, turbidite system and turbidite fan will be used indistinctly to refer to the same geological concept). There is little understanding of this play because of the scarce data available, however, it is believed to have a big potential due to the following reasons:

- These wedges are considered to be a good reservoir by Seldal (2005). This article gives some good average porosity and net to gross values for three wells drilled through these sandstones (*table 1*).
- Exploration within the Hammerfest Basin has been mostly focused in the Jurassic. This could explain the fact that only three wedges have been found so far with good reservoir quality sandstones, while the remaining wells drilled in the south western Barents Sea, which were targeting Jurassic sandstones, found mainly claystones in the Lower Cretaceous.
- Almost all the wells drilled through the Lower Cretaceous claystones have hydrocarbon shows according to NPD (2015); Seldal (2005). This a good indication of the presence of migration routes from the source rocks into this stratigraphic unit.
- Hydrocarbon shows almost disappear in the Upper Cretaceous, indicating the possible presence of a good seal in the region (Seldal, 2005).
- Well 7019/1-1, located in the Troms-Finnmark Fault Complex, was drilled in the tip of what it is thought to be a mega-fan according to seismic mapping (Seldal, 2005). The well encountered gas-bearing sandstones with an average net sand of 52 meters and 13% porosity, although there is potential for better quality sandstones further south in the structure (Fjeld, 2014). Furthermore, the recent discovery in the Salina Prospect in 2012 proves finally the success of this play.

WELL NAME	NET TO GROSS	AVERAGE POROSITY
7120/1-2 (Hauterivian)	0,43	13%
7120/1-2 (Valanginian)	0,90	16%
7120/10-2	0,94	15,8%
7122/2-1	0,87	17%

Table 1 – Average values for the reservoir properties of wells 7120/1-2, 7120/10-2 and 7120/2-1 (Seldal, 2005).

These sandstone wedges have been mapped at different levels within the Lower Cretaceous with a general trend of decreasing size with time (Seldal, 2005). However, this thesis focuses only on the wedges from the Knurr Formation (Figure 3). The Knurr Formation is defined by Dalland et al. (1988) as dark to greyish-brown claystones interbedded with thin limestones and dolomites, as well as sandstones which are seen in the unit's lower parts disappearing laterally into the Hammerfest Basin. According to dinoflagellates and foraminifera, the age of this formation is suggested to be Ryazanian/Valanginian to early Barremian (Dalland et al., 1988). However, there is poor age control in the wells of this stratigraphic unit mainly due to the scarce core data available. In an attempt to constrain the uncertainty in age control, a sequence stratigraphy analysis was carried out in a research study as part of the LoCra Project (Marin et al., 2014). Six sequences were discerned in the Lower Cretaceous which are defined based on maximum flooding surfaces (MFS), dividing each sequence into a progradational and a retrogradational unit (*figure 5A*). In this research study the Knurr Formation is believed to belong mainly to the first sequence (*figure 5B*).

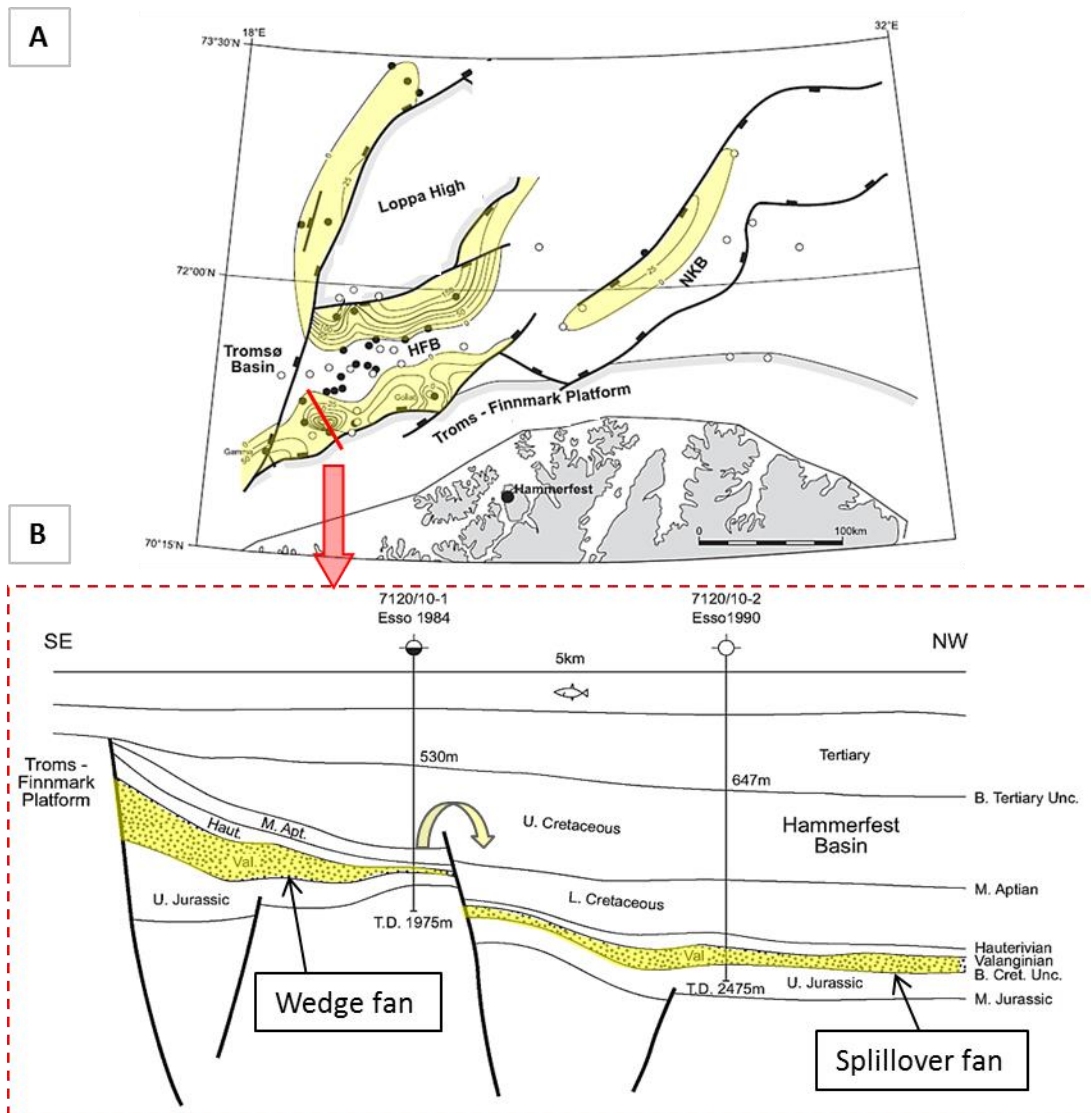


Figure 4– A) Map view of the Hammerfest Basin showing the distribution of the Lower Cretaceous sandstone wedges. B) Cross section over the southeastern flank of Hammerfest Basin, explaining the play concept of «hanging-wall wedge fans and spill over fans» (modified from Seldal (2005))

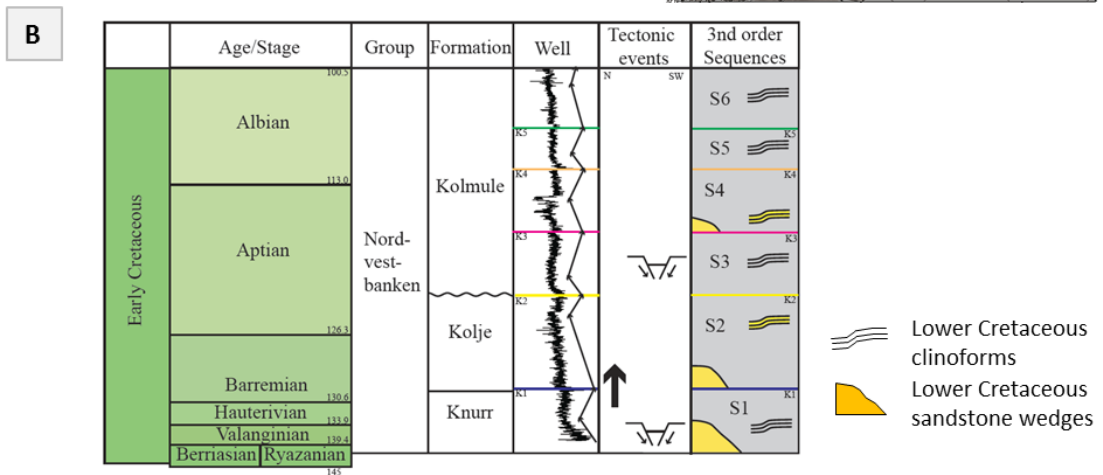
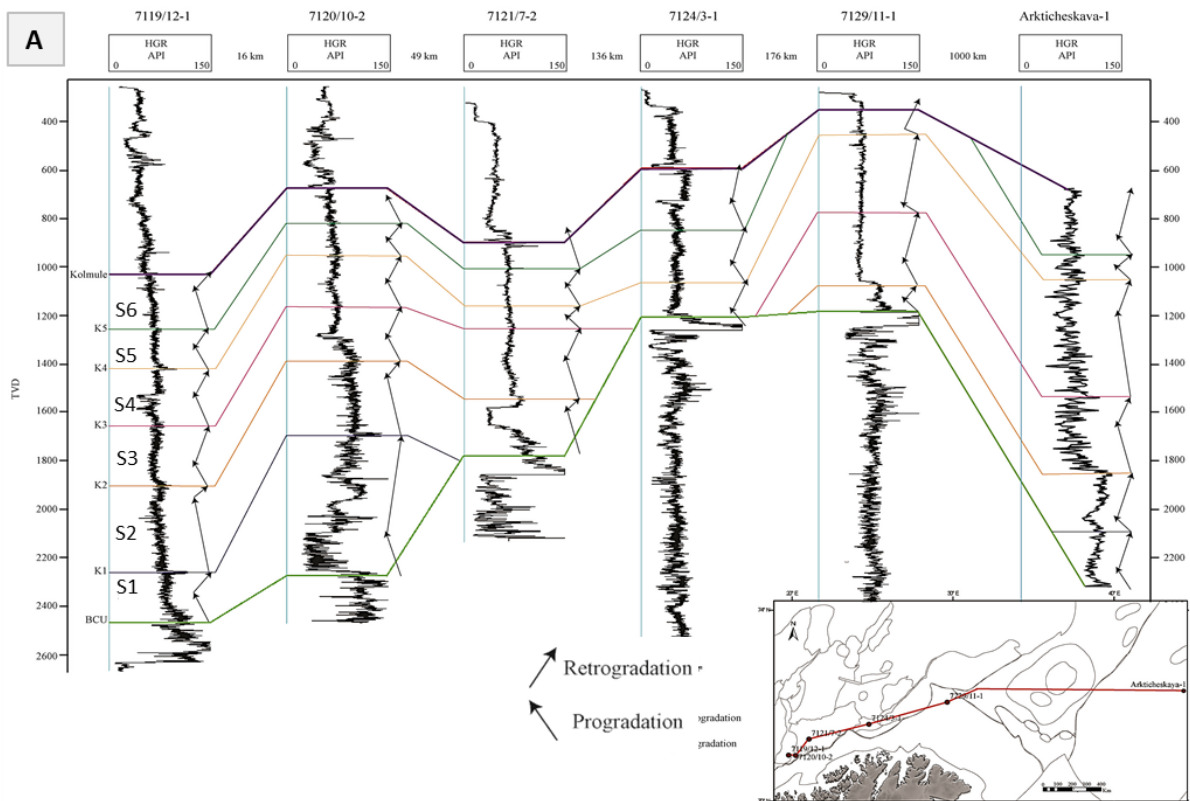


Figure 5– A) Division of the Lower Cretaceous in six sequences (S1-S6) based on maximum flooding surfaces. B) Geological time estimated for each sequence and their associated geological formations (modified from Marin et al. (2014)).

2. TURBIDITES BACKGROUND

A turbidite is the deposits of a turbiditic current. It is theoretically defined from outcrop observations as a deposit with an upward-fining grain size which is divided in five sequences, each one with its own characteristic sedimentary structure (*figure 6A*) (Walker, 1976). However, a turbidite with the complete sequence is rarely found. Turbiditic currents are density currents composed of suspended sediment and water and are the primary mechanism for transporting sediment to submarine fans (Normark et al., 1979). Submarine fans are divided into three different parts according to their environmental interpretation: inner fan, mid fan and outer fan, each of them presenting various characteristic facies (*figure 6B*). The classical turbidites tend to form on the lobes and the outer fan, while the more massive sandstones with channel-type sedimentary structures form on the inner fan or channelized part of the lobes (Walker, 1976).

There are four types of submarine fans depending on the dominant grain size of the fan system: Gravel-rich systems, sand-rich systems, mixed mud/sand-rich systems and mud-rich systems. *Table 2* explains the main characteristics according to Richards and Bowman (1998) for the sand-rich and mixed mud/sand rich systems which are the two relevant ones for this master thesis. In this article, the authors set the framework for understanding the broad scale reservoir architecture and wireline-log character for these types of fan systems. *Figure 7* summarizes the wireline-log characters of the different environments within the sand rich and the mud/sand-rich turbidite systems, based on (Richards and Bowman, 1998).

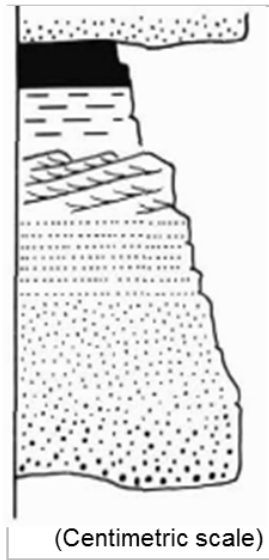
Pyles et al. (2013) presents an experiment which documents that turbidites are very efficient system for hydrodynamically fractionating minerals on the basis of their settling velocity. According to this article, settling velocity is mainly controlled by mineral grain size; however, density and angularity also have an important effect on it. "Angular grains have higher drag force, and therefore lower settling velocity, than spheres of equivalent volume, just as spherical, relatively high-density grains have a higher settling velocities than spherical lower-density grains of equivalent volume" (Pyles et al., 2013). Considering this, denser and rounded minerals will tend to deposit in the proximal areas of a turbidite fan while lighter and angular ones tend to do so on the distal parts of the fan (*figure 8A*). The results of the experiment showed

that the concentration by volume of high-density grains decreased by more than ~50% in the distal areas while the concentration of angular grains increased by ~60% (figure 8B). The understanding of the mineral distribution within a turbidite system is important in a petrophysical evaluation due to the effect of mineralogy on the calculation of porosity.

SAN RICH FAN	MIXED MUD/SAND-RICH FAN	
Channelized sand bodies in the upper fan passing down-dip into channelized lobes.	Channel-levee complexes in the upper fan passing down-dip into depositional lobes	
Sand/shale ratio higher than 70 % through the whole system	Sand/shale ratio between 30-70 % through the extent of the system, decreasing towards the distal areas	
Small scale (1-50 km radius)	Moderate scale (10-350 km radius)	
Reservoir facies are dominated by high density currents and/or debris flows arranged into broad, lenticular channels and lobate, channelized sheets.	Reservoir facies are highly variable with a general increase in mud content towards the distal parts of the fan	
	Channel-fill facies vary from high density turbidites to fine-grained, thin-bedded turbidites and hemipelagic mudstones.	Depositional lobes are very heterogeneous. The core may be dominated by thick-bedded high density turbidites, passing into thin-bedded turbidites towards the lobe margins.
Limited range of log motif. Blocky to poorly develop shaling-upwards log signature appears to dominate reflecting the sand-rich nature of both the channelized sand bodies and the channelized lobes	Wide range in log responses depending on location.	
	At the levee margin: - Cleaning upwards units reflecting stacking of thin bedded turbidites deposited by overbank lows - Broadly shaling-upwards or sometimes ratty trend reflecting stacked channel-fill turbidites	Depositional lobes display erratic but broadly cleaning-upwards grading into shaling-upwards signatures representing the movement of the lobes.

Table 2 – Main characteristics from sand-rich fans and mixed mud/sand-rich fans, as it is explained in the article by Richards and Bouman, 1998.

A BOUMA MODEL
CLASSICAL TURBIDITE



- E - Pelitic division, partly deposited by turbiditic current, partly hemipelagic
- D - Faint parallel laminations of silt and mud
- C - Ripple cross-laminated fine sandstones
- B - Paralell laminated sandstones
- A - Graded or massive sandstones

B SUBMARINE FAN ENVIRONMENTAL MODEL

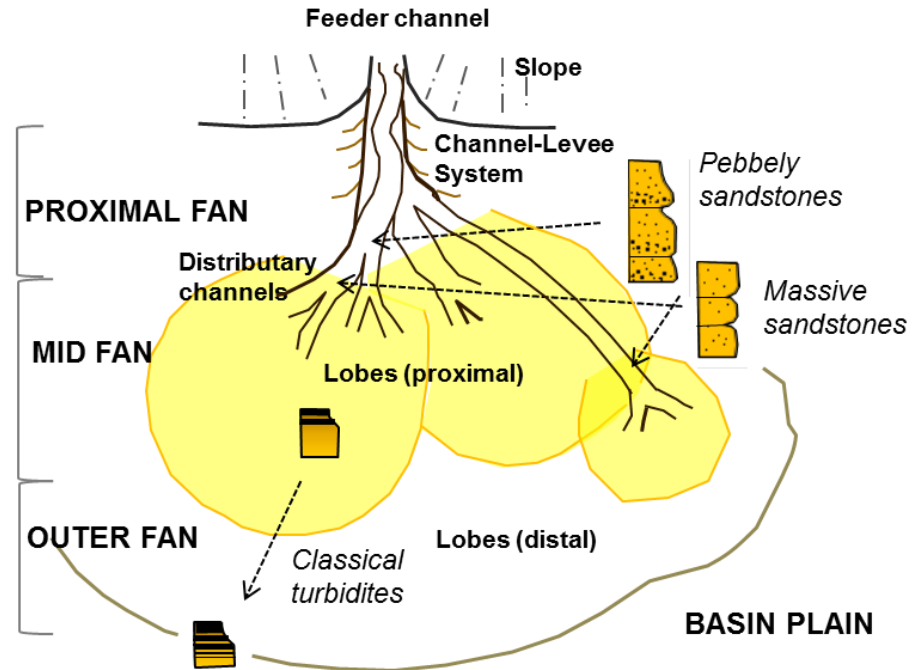
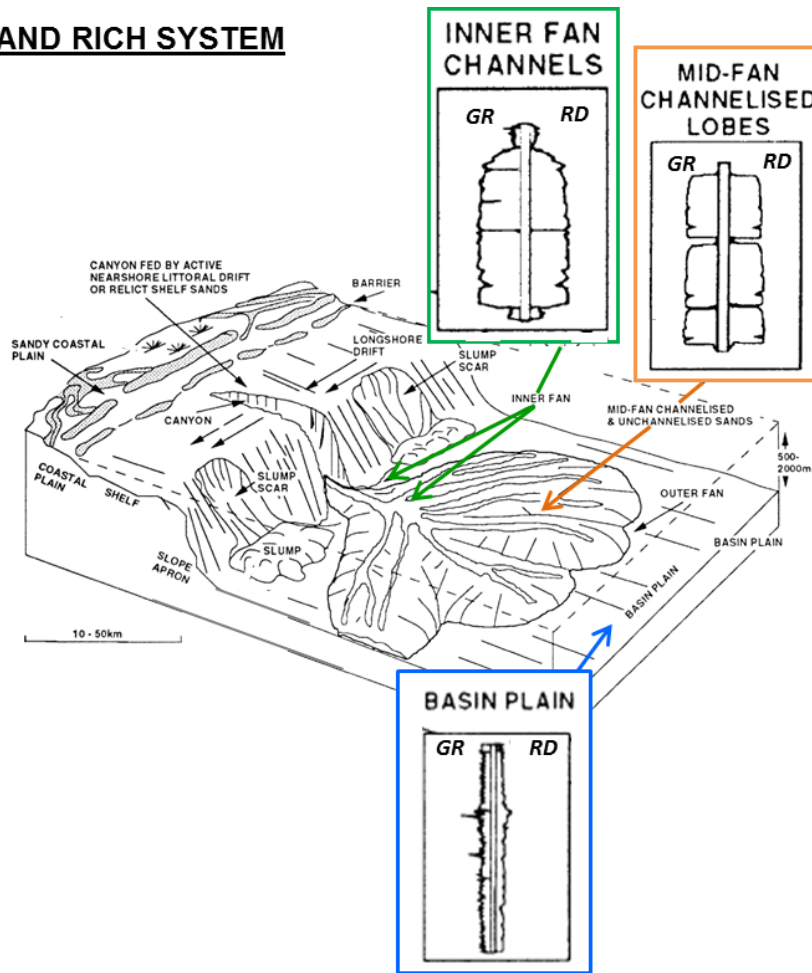


Figure 6– A) Description of the Bouma turbidite facies model, consisting of five distinctive divisions. B) Environmental model of a submarine fan showing the three main fan zones with their most characteristic lithological facies (modified from Walker (1976)).

SAND RICH SYSTEM



SAND-MUD RICH SYSTEM

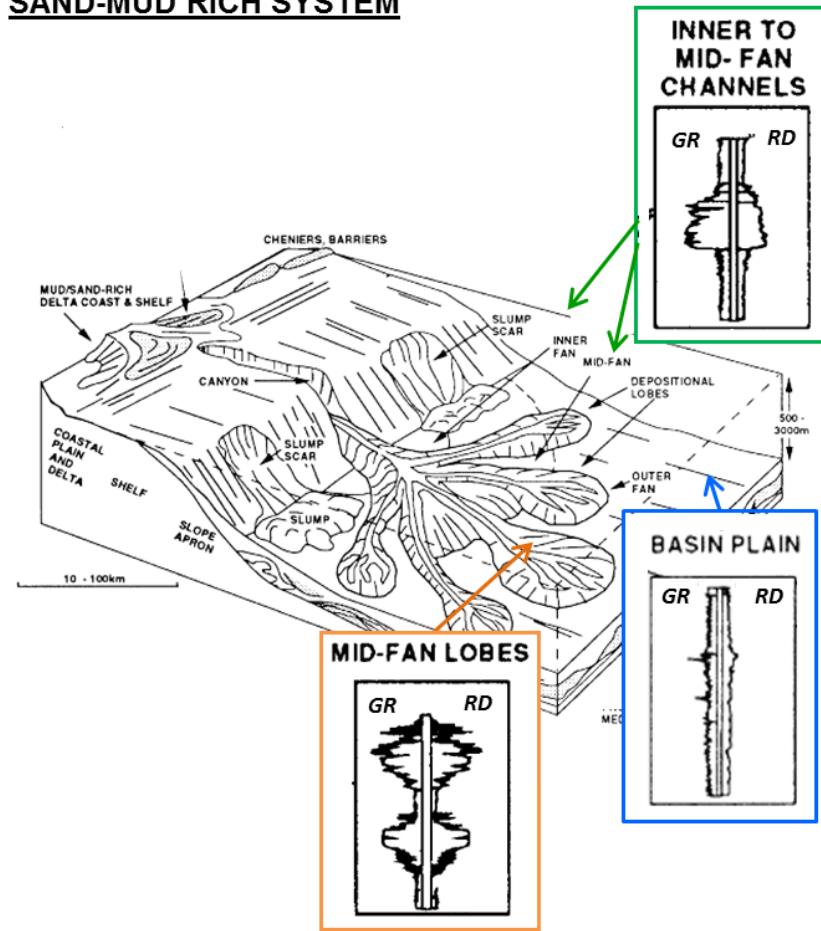


Figure 7– Gamma ray and resistivity log signatures of the different depositional environments within a sand rich system and a sand-mud rich turbidite system (modified from Richards and Bowman (1998))

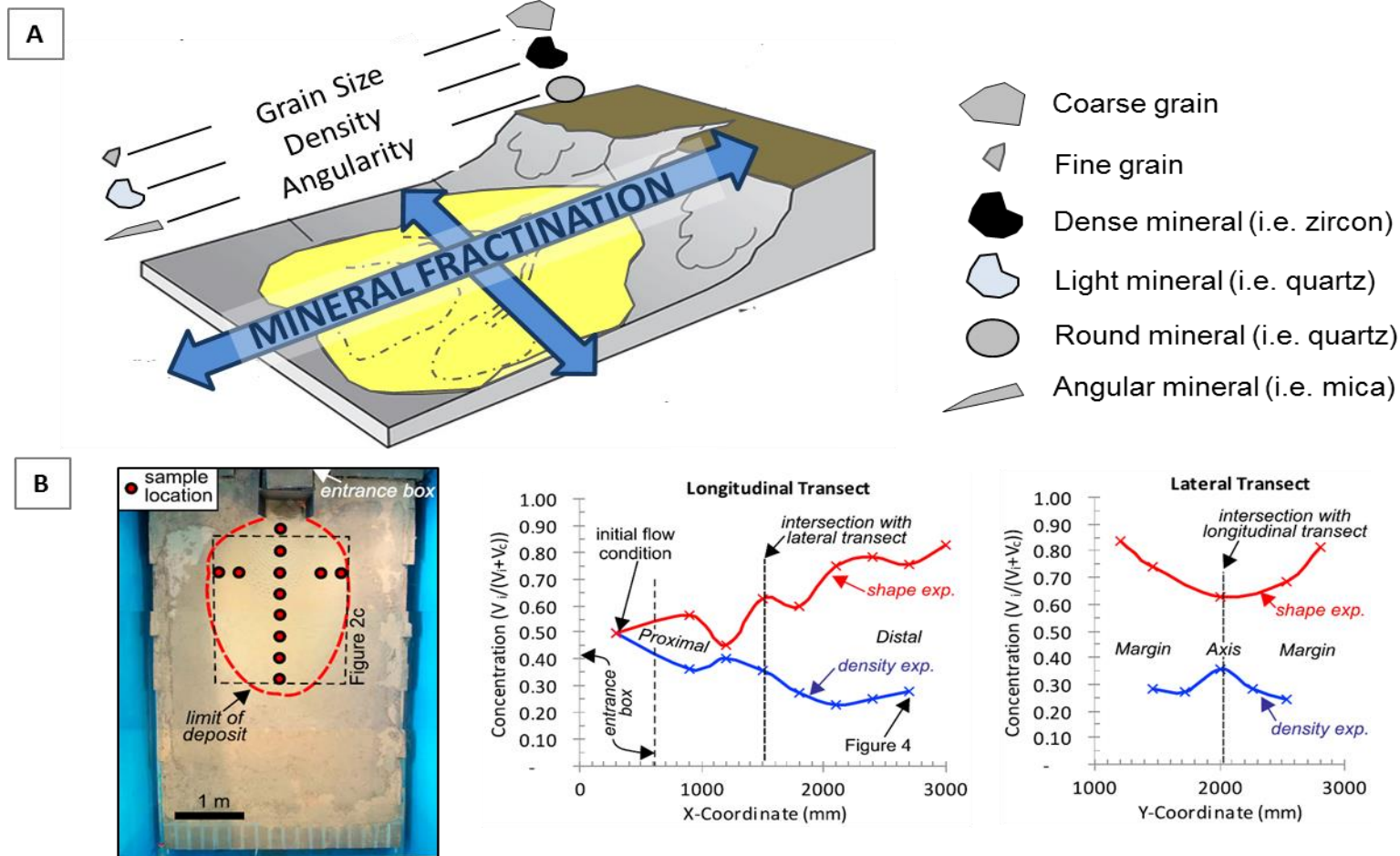



Figure 8– A) Sketch explaining how mineral fractionation function in a turbidite fan. Fine, light and angular minerals tend to deposit towards the distal parts of the fan while coarse, dense and rounded tend to do so in the proximal areas. B) Figures from the article by Fulanito, illustrating the results of two experiments performed to document the effect of density and shape in mineral fractionation over a turbidite fan (figure 8B modified from Pyles et al. (2013)).

3. DATA

The main dataset used for this study comprises the following:

- 1) The log-suit of wells 7122/2-1, 7120/1-2, 7120/2-2, 7120/10-2 (*figure 1*), provided by the NPD (2015).
- 2) Well reports, conventional core analysis reports with lab measurements of porosity, permeability and grain density, core and cuttings descriptions and high resolution photos of the cores, form NPD (2015).
- 3) A collection of 16 thin sections from different levels within Knurr Formation. The sections were as part of the LoCra Project for the research by Matthews et al. (2015) on provenance studies.

A summary with the main information from the studied wells (NPD, 2015), as well as a list with the log-suits and the number of thin sections available for each well is provided in *table 3*.

WELL NAME	7122/2-1	7120/1-2	7120/2-2	7120/10-2
LOCATION	Hammerfest Basin	Hammerfest Basin	Hammerfest Basin	Hammerfest Basin
YEAR	1992	1989	1991	1990
DISCOVERY	No (No shows in Knurr Fm)	Yes (Technical discovery)	No (oil shows in Knurr Fm)	No (No shows in Knurr Fm)
TOTAL DEPTH (MD)	2120 meters	2630 meters	2794 meters	2500 meters
TARGET	Valanginian/ Hauterivian sandstones	Aptian and Hauterivian sandstones	Aptian and Hauterivian sandstones	Valanginian sandstones
CORED	99 meters in Knurr Fm	11 meters in Knurr Fm	22 meters in Knurr Fm	8,5 meters in Knurr Fm
TESTS (DST)	No	Yes 	No	No
<div style="border: 1px solid black; padding: 5px; display: inline-block;"> At 1888,5 m – Production test + segregated sample (0.0012 m³ oil + 0.074 m³ gas) </div>				

LOG SUIT	CAL, GR, NPHI, RHOB, DT, RD, RM, RS, K, TH, U	CAL, GR, NPHI, RHOB, DT, RD, RM, RS, K, TH, U	CAL, GR, NPHI, RHOB, DT, RD, RM, RS, K, TH, U	CAL, GR, NPHI, RHOB, RD, RM, RS
CORE LAB MEASSUREMENTS	porosity, grain density, permeability	porosity, grain density, permeability	porosity, grain density, permeability	porosity, grain density, permeability,
N° OF THIN SECTIONS	6	3	4	3

Table 3 – Main information of the four study wells.

4. METHODOLOGY

4.1. DATA QUALITY CHECK AND ZONATION

The quality of the logs is analyzed using the caliper as a reference. After correcting any possible error, the log suit signature is analyzed to define a possible zonation of the reservoir to use as a framework during the evaluation.

4.2. LITHOLOGY IDENTIFICATION

In order to interpret lithology, data coming directly from the drilling (mud log report, cores and thin sections) is compared with log data. The comparison between the two datasets is carried out by a horizontal routine. This routine starts with observations of the mud log and core data for the identification of the gross lithology. The results are then compared with the gamma ray log at the same depths and with the remaining wells afterwards in a horizontal manner. If lithology is consistent, meaning that all logs agree with the lithology observed in the drilling data, the lithology is noted. When there is inconsistency among all logs, the anomalous logs have to be identified and explained. This is an iterative process until the whole well is interpreted. The neutron-density cross-plot is also useful for the reconstruction of lithology.

4.3. PETROGRAPHIC ANALYSIS

The study of thin sections is performed using a petrographic microscope. Mineralogy, average grain size, angularity and sorting are described for each thin section. In addition, some sections are selected to perform a modal analysis with the point counting technic using the software JMicrovision (Roduit, 2015). For each thin section, three digital photos are taken and 300 points are counted per photo over a random grid. This is done to achieve a statistically correct representation of each thin section. Unfortunately, the thin sections are not impregnated with blue epoxy which complicates the identification of porosity.

4.4. DEPOSITIONAL ENVIRONMENT ANALYSIS

Although a proper analysis of the environment of deposition is not the main purpose of this thesis, its broad scale understanding is important because of its implications in porosity and permeability calculations. This analysis is carried out in three steps:

1- Definition of lithofacies and log facies.

Lithofacies are defined based on lithology, grain size, sorting, content of clay and sedimentary structures by the study of both core photos and thin sections. Considering that the properties measured by logs provide a representation of primary depositional facies (Richards and Bowman, 1998) different log facies are also determined. Log facies are mainly defined based on GR baseline, GR shape and neutron-density separation.

2- Calibration of log facies with core data.

For log facies to have a geological meaning they have to be calibrated with core data. The purpose of the definition of log facies is to be able to extrapolate the lithofacies in areas where there are no core data so the depositional environment may be interpreted.

3- Analysis of the gamma ray and resistivity signatures for the recognition of fining upwards (FU) and coarsening upwards (CU) trends.

4.5. PETROPHYSICAL EVALUATION

In a petrophysical evaluation, the availability of core data is of high importance for calibration, in order to be confident in the final results. In this project, modal analyses of thin sections are available for calibration of the volume of clay log (Vcl) and the log-mineral volumes (Vmi), as well as lab measurements of grain density, porosity and permeability for calibration of the final matrix density log (RHOMA), effective and total porosity logs (PHIE, PHIT) and horizontal permeability log (KH) respectively.

Considering the availability of these core data, the general workflow in this evaluation follows an iterative process of two steps:

- 1) Definition of the computing parameters for the reservoir properties.
- 2) Modification of the computing parameters until a considerably good fit between the calculated logs and the core data is reached.

Only the water saturation log cannot be calibrated because lab measurements are not available for these wells.

The petrophysical evaluation is done with the software Interactive Petrophysics™ (IP™) (Senergy Software, 2011).

4.5.1. Volume of clay

The computation of the volume of clay log (V_{cl}) is done with the Clay Volume interpretation module in IP™. This module offers different logs to use individually or in combination as clay indicators. In this project, the gamma ray and the neutron-density combination are used for this purpose.

- 1- Volume of clay from gamma ray (V_{cl-GR}).

Gamma ray is usually the most used log as a clay indicator because, even though the gamma ray values for pure clay may vary a lot, it is usually quite constant for any one area (Rider and Kennedy, 2011). Therefore, a linear relationship from 1-100% may be constructed between gamma ray and the volume of clay (*equation 1*) if a claystone interval is known in the area and formation of study.

$$V_{cl-GR} = \frac{GR_{log} - GR_{min}}{GR_{max} - GR_{min}} \dots\dots\dots [Equation 1]$$

GR_{min} is the minimum average gamma ray value considered as clean sand (0% clay) and GR_{max} is the maximum average gamma ray value considered as clean clay (100% clay). These two average values are called the sand line and the clay line respectively.

Care should be taken however when evaluating gamma ray since there are some detrital minerals which are radioactive, like feldspars and micas that may lead to wrong interpretations of the volume of clay. For this reason it is always good to compare the gamma ray results from with other clay indicators.

2- Volume of clay from neutron-density (V_{cl-ND}).

The neutron-density crossplot is also used very often as a clay indicator together with gamma ray. Three end members are empirically defined in the neutron-density crossplot, 100% wet clay (clay point), 100% matrix (matrix point) and 100% porosity (fluid point). The wet clay point is chosen in the bottom right edge of the crossplot within the clay population. The matrix and fluid points are defined based on a “sand-line” which is chosen to be located within the clean sand population. When the crossplot is compositionally divided in this way, V_{cl-ND} can be estimated.

The final Vcl is the minimum curve resulting from the comparison between V_{cl-GR} and V_{cl-ND} . The minimum is generally chosen and not the average because these methods tend to over-estimate Vcl(Rider and Kennedy, 2011).

4.5.2. Porosity

Effective (Φ_E) and total (Φ_T) porosity are calculated with the Porosity and Water Saturation interpretation module in IPTM by using *equations 2 and 3*.

$$\Phi_E = \frac{\rho_{ma} - V_{cl}(\rho_{ma} - \rho_{Wcl}) - RHOB}{\rho_{ma} - \rho_f} \dots\dots\dots [Equation 2]$$

$$\Phi_T = \Phi_E + V_{cl} * \Phi_{cl} \dots\dots\dots [Equation 3]$$

In these equations, ρ_{ma} is the matrix density, ρ_f is the density of mud filtrate or pore fluid, ρ_{Wcl} is the wet clay density and Φ_{cl} is the porosity of the clay ($\Phi_{cl} = V_{cl} (wet) - V_{cl} (dry)$). The calculation of porosity when the matrix density is constant (i.e. the rock is composed only of quartz) is quite straightforward; however, the matrix density varies generally across the reservoir section due to changes in mineralogy or in the mineral

volumes. In these cases, a variable matrix density has to be calculated from *equation 4* and the calculation of porosity becomes more challenging.

$$\rho_{ma} = \sum_{i=1}^n \rho_i * V_i \dots\dots\dots [Equation 4]$$

As it can be seen from equation 4, the matrix density is dependent on the number of minerals constituting the reservoir rock (*i*), the density of these minerals (ρ_i) and the volumes of the minerals (V_i). The issue with this calculation is that the reservoir mineralogy is only known from cored intervals. Therefore, it is necessary to extrapolate the results from core data to the rest of the reservoir, where mineralogy cannot be directly measured. This is done by the definition of a mineral model that uses as inputs a selected number of minerals from the results of the petrographic analysis and then calculates their volumes over the entire well based on the responses of a particular log set. Mineral models are built in IP™ using the “multimineral analysis” option in the Porosity and Water Saturation interpretation module. This option uses NPHI, RHOB, DT and PEF to calculate models of three or four minerals. However, since PEF is not available for any of the wells in this project, models with a maximum of three mineral are calculated. The “multimineral analysis” option uses the Matrix Identification Plot (MID) by Schlumberger (1997) to build the mineral models, which is a crossplot of the apparent matrix density (RHOMAPP) and the apparent matrix transit time (DTMAPP). The values to plot in the MID Plot are calculated in three steps:

- 1- A pure sandstone and a pure limestone mineral models are assumed for the reservoir and the density and neutron porosities (Φ_D , Φ_N) are calculated for each of them (*equation 5*).
- 2- With the resultant density and neutron porosity values, the neutron-density crossplot porosity (Φ_{N-D}) is calculated (*equation 6*).
- 3- RHOMAPP and DTMAAPP are finally calculated based on the neutron-density crossplot porosity (*equations 7 and 8*).

$$\Phi_D = \frac{\rho_{ma} - RHOB}{\rho_{ma} - \rho_f} ; \quad \Phi_N = NPHI + lithological\ correction \dots\dots\dots [Equation 5]$$

$$\phi_{N-D} = \phi_{D_sand} + \frac{\phi_{N_sand} - \phi_{D_sand}}{1 - (\phi_{N_sand} - \phi_{N_lime}) / (\phi_{D_sand} - \phi_{D_lime})} \dots\dots\dots [Equation 6]$$

$$RHOMAPP = \frac{RHOB - \phi_{N-D} * \rho_f}{1 - \phi_{N-D}} ; \quad DTMAPP = \frac{DT - \phi_{N-D} * \rho_f}{1 - \phi_{N-D}} \dots\dots\dots [Equations 7 and 8]$$

A mineral model is defined as a triangle in the MID Plot where the apexes represent the RHOMAPP and DTMAPP values of the three minerals selected as inputs from the petrographic analysis. The volume of each mineral for each data point in the well is calculated considering the position of the points in the triangle relative to the position of the three mineral end members. The estimation of the mineral end members is done by calibration of the resulting mineral volumes with the volumes calculated from thin sections. Furthermore, the resulting wet clay volume calculated from the mineral models has to fit with the Vcl log. The final RHOMAPP and DTMAPP end members values might be different from their true density and sonic values if the selected input minerals are not the standard Limestone / Dolomite / Quartz. This is because the apparent crossplot porosity that is used for the calculation of RHOMAPP and DTMAPP is based on pure sandstone and limestone models, which might be not realistic.

A model is first built for well 7122/2-1 to use as a reference because this well has a continuous core which allows for better calibration and thus, more confidence in the resulting model. This model is then tried in the rest of the wells and the mineral end members adjusted in each of them until the best fit with core data is reached. Finally, if a model results very different from the reference one after calibration, it means that the mineral inputs of this model should be reconsidered and a different model should be tried.

Once the mineral models are defined, matrix density is computed using *equation 4* with the volumes calculated from the mineral models and the true densities of the minerals selected as inputs. Finally, the final effective and total porosity logs can be computed from *equations 2 and 3*.

The fluid density is assumed to be the same as the density of the mud; however, there is no data to estimate its value. Therefore a standard value of 1,03 g/cc is chosen to be used in the calculations (Lehne, 2015).

4.5.3. Water saturation

Water saturation is calculated with the Porosity and Water Saturation interpretation module in IP™, which offers several functions to calculate water saturation. The use of each of these functions generally depends on the type of data available. In this study, considering that some reservoir intervals are shaly-sands and also that neither special core analyses (SCAL) rock electrical-properties data nor SCAL capillary pressure data is available, Indonesia equation (*equation 9*), developed by Poupon and Leveaux (1971), is the best option to calculate water saturation. The computing parameters for the calculation of the water saturation are the true resistivity (R_t), the water resistivity (R_w), clay resistivity (R_{cl}), the tortuosity factor (a), the cementation factor (m) and the saturation exponent (n), apart from the already calculated effective porosity (Φ_E) and the volume of clay (V_{cl}).

$$\frac{1}{\sqrt{R_t}} = \left[\frac{V_{cl}^{(1-V_{cl}/2)}}{\sqrt{R_{cl}}} + \frac{\Phi_E^{m/2}}{\sqrt{(a \cdot R_w)}} \right] * S_w^{n/2} \dots\dots\dots [Equation 9]$$

Clay resistivity is the average value of the resistivity across the clay intervals and it is calculated interactively from the Interactive Plot in IP™. Water resistivity can be calculated from any water bearing clean sand interval in the reservoir considering that in these intervals it holds that $R_w = R_t / F$. Thus, water resistivity can be calculated if the formation factor (F) is known. Formation factor can be calculated through the relationship $F = a / (\Phi^m)$. Parameters “a” and “m” are obtained from special core analyses (SCAL) or otherwise theoretical values can be assumed from bibliography. The Pickett Plot, which relates porosity with resistivity, is a graphical way to solve water resistivity and the formation factor.

4.5.4. Permeability

The approach used to calculate permeability is based on the establishments of trends using core data measurements. Core data values have to be corrected for overburden to simulate insitu reservoir conditions ($K_{core}=KHLC=KHL*0.75$ / $\Phi_{core}=PORC=PORO*0,98$). These trends are built based on linear regression lines (equation 10), where core porosity (Φ_{core}) is the independent variable and core permeability (K_{core}) is the dependent one.

$$\log(k_{core}) = a + \Phi_{core} * b \dots \dots \dots [Equation 10]$$

From these trends one can generally infer the strong correlation between porosity and permeability. However, very often there is not a single porosity-permeability trend representing one reservoir. This is because permeability is also controlled by rock texture (in terms of grain size, sorting and amount of depositional matrix) and diagenesis. According to Cade et al. (1994), the best way to evaluate porosity-permeability trends is to remove the primary textural controls from the data set and then evaluate the effect of diagenesis. In order to follow this approach, the data set is divided in lithofacies, since they are defined based on type of lithology and texture. Once the different trends are established for each lithofacies, the permeability log is computed upon the wireline logs.

It is also possible to calculate permeability from nuclear magnetic resonance logs, full-wave acoustic log or from Timur's relationship, which uses porosity and water saturation estimations. However, these methods cannot be used in this project since neither nuclear magnetic resonance logs nor full-wave acoustic log are available for these wells and water saturation is too high to be used it for this purpose. In any case, a predictive method based on core data is much likelier to succeed than a non-predictive one (Hearst et al., 2000).

4.5.5. Net to gross

The calculation of the net to gross is based on cutoffs that are applied to specific reservoir properties in order to discern between unproductive or uneconomic layers. In

general, cutoffs are applied to clay volume, porosity, permeability and/or water saturation, depending on the results from the evaluation. Histograms of the calculated reservoir properties should be analyzed in order to understand which one will affect the most for the final estimation of the net pay. For example, when reservoirs are shallow it is common that variations in the porosity cutoff do not influence much the final net pay, however, small variations in the Vcl could lead to important differences in the resultant net sand. In the Norwegian Continental Shelf it is common to use a cutoff on the permeability log of 0,05 mD (Lehne, 2015). However, since permeability logs are not always computed, this cutoff is normally extrapolated to a porosity value, using a porosity-permeability plot that can be used for all the wells in a field. In this project, Vcl, PHIE and Kh are analyzed by the use of histograms to determine which one give the most appropriate net sand results.

5. DATA QUALITY CONTROL AND ZONATION

The quality of the data is in generally good except for well 7120/10-2. In this well, the logs show bad quality in the interval 1745-2100, probably due to problems during data acquisition (*figure 9A*). Furthermore, some point data in wells 7120/1-2 and 7120/2-2 exhibit very high neutron, very low density and high caliper (*figure 9B*). These data are interpreted as washouts and they are corrected.

Once the data are corrected, the log suit is analyzed together for each well in order to establish a first zonation in the reservoirs to use as a framework for the evaluation. Knurr is divided in two zones in each well: S1-Lower and S1-Upper (*figure 9C*). This division is based on the similarity of the log responses over each zone and agrees with the progradational and regradational sections respectively from the division of Sequence 1 by Marin et al. (2014). Zone S1-Upper of well 7120/10-2 is not evaluated in the project due to the quality problems of the logs in this section.

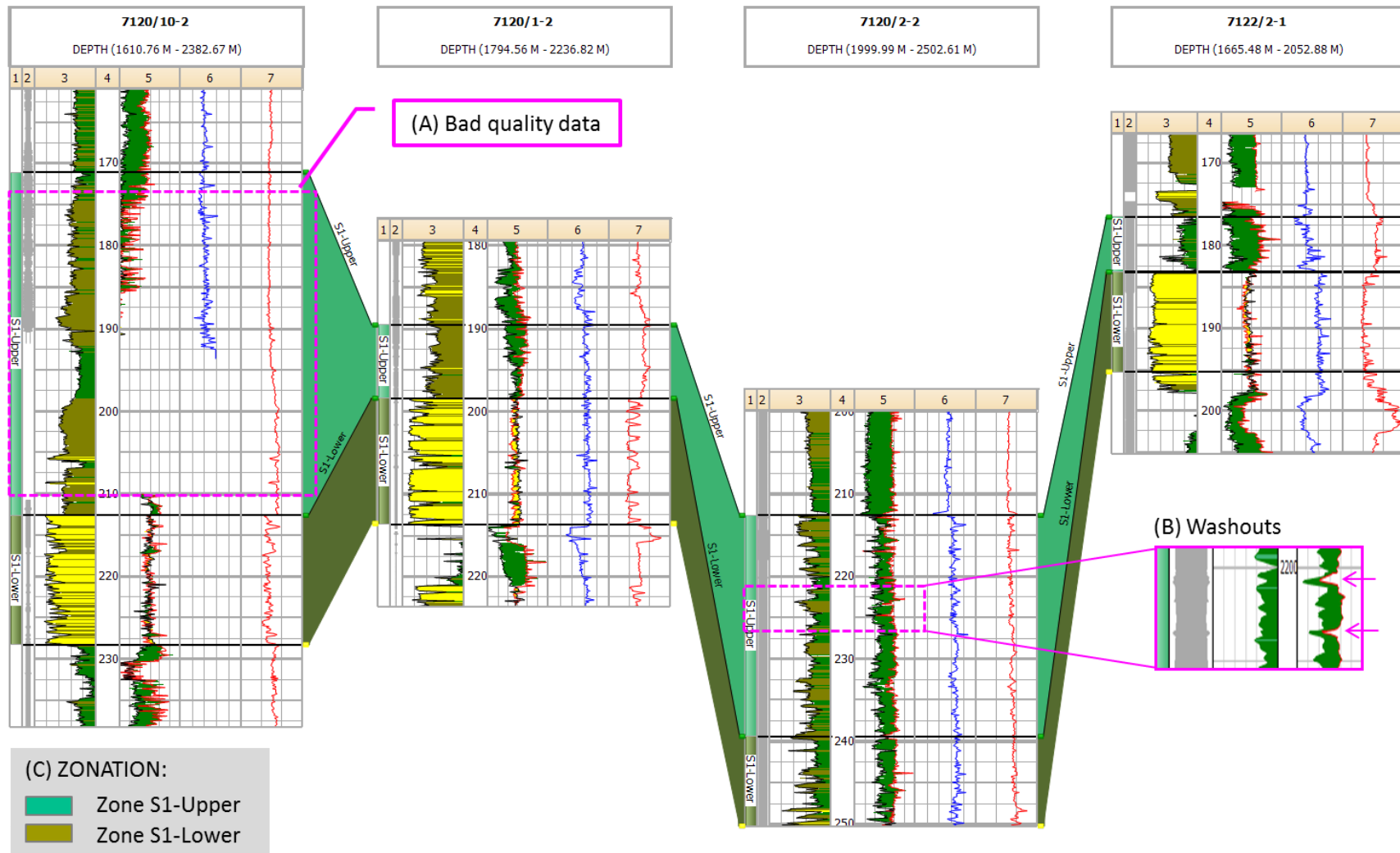


Figure 9– A) Bad quality data probably due to acquisition problems. B) Washouts leading to erroneous measurements in RHOB and NPHI. C) Zonation of Knurr Formation based on the similarity of the log responses over each zone.

6. LITHOLOGY IDENTIFICATION

The differences in lithology between the four wells can be easily observed in the neutron-density cross plot with gamma ray in the Z axis (*figure 10*). Five main lithologies can be distinguished: conglomerates, sandstones, shaly-sandstones, sandy-shales and claystones.

Well 7122/2-1 presents several peculiarities. First of all, it shows a very sharp lithological change, with clean sands in the lower zone and claystone in the upper one. In fact, it is the only well that presents an almost 100% claystone interval, being siltstone its closest lithology for the rest of the wells. It is also very interesting to notice about the conglomeratic intervals in zone S1-Lower of this well. These conglomerates have a gamma ray and neutron-density responses similar as for shales and without core data they could be easily mistaken by this lithology. The reason for this might be the big claystone fragments observed from core data. However, they present a distinctive characteristic that makes these conglomerates recognizable, the high U-Sp and the presence of pyrite). The high U-Sp can be analyzed in the Computer Processed Interpretations (CPI) but the presence of pyrite is better evaluated in the neutron-porosity crossplot because heavy minerals (i.e. pyrite) produce the effect of increasing RHOB but not affecting NPHI. Finally, it can be observed the effect of calcite cement closing almost all the porosity (blue circle) in few horizons. This characteristic is also present in wells 7120/1-2 and 7120/10-2. At a first glance, the sandstones in wells 7122/2-1, 7120/1-2 and 7120/10-1 seem to have good porosity around 15 to 20%. Well 7120/2-2 is mainly composed by shaly sandstones although thin layers of sandstone are also identified, with lower porosities, of over 10%.

The resultant lithological column obtained from the horizontal routine is presented for each well in figure 11. Given these results, the upper section of well 7120/2-1 is not evaluated in this project because it is not considered as a reservoir, as it is claystone the main lithology identify.

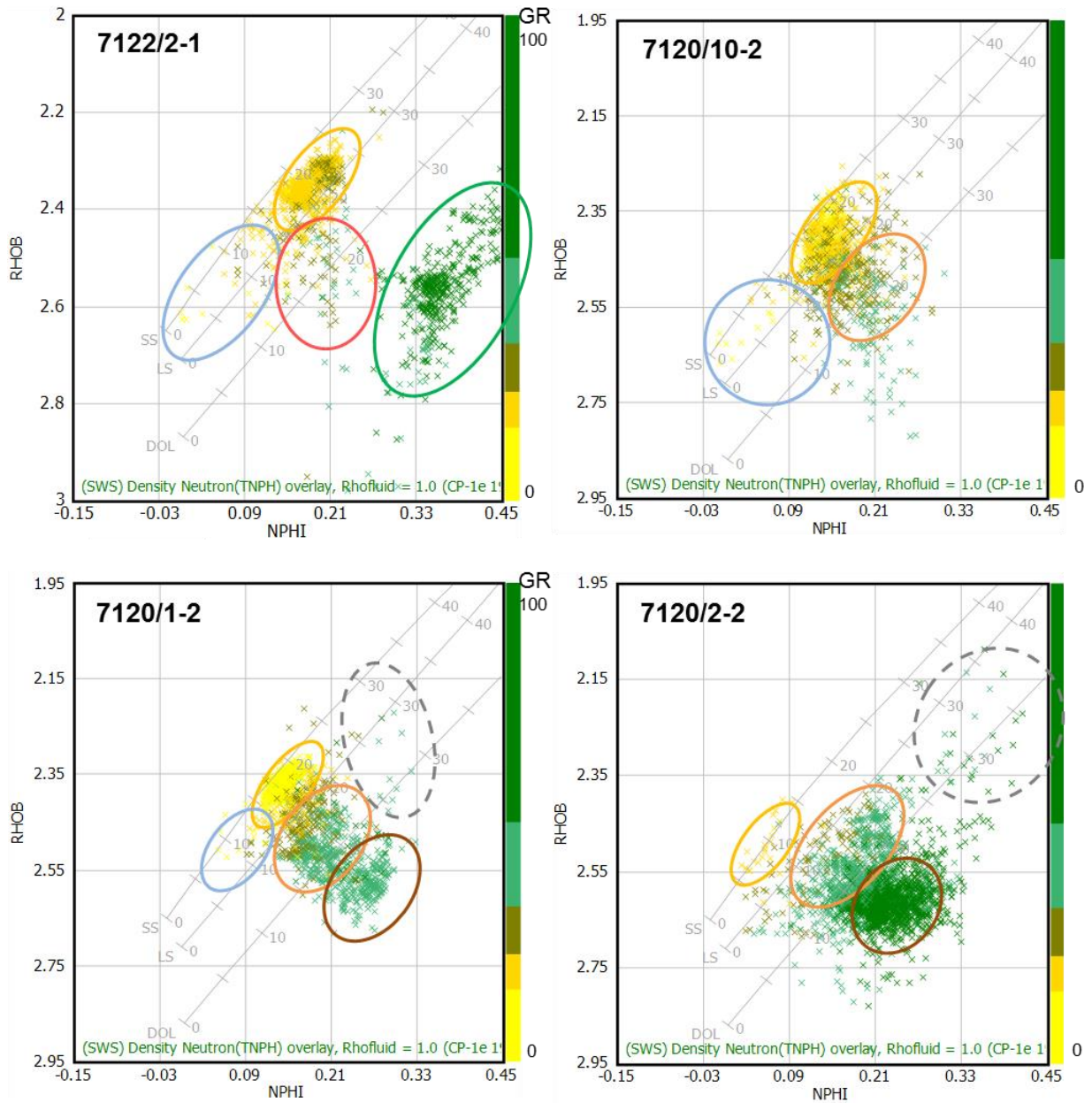


figure 10– neutron-density crossplots for each of the wells under study. different lithologies are marked with colored circles. yellow: sandstones; green: shales; orange: sandy-shales; brown: shaly-sands and blue: calcite cemented horizons. the grey circle shows the anomalous data due to washouts

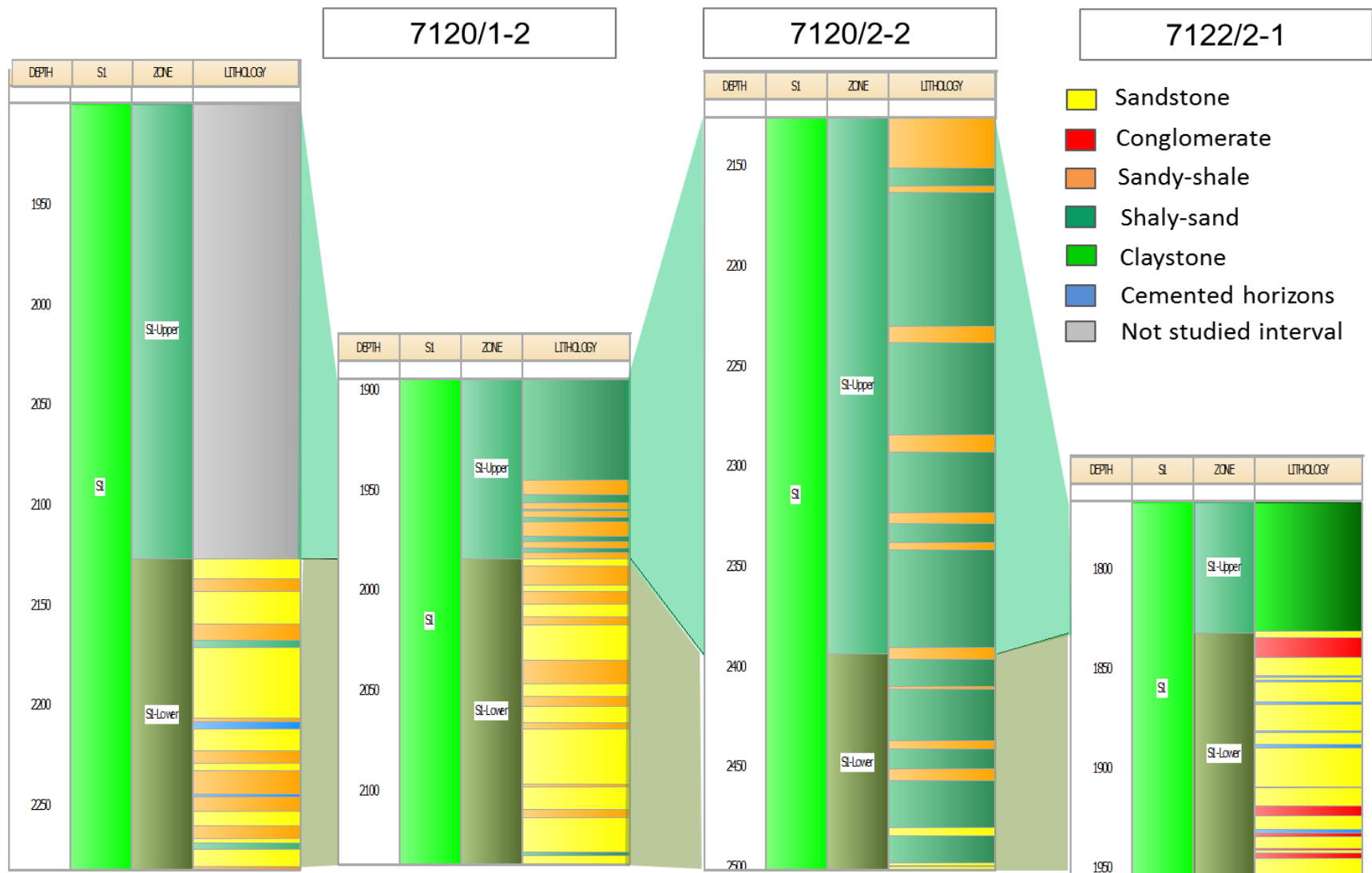


Figure 11– Lithological columns for the study wells. The wells are aligned to the base of S1 sequence

7. PETROGRAPHIC ANALYSIS

Due to the time constrain of the project, a detail petrographic analysis is not possible. Therefore, this analysis focuses in three blocks:

- Understanding of the main mineralogy of the different reservoirs to identify the mineral inputs for the petrophysical mineral models.
- Modal analysis considering only the mineral inputs previously defined in order to calculate the volumes of each mineral for later use in calibration of V_{cl} and V_{mi} .
- Recognition of the rock main textural characteristics as well as the main diagenetic processes as a tool for lithofacies identification and for a better understanding of porosity-permeability trends.

The results from the study of xx thin sections as wells as the results from the modal analysis are summarized in *table 4*. The value ranges of grain size, sorting and roundness to define rock texture are given considering the categories published by Pettijohn et al. (1973).

According to the classification by Pettijohn et al. (1973), these sandstones can be divided in two groups (figure 12): subarkoses (figure 13A) and feldspatic wackes (figure 13B). It is observed that the mineralogy of the four turbidite systems is very similar. The rocks in all of them are mainly composed of quartz, feldspar, clay minerals and micas. The type of clay is difficult to identify by thin sections. However, in all the wells, kaolinite and illite have been sometimes recognized (figure 13C-D). Micas are generally observed as fine grained minerals in the wack samples (figure 13E). Their volumes, however, seem noticeable reduced in those samples formed by clean sands. Carbonates are also observed as shell fragments and carbonate cement in some localized horizons over then entire well, associated with clean sands (figure 13F). Finally, accessory minerals are also identified which are generally classified as heavy minerals (figure 13G). Matthews et al. (2015) is currently doing a heavy mineral analysis as part of the provenance studies of the Lower Cretaceous sandstones. Until now, they have qualitatively identified the heavy mineral assemblage in several wells in the Barents Sea, including three of the study wells in

this thesis. The heavy mineral assemblage for these three wells is shown in *table 5*. Porosity is easily recognized in the clean sandstones with big grain sized (figure 13H), but it results very challenging to do so in the finer samples.

The rocks also seem very similar regarding diagenesis. Compaction and silica cementation are the main diagenetic processes observed affecting these reservoirs. Poiquilotopic carbonate cement is also observed in some horizons, as it was mentioned before. In these horizons porosity is noticeable reduced or even almost inexistent. Alteration of grains is rarely seen and that is why the clay matrix in these sandstones is considered mainly depositional, transported within the turbidite system. Only in well 7120/2-2, in the more sandy layers, some feldspars are observed that seem to be altering to illitie (figure 13I). Also in this well and associated as well with the more sandy layers, moldic porosity is observed which is interpreted as secondary porosity probably due to the dissolution of grains (figure 13J).

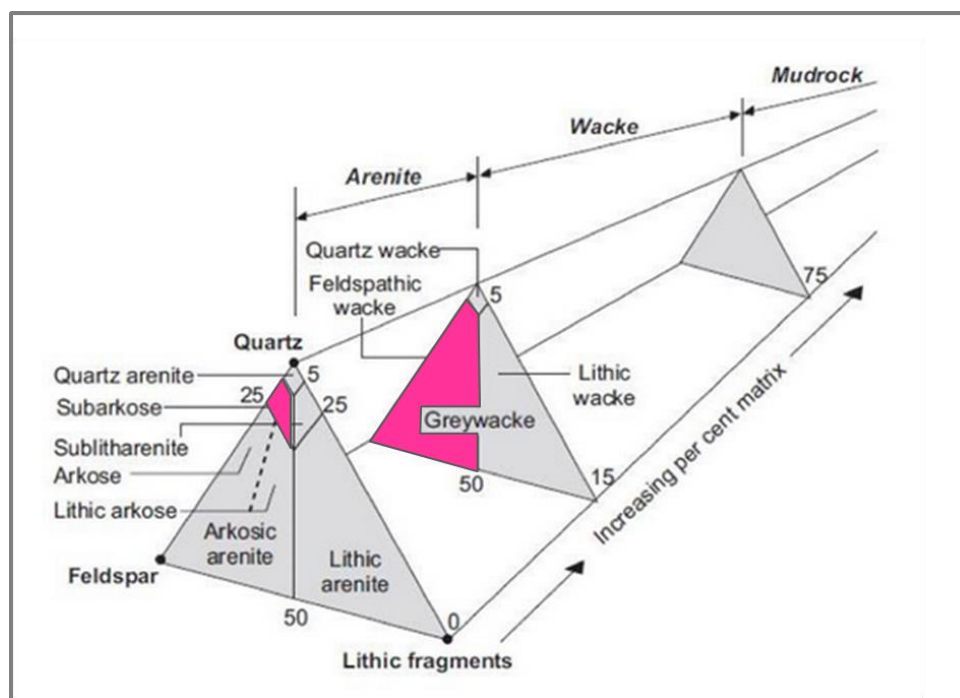


Figure 12– Pettijohn classification of sandstones. In pink, the fields to which the study samples belong to: subarkose/feldspathic wacke (Pettijohn et al., 1973).

TS	Well	Depth (m)	Grain Size	Roundness	Sorting	Modal analysis	Qtz+Fds	Lith	Mosc	Biot	Hm +	Calc	Clay	Pore	Other
	7122/2-1	1869,6	Coarse	Subrounded	Poorly sorted		0,680		0,035	0,000	0,000		0,055	0,215	0,015
	7122/2-1	1884,35	Coarse	Subrounded	Poorly sorted		0,700		0,000	0,000	0,000		0,050	0,200	0,05
	31b		Pebbles	Subangular	Very poorly sorted	No	X	X	No	No	X	X	X	X	
	7122/2-1	1925,95	Medium - coarse	Subrounded	Well sorted		0,798		0,000	0,000	0,013		0,020	0,153	0,015
	125		Medium	Rounded	Well sorted	No	X		X				X		
	7122/2-1	1909,8	Medium	Subrounded	Very well sorted		0,795		0,000	0,000	0,005		0,025	0,170	0,000
20	7120/1-2	1958,3	Fine	Subangular	Moderately sorted		0,715		0,000	0,000	0,005		0,055	0,060	0,016
12	7120/1-2	12b	Medium to fine	Subrounded	Poorly sorted		0,890		0,000	0,000	0,010		0,013	0,087	0,000
11	7120/1-2	11b	Fine to very fine	Subangular	Moderately sorted		0,667		0,010	0,000	0,000		0,260	0,063	0,000
	7120/2-2	2163,4	Silt	Angular	Moderately sorted	No	X		X	X			X		
	7120/2-2	2396,8	Medium to Fine	Subangular	Poorly sorted		0,585		0,000	0,000	0,005		0,365	0,035	0,000
	7120/2-2	2196,8	Very fine to silt	Angular	Poorly sorted		0,350		0,055	0,030	0,000		0,565	0,000	0,000
	7120/2-2	2187,65	Fine	Angular	Moderately sorted		0,360		0,028	0,030	0,005		0,523	0,048	0,015
	7120/10-2	2134,85	Medium	Subangular	Poorly sorted		0,735		0,000	0,020	0,020		0,090	0,125	0,010
	7120/10-2	2130,3	Very fine	Angular	Poorly sorted		0,580		0,090	0,040	0,010		0,195	0,080	0,000
	7120/10-2	2130,75	Medium	Angular	Poorly sorted		0,850		0,000	0,000	0,000		0,060	0,090	0,000

Table 4 – Thin section analysis

WELL	HM Assemblage
7122/2-1	trm, rt, apa, pyr, zr, mosc
7120/1-2	apa,chl,sp,zr, mos, biot
7120/2-2	gar, chl, sp, zr, mosc, biot
Heavy minerals densities (g/cc)	
Apatite (apa)	3,2
Chlorite (chl)	2,8
Tourmaline (trm)	3,2
Spinel (sp)	3,8
Garnet (gr)	4,31
Zircon (zr)	4,5
Pyrite (pyr)	4,99
Rutile (rt)	4,24
Magnetite (mg)	5,08
Biotite (biot)	2,99
Moscovite (mosc)	2,82

Table 5 – Heavy mineral assemblage for wells 7122/2-1, 7120/1-2, 7120/2-2 (data from Matthews et al. (2015)).

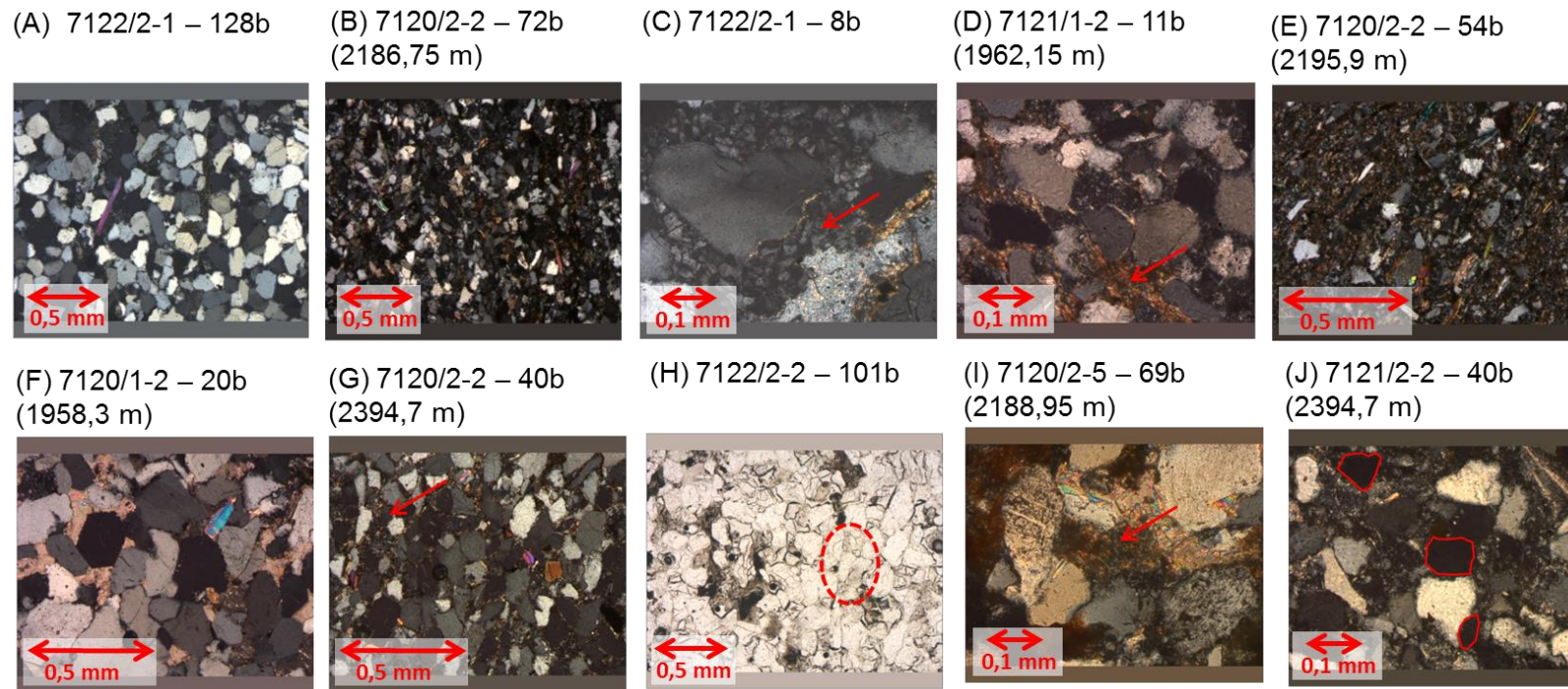


Figure 13 – A) Subarkose, B) Feldspathic wacke, C) Kaolinitic, matrix, D) Illitic matrix, E) Fine grains of muscovite observed in a wacke sample (high birefringence minerals with tabular shape), F) Carbonatic cement, G) Heavy minerals, H) Porosity in a coarse grained sandstone (porosity appears with very high relief), I) Mineral alteration, J) Moldic porosity

8. ENVIRONMENTAL ANALYSIS

8.1. RESULTS: LITHOFACIES, LOG FACIES AND GAMMA RAY SIGNATURE

From the study of thin sections and cores six lithofacies are defined. A description of each of this lithofacies and an example from thin section and core is shown in *table 6A-B*. Lithofacies are analyzed in the NPHI-RHOB cross-plot and also adding the GR in the Z axes in form of a 3D plot (*figure 14A*). It is observed that each lithofacies is plotted within a distinctive cluster, indicating that the neutron, density and gamma ray logs can be used as well to define lithofacies and estimate their distribution along the non-cored part of the well. Taking this into account, seven log facies are also defined based on GR baseline, GR shape and neutron-density separation (*table 7*). These log facies are also plotted in the neutron-density crossplot where it can be observed the correlation between the lithofacies and log facies clusters. Only LogF5 seems to overlap part of LogF4 and LogF6.

	LITHOLOGY	ANGULARITY	SORTING	GRAIN SIZE	MATRIX	GENERAL DESCRIPTION	
LF1	Conglomerates	Subrounded to subangular	Poorly sorted	Pebbles	Sandy matrix	Matrix supported conglomerate with no visible sedimentary structures. No visible gradation in either clasts or sandy matrix. Presence of erosive bases. Grains are silica cemented and some horizons present calcite cement.	Photos in next page
LF2	Sandstones	Subangular to subrounded	Moderately to poorly sorted	Coarse to medium	Clay matrix (<15%)	Massive sandstone with no gradation. Grains are silica cemented and some horizons present calcite cement.	Photos in next page
LF3	Sandstones	Subangular to subrounded	Moderately to well sorted	Medium	Clay matrix (<15%)	Sandstones with low angle cross-stratification and planar lamination. Finning-upwards (FU) units can be sometimes recognized. Grains are silica cemented and some horizons present calcite cement.	Photos in next page
LF4	Sandstones	Subangular to subrounded	Poorly sorted	Coarse-fine	Clay matrix (<15%)	Sandstones with cross-stratification and planar lamination that are organized in finning-upwards (FU) sequences. In some of these sequences erosive bases can be distinguished. Grains are silica cemented and some horizons present calcite cement.	Photos in next page
LF5	Shaly-sandstones	Subangular	Moderately sorted	Medium to very fine	Clay matrix (<15% and >15%)	Heterolithic facies formed by alternation of sandstone layers with shale layers which are organized in FU units. Visible structures include low angle cross-stratification, planar lamination and small scale current ripples. Grains are silica cemented and some horizons present calcite cement as well.	Photos in next page
LF6	Sandy-shales	Subangular	Moderately sorted	Silt and clay	Clay matrix (>15%)	Sandy-shales formed by a mixture between silt and clay with intercalation of thin stringers of very fine sandstones.	Photos in next page

Table 6A – Description of lithofacies

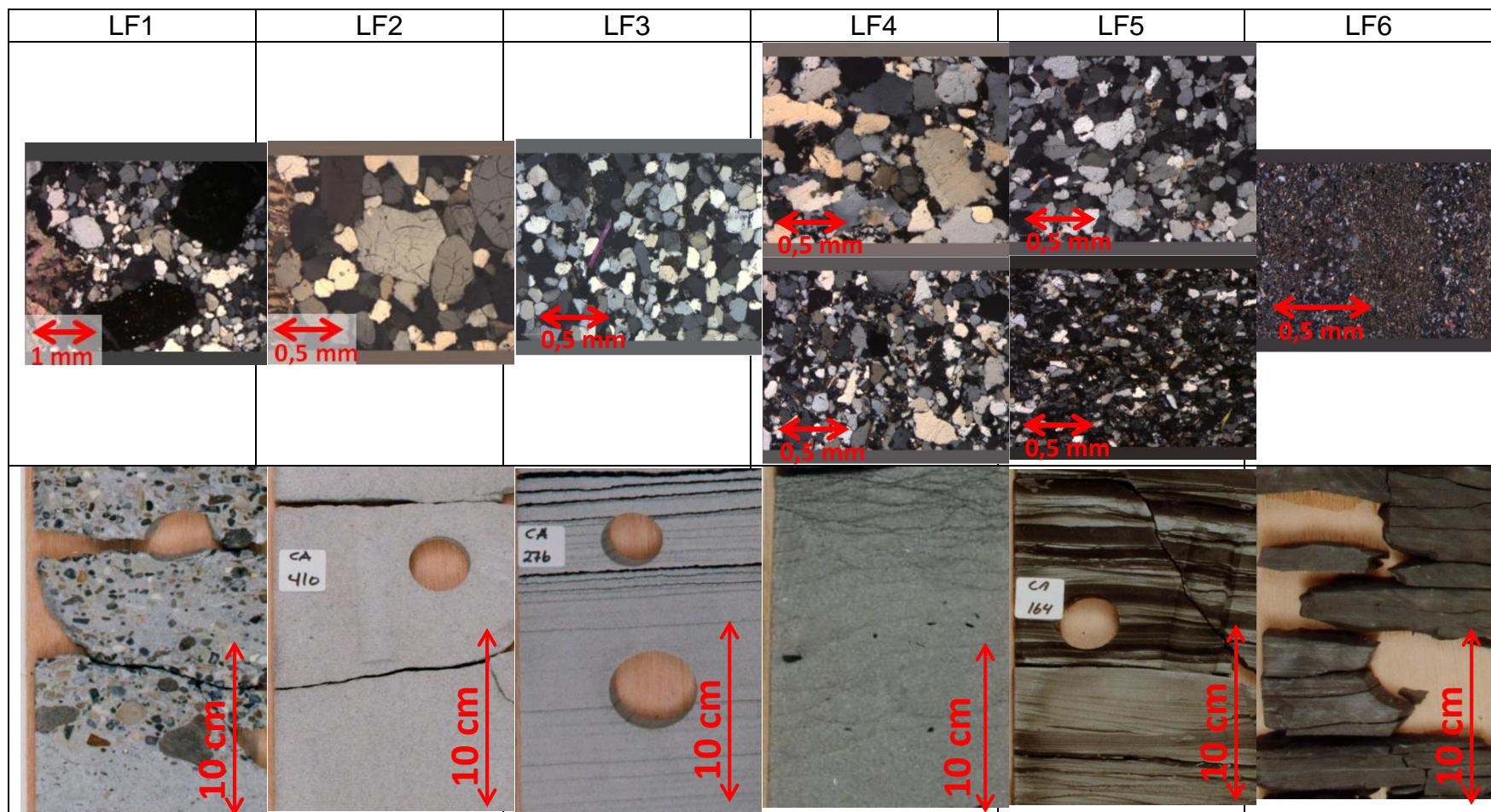


Table 6B – Photos from thin sections and cores that represent typically each of the lithofacies

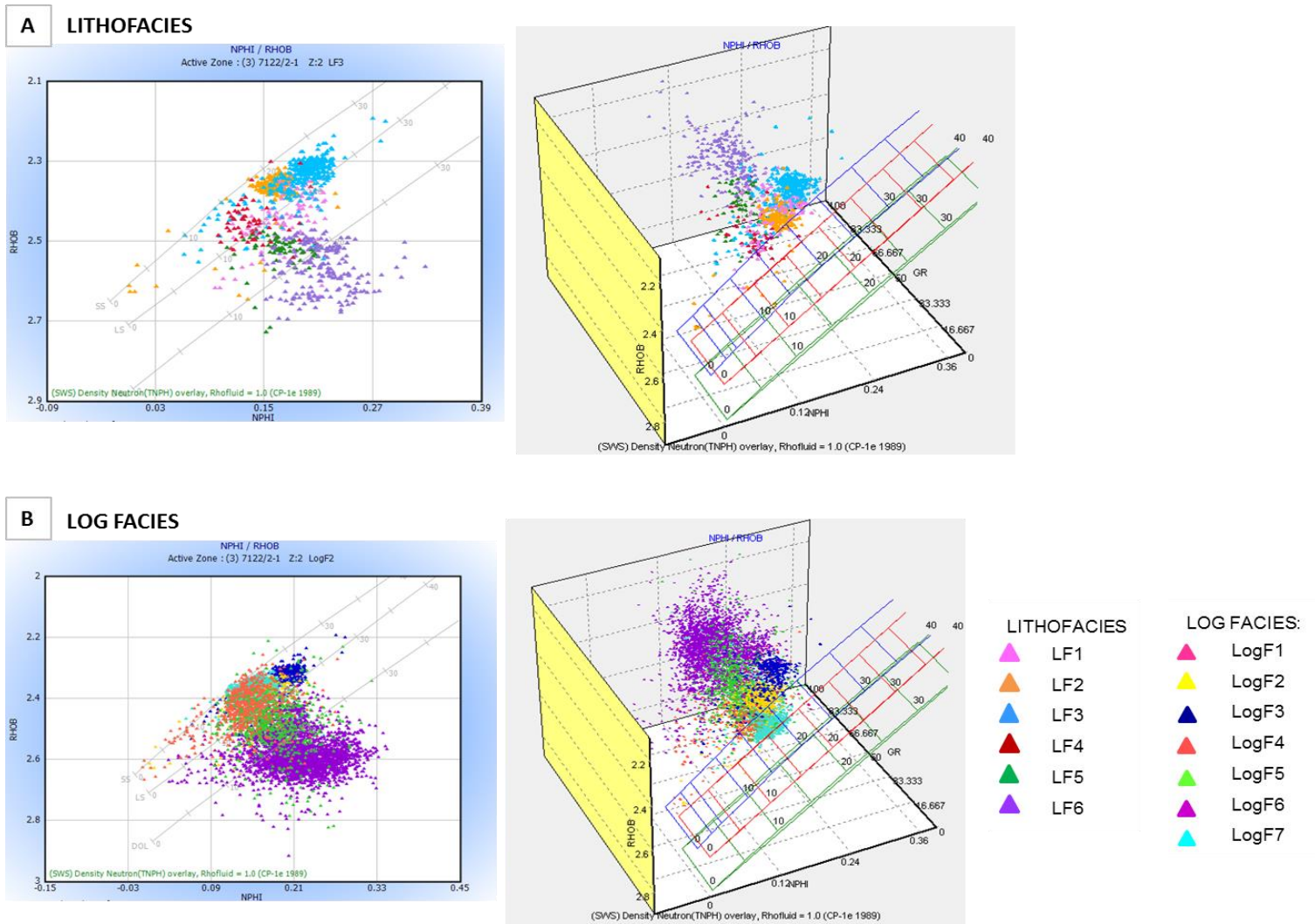


Figure 14– Neutron-Density crossplot and Neutron-Density-Gamma ray 3D plot displaying the lithofacies (A) and log facies (B) described in the study

LogF1		<ul style="list-style-type: none"> - GR baseline is 65° API - The U-spectral GR present characteristic high values (>6, 5° API) - NPHI-RHOB shows a typical shale-type crossover with a separation of 0.5 neutron units average 	
LogF2		<ul style="list-style-type: none"> - GR base line is 35° API - GR presents blocky shape - NPHI-RHOB presents generally constant values with typical sand-type crossover with a separation of ~0.8 neutron units 	
LogF3		<ul style="list-style-type: none"> - GR base line is 45° API - GR presents blocky shape - NPHI-RHOB shows the typical sand-type crossover of ~0.5 neutron units - Punctual changes to shale-type crossover. 	
LogF4		<ul style="list-style-type: none"> - GR baseline is 35° API - GR shows FU units of metric scale - NPHI-RHOB shows changes from sand-type to shale-type crossover following the FU units in the GR. - Sand type crossover is more frequent and has a separation of ~0.5 porosity units 	

Table 7 – Description of log facies based on the gamma ray base line, gamma ray shape and neutron-density separation. A core-photo of their correlative lithofacies is also included for a better understanding.

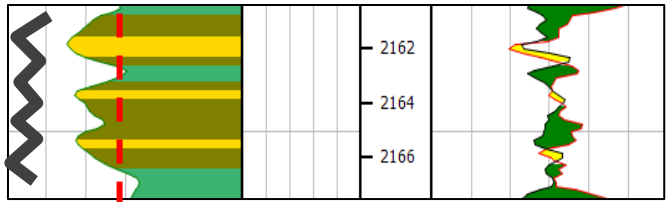
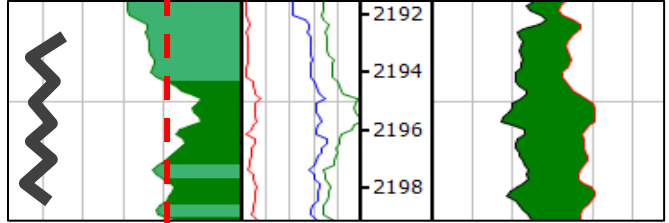

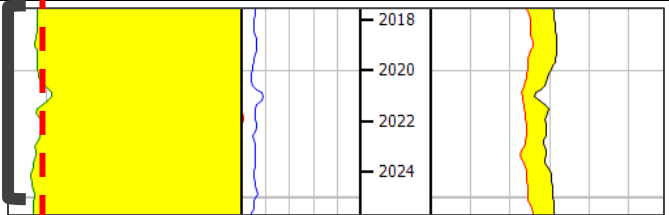
<p>LogF5</p>		<ul style="list-style-type: none"> - GR baseline is 7° API - GR shows ratty pattern - NPHI-RHOB shows changes from sand-type to shale-type crossover - Shale-type crossover is more frequent and has a separation of ~1 porosity units 	<p>Mix between LF4-LF and LF6-LF5</p>
<p>LogF6</p>		<ul style="list-style-type: none"> - GR baseline is 95° API - GR shows ratty pattern - NPHI-RHOB shows shale-type crossover with a separation of ~2 neutron porosity units 	
<p>LogF7</p>		<ul style="list-style-type: none"> - GR presents blocky shape - GR base line is 20° API - NPHI-RHOB presents generally constant values with typical sand-type crossover with a separation of 0.8 neutron porosity units - 	<p>No core</p>

Table 7- (Continuation)

Finally, the signature of the gamma ray and the resistivity are analyzed together in a bigger scale resulting in the following observations (*table 8*):

Well 7122/2-1 (S1-Lower)	- Serrated blocky along the whole section for both GR and RD
Well 7122/1-2 (S1-Lower)	- Serrated blocky signature for LogF7 in both GR and RD - LogF5 presents generally a coarsening- upwards signature in both GR and RD
Well 7122/1-2 (S1-Upper)	- GR presents a coarsening-upwards/finning-upwards signature across the whole section - RD does not define any clear trend
Well 7122/2-2 (S1-Lower)	- GR presents a coarsening-upwards/finning-upwards signature across the whole section - RD does not define any clear trend
Well 7122/2-2 (S1-Upper)	- GR presents a coarsening-upwards/finning-upwards signature across the whole section - RD does not define any clear trend
Well 7122/10-2 (S1-Lower)	- GR presents a coarsening-upwards/finning-upwards signature across the whole section - RD also presents a coarsening-upwards/finning-upwards signature across the whole section

Table 8 – Description of gamma ray and resistivity signatures.

A summary with the lithofacies, log facies and gamma ray/resistivity signature observed for each well is shown in *figure 15A-F*.

8.2. INTERPRETATION OF DEPOSITIONAL ENVIRONMENT

The interpretation of each of the lithofacies is explained below:

- LF1: The poorly sorted and matrix supported nature of the conglomerates suggest a rapid deposition probably by debris flows. Debris flows and other type of mass transport flows are common in the upper part of the turbiditic fans, close to the slope.

- LF2: The massive appearance of these sandstones, which are coarse grained and poorly sorted, indicates a deposition by high density turbiditic currents from the proximal fan. The fact that LF2 appears together with LF1, give support to a proximal depositional environment for these two lithofacies.
- LF3: These sandstones are interpreted as turbidites deposited in a more distal part of the fan, compared with sandstones from LF1. This is based on the finer grains of these deposits, and it is also supported by the presence of lamination. The recognition, sometimes, of over one meter finning-upwards units with cross stratification, may indicate that these sandstones are channel related.
- LF4: This lithofacies is interpreted as amalgamated channel-fill turbidites. The base of this interpretation is the organization of the sediments in finning-upwards units of around one meter with erosive bases and the presence of cross-stratification.
- LF5: Thin bedded turbidites forming finning-upwards units of centimetric scale represent this lithofacies. Some of these turbidites present a structure very close to the typical Bouma Sequence, with massive appearance in the base, lamination in the middle part and small scale current ripple at the top. These types of turbidites are very common in the fan lobes.
- LF6: The mix of silt and clay that characterize this lithofacies indicates a deposition in the outer fan. It can be interpreted as a mix between hemipelagic sedimentation interfingered with low density turbiditic currents that managed to reach far distances. These very fine sediments could also be interpreted as deposition during the abandonment of the fan system or the fan-lobes.

The calibration of log facies with core data shows that LogF1, LogF2, LogF3, LogF4 and LogF6 can broadly described LF1, LF2, LF3, LF4 and LF6 respectively while LogF5 represents sometimes a mixture between LF4 and LF5 and sometimes between LF5 and LF6. LogF7 could not be calibrated since there is no core data that corresponds to this interval, however, due to its similarity with LogF5 and considering the lithological information from cuttings and logs, this log facies is interpreted as high density turbidites from the proximal fan.

The final interpretation of the environment of deposition for the different wells, considering the analysis of the lithofacies, the log facies and the gamma ray/resistivity signatures together, is explained next.

Well 7122/2-1(S1-Lower)

This well is the only one presenting a continuous core which makes easier and more certain its final environmental interpretation. The lithofacies observed suggest this section to be interpreted as the transition from a proximal turbiditic fan with deposition of high density turbiditic currents mixed with debris flows, to a more distal fan with deposition of laminated turbidites and sometimes channel related sandstones. Finally, the uppermost part of the section changes back to a proximal environment. The blocky pattern observed in the gamma ray signature through the whole section suggests that this turbiditic fan is a sand-rich system. The more distal part of the section might represent the channelized lobes typical from this type of systems which do not reflect shaling-upwards signature in the gamma ray and resistivity due to the low content of shale in the system.

Well 7120/1-2 (S1-Lower)

In this section it was observed mostly the presence of LogF7 with some punctual intercalation of LogF6. The gamma ray and resistivity signatures together with the interpretation of log facies, suggests the interpretation of this section as the inner to mid fan channel-levee system in a mud-sand rich system. LogF7 represents the channels while LogF5, with a coarsening-upwards signature, might be the leveed part of the system.

Well 7120/1-2 (S1-Upper)

This sequence can be divided in two zones, both of them representing the distal part of a turbiditic fan. In the lower part, LogF5 is observed while in the upper part LogF6 is present, meaning that the environment becomes more distal towards the top of the sequence, with deposition of thin-bedded turbidites passing into a more pelagic type of sedimentation. Although the resistivity log is not determinative, the CU-FU signature in the gamma ray suggests that these sediments form part of the depositional lobes of a mixed sand-rich fan system.

Well 7120/2-2 (S1-Lower)

LogF6 is mostly distributed along S1-lower in this well. This indicates a very distal environment of deposition within the turbiditic fan, with low density turbiditic currents and hemipelagic sedimentation. However, the fact that LogF4 is also observed intercalated between this distal sediments in few places, suggests that some high density currents were able to reach these distal areas. The CU-FU signature of the gamma ray suggests, as in S1-Upper of Well 1-2, sedimentation in the depositional lobes of a mixed sand-rich fan system, however it is far away, probably in the outer fan already. The high density turbidites from LogF4 might represent channels cutting these lobes.

Well 2-2 (S1-Upper)

The upper part of sequence1 in well 2-2 is very similar to the lower part of the sequence in terms of facies and gamma ray signature and it is also interpreted as a distal environment in the very distal part of the lobes. The main difference is that the channel-fill turbidites represented by LogF4 do not appear.

There is, however, another interpretation of this depositional environment given in the research study by Sandvik (2014). In this study, the analysis of the real cores showed some sedimentary features typical from shallow environments. This has not been observed in this project probably due to the limitations related to the analysis of core photos and not the real core. The observations in this research suggested this environment to be interpreted as a shallow marine interdistributary bay or lagoon with development of washover fan deposits.

Well 10-2

Amalgamated channel-fill turbidites with intercalation of stacked thin bedded turbidites are interpreted in this well as is suggested by the mix of LogF4 and LogF5 in this section. The resistivity and the gamma ray signature show CU-FU trends, typical from depositional lobes. The difference with wells 1-2 and 2-2 is that this well was probably drilled in a much proximal location within the lobes of this turbiditic system, close to the main channel-levee complex. This area within the fan is the middle fan, where facies from the distributary channels within the lobes, represented

by LF4, are mixed with bedded-turbidites forming the actual lobe, represented by LF5.

Figure 15A-F summaries the final interpretation of the depositional environment for each well taking into account the lithofacies, the log facies, and the differences in the gamma ray and resistivity signatures.

Overall, S1-Lower represent more proximal environments than S1-Upper, except for well 7120/2-2 S1-Lower that represents distal areas in the turbidite fan. The NPHI-RHOB cross-plot shown in *figure 13* can be used for the analysis of reservoir quality, as a first approximation. Taking into consideration that LogF1, LogF2 and LogF7 represent proximal fan facies, LogF3 and LogF4 middle fan facies and LogF5 and LogF6 distal fan facies, it can be observed that proximal environments show high porosity clean sands while distal environments show a noticeable increase in shale that might also decrease the reservoir quality. This indicates that reservoir quality it is directly related with the type of depositional environment within a turbidite system.

The fact that the turbidite fans in the eastern Hammerfest Basin are classified as mud-sand rich systems while the one in the west is interpreted as a sand rich system, suggests that there are differences in the source area between the east and the west. It seems that the rocks that were eroded during the Lower Cretaceous in the western Loppa High were richer in sand content than the rocks in the eastern Loppa High and Finnmark Platform. Therefore, the turbidite systems in the east of Hammerfest Basin might tend to be more sand prone while in the west may tend to be more mixed.

The reason for the high uranium content that is observed in the conglomerates in well 7122/2-1 might also be related with the different source area of this turbidite fan compared with the systems in the west. As it was mentioned in the lithological analysis, claystone fragments are observed in these conglomerates. These clastones could be the reason for the high Uranium content observed in the GR-Spectral if the claystones were very rich in organic matter. It is known that the formation stratigraphically bellow Knurr is a well-known hot shale in the area, Hekkingen Formation. Therefore, the presence of these high Uranium content conglomerates might indicate that Hekkingen Formation was being eroded during the

Early Cretaceous in the eastern areas of Loppa High, resulting in sediments that were transported into the Hammerfest Basin by turbidity currents (and leading to the formation of the reservoir drilled by well 7122/2-1).

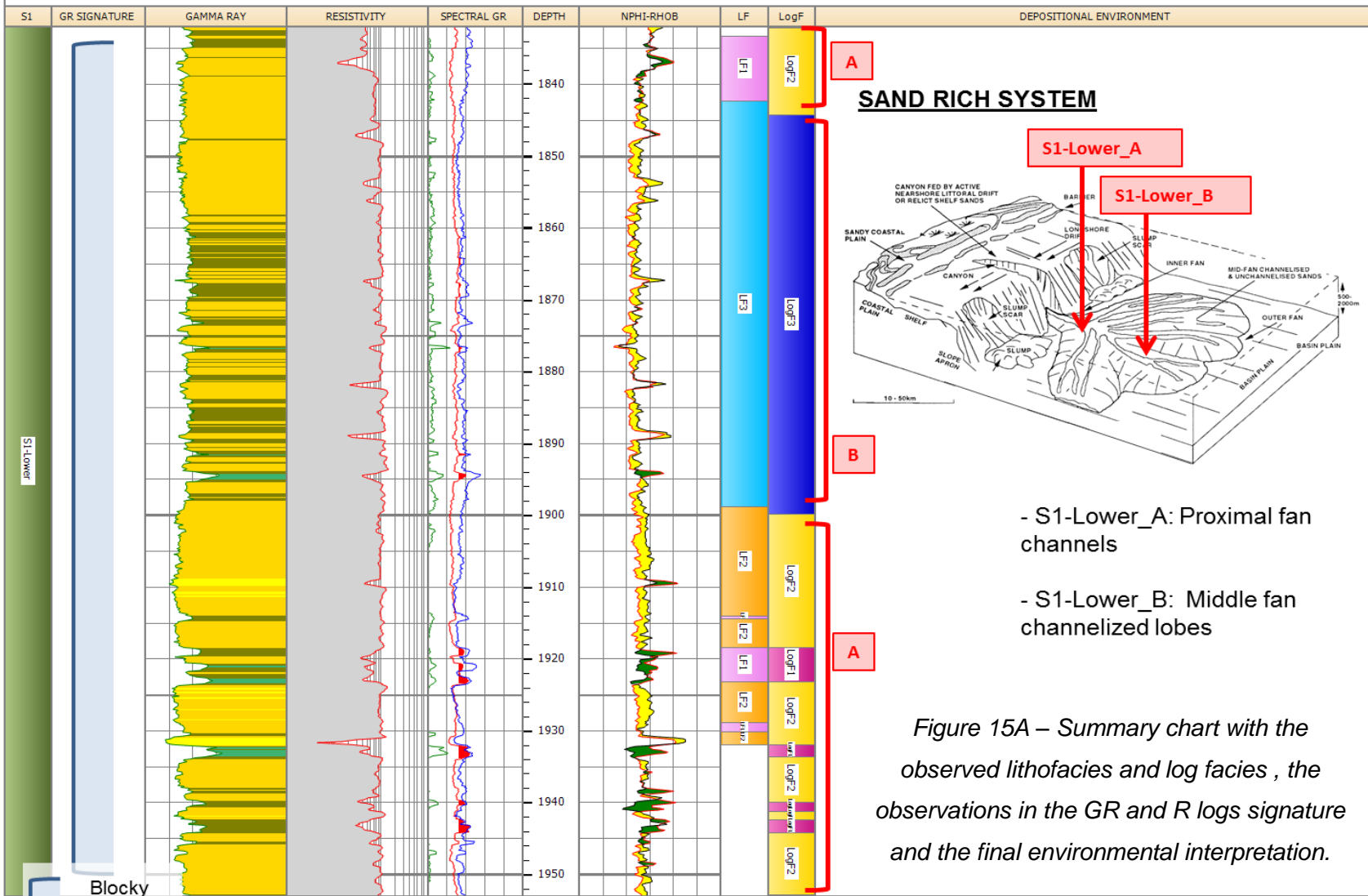
Scale : 1 : 500

DB : IP-Data (3)

7122/2-1

DEPTH (1832.05M - 1953.05M)

06/03/2015 18:25



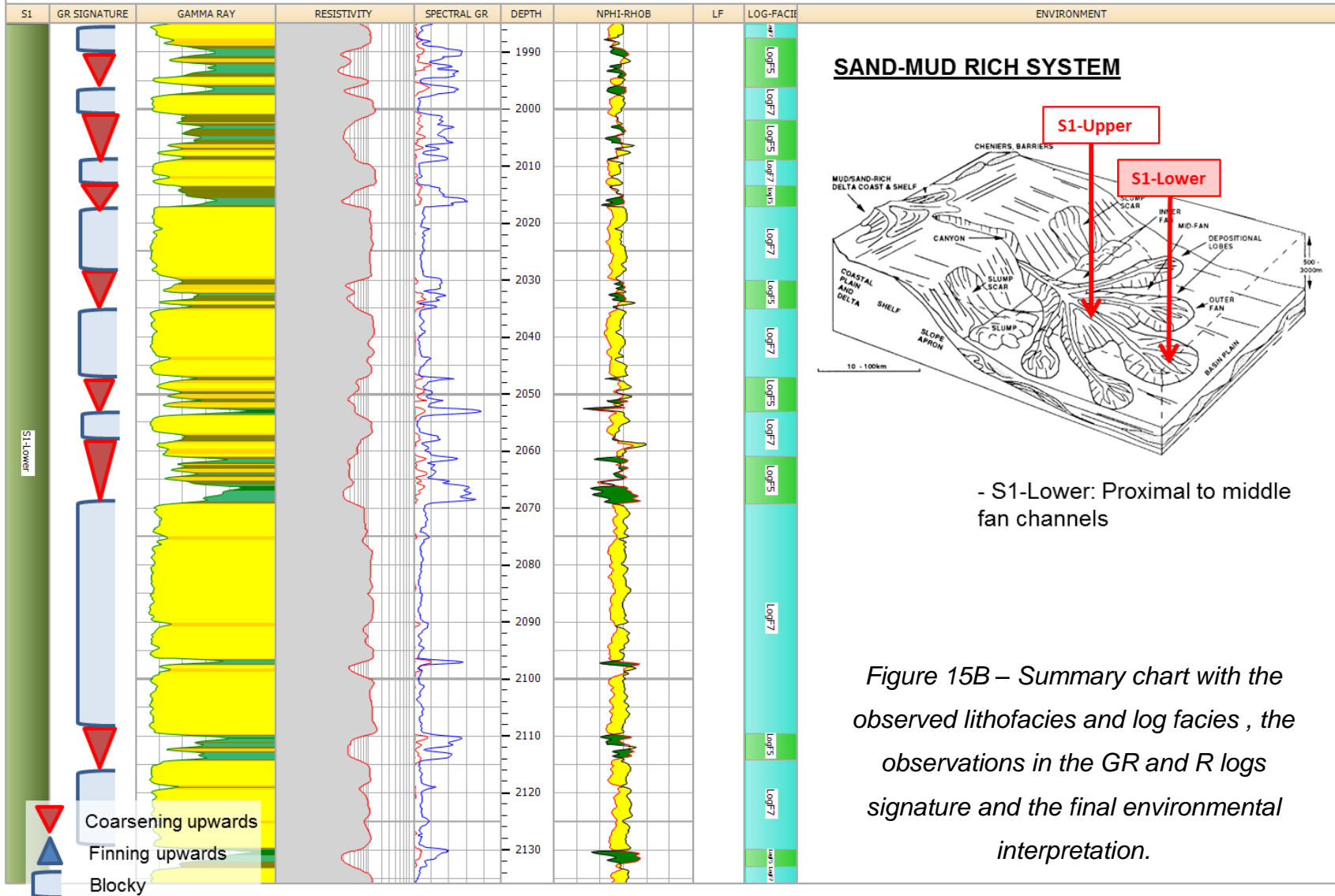
Scale : 1 : 600

DB : IP-Data (2)

7120/1-2

DEPTH (1985.06M - 2135.93M)

06/03/2015 19:06



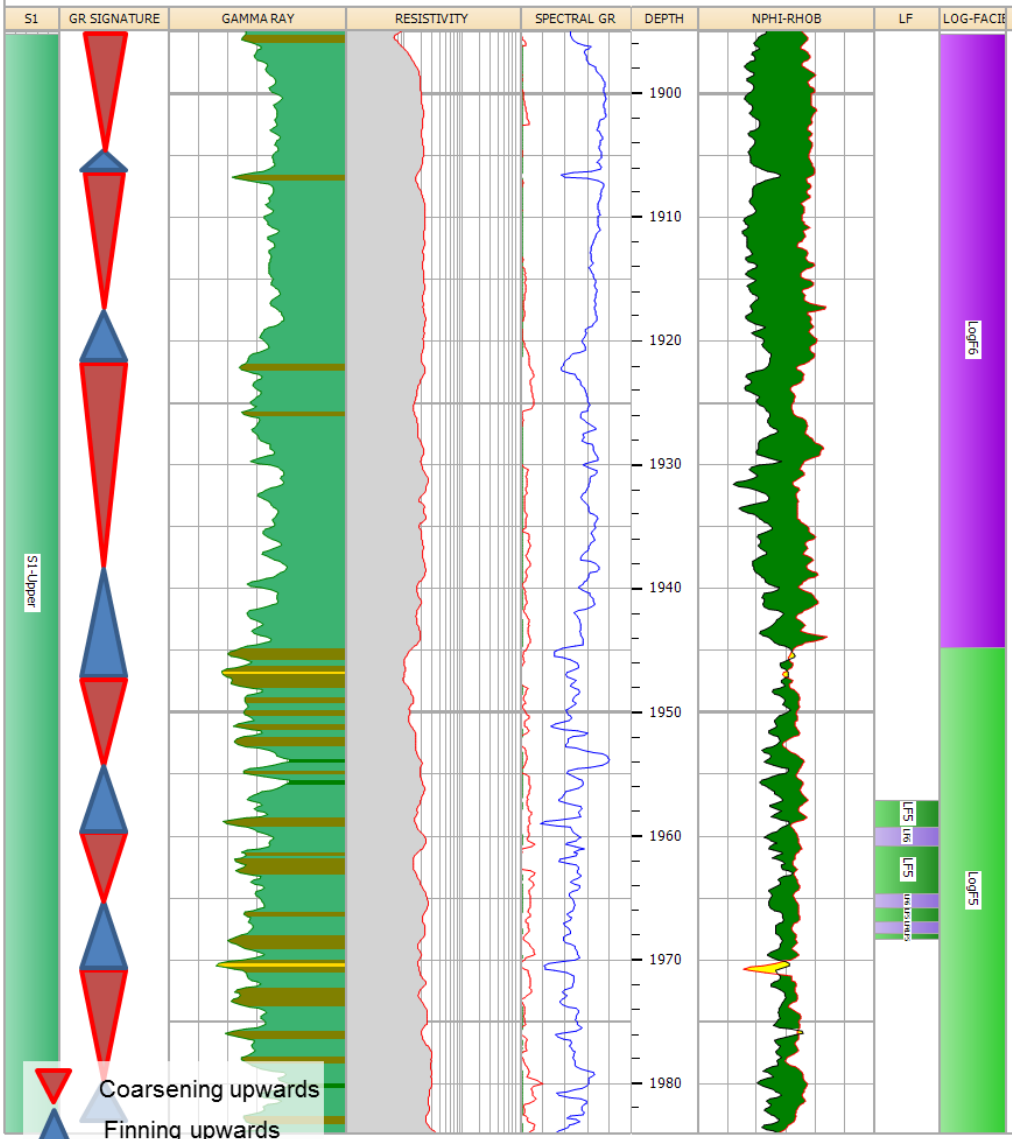
Scale : 1 : 350

DB : IP-Data (2)

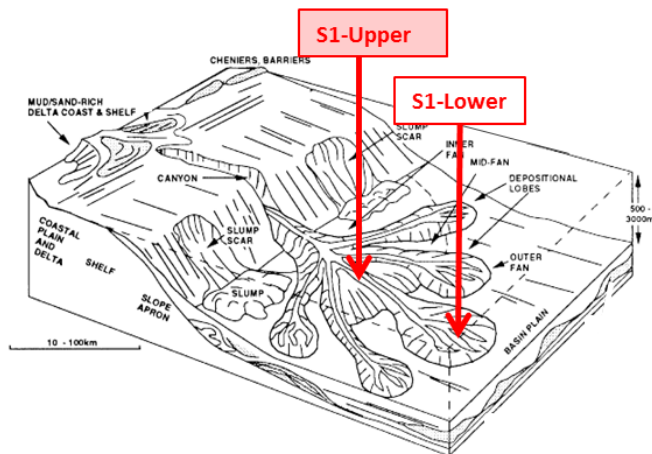
7120/1-2

DEPTH (1894.99M - 1983.99M)

06/03/2015 19:02



SAND-MUD RICH SYSTEM



- S1-Upper: Middle fan lobes (distal areas)

Figure 15C – Summary chart with the observed lithofacies and log facies , the observations in the GR and R logs signature and the final environmental interpretation.

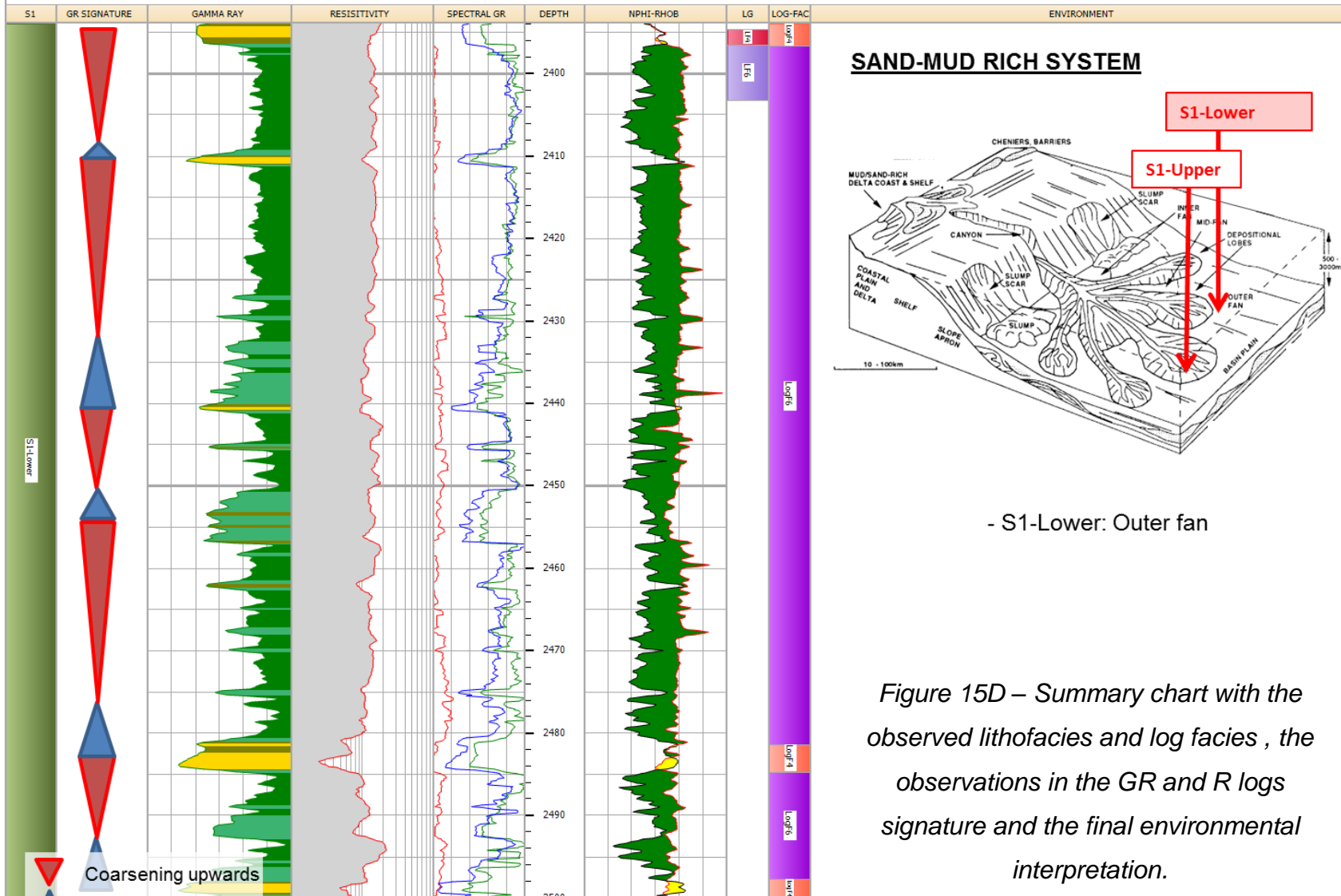
Scale : 1 : 400

DB : IP-Data (4)

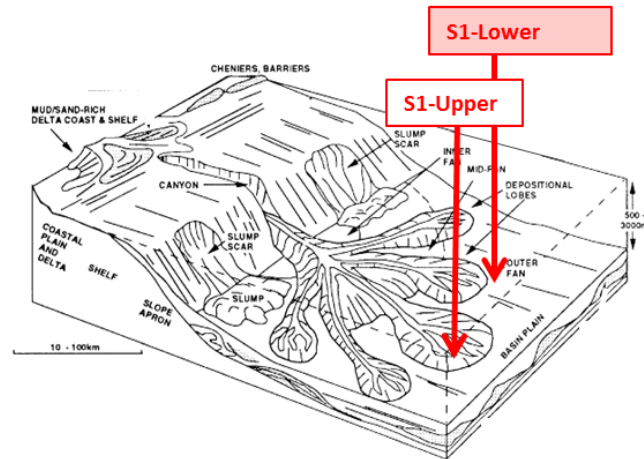
7120/2-2

DEPTH (2393.95M - 2500.02M)

06/03/2015 19:29



SAND-MUD RICH SYSTEM



- S1-Lower: Outer fan

Figure 15D – Summary chart with the observed lithofacies and log facies , the observations in the GR and R logs signature and the final environmental interpretation.

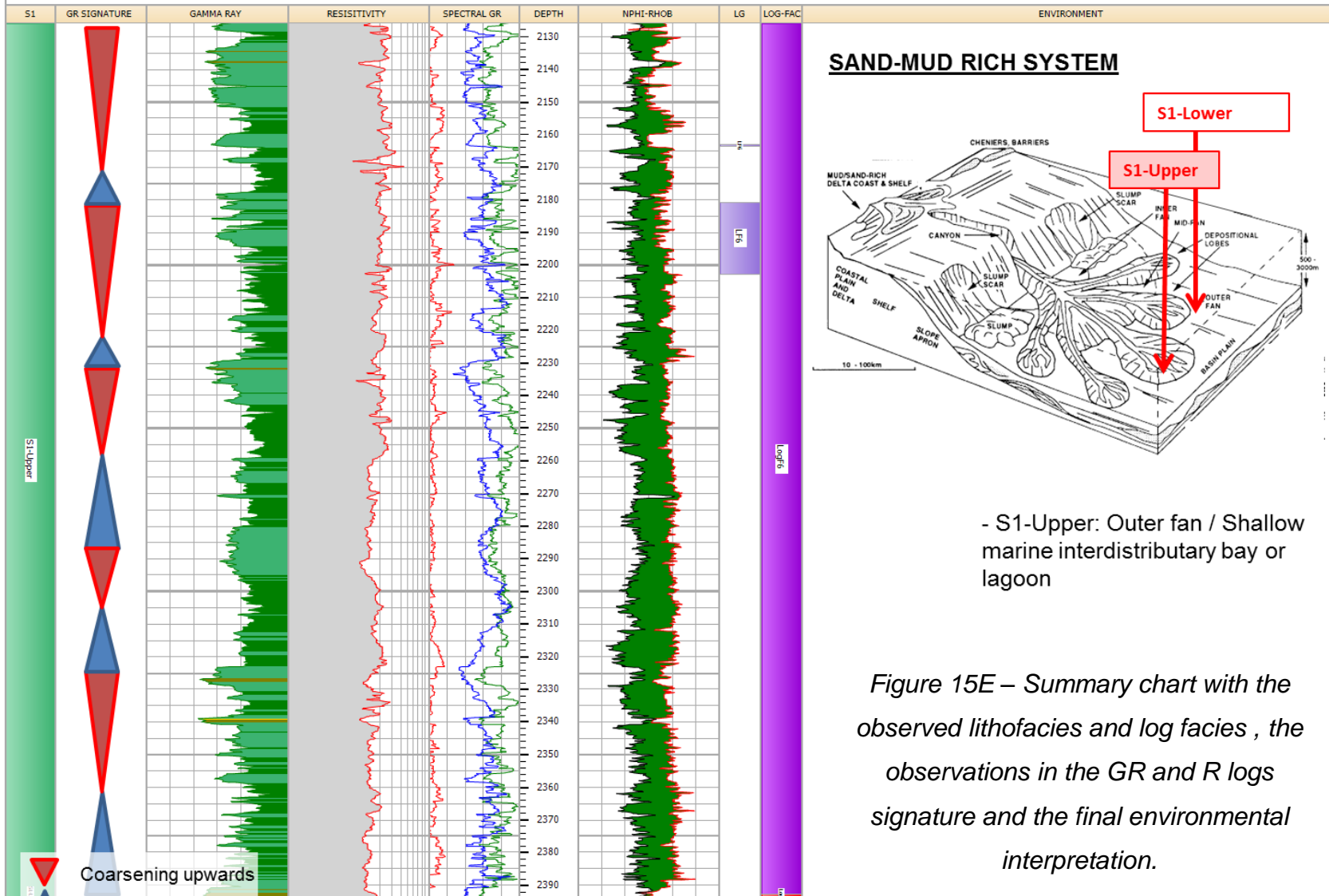
Scale : 1 : 1000

DB : IP-Data (4)

7120/2-2

DEPTH (2126.03M - 2393.95M)

06/03/2015 18:38



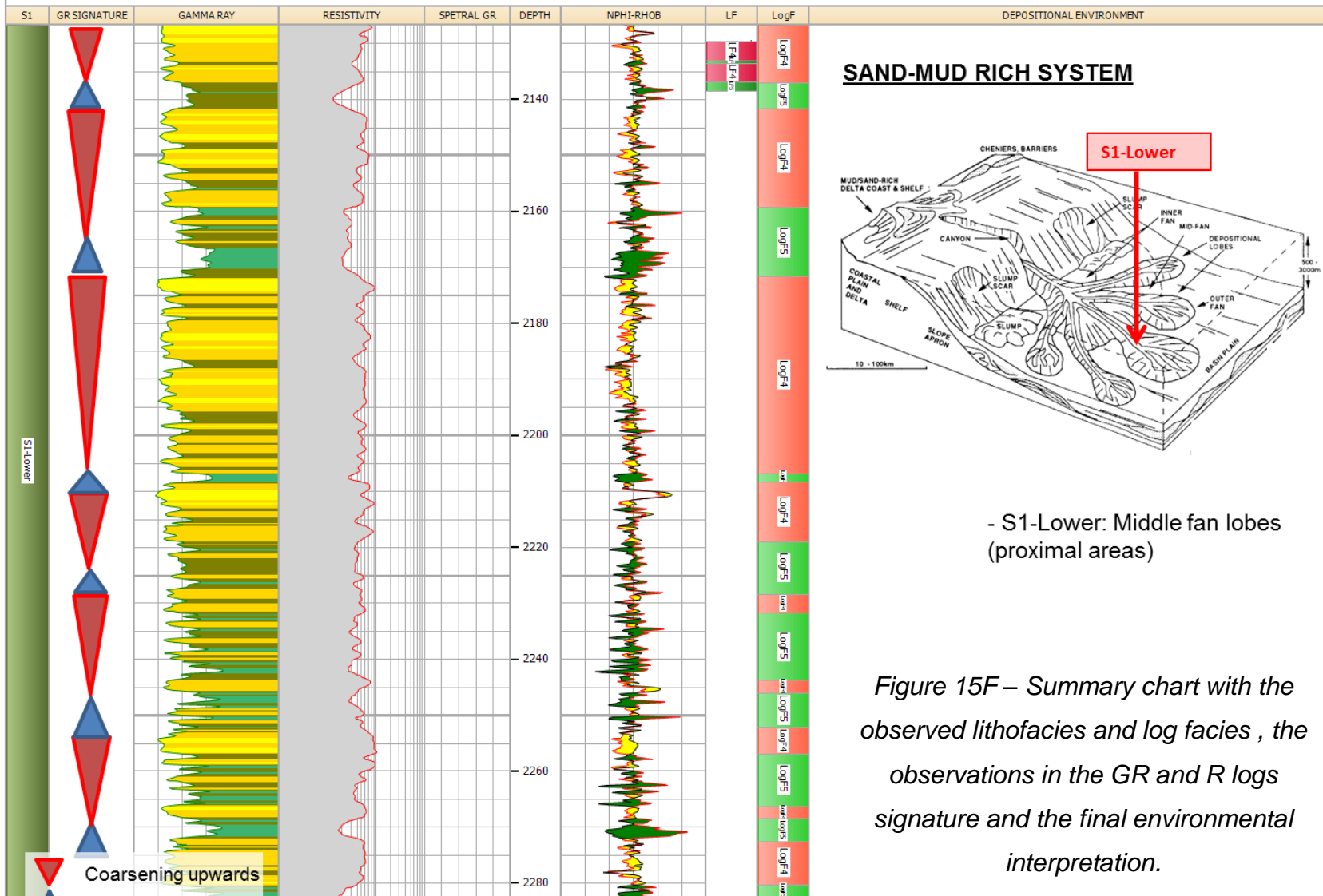
Scale : 1 : 600

DB : IP-Data (1)

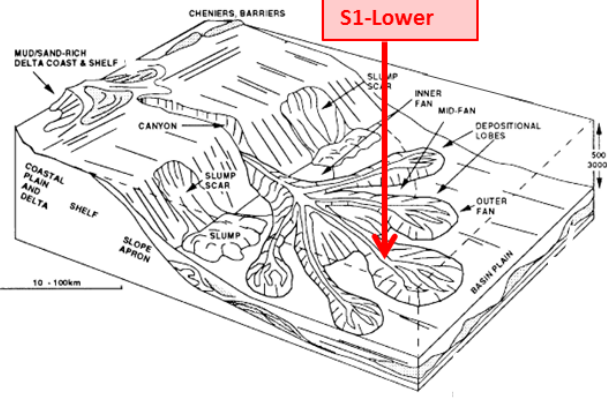
7120/10-2

DEPTH (2126.79M - 2282.7M)

06/03/2015 19:24



SAND-MUD RICH SYSTEM



- S1-Lower: Middle fan lobes (proximal areas)

Figure 15F – Summary chart with the observed lithofacies and log facies , the observations in the GR and R logs signature and the final environmental interpretation.

9. PETROPHYSICAL EVALUATION

9.1. DEFINITION OF THE COMPUTING PARAMETERS

A summary with all the computing parameters used for the calculations of the reservoir properties is included in Appendix 1.

9.1.1. Volume of clay parameters

In this project, it was observed from the lithological analysis that a claystone interval within Knurr Formation is only present in well 7122/2-1 S1-Upper, being siltstone the closest lithology for the other three wells. The V_{cl} parameters from this claystone interval in well 7122/2-1 are taken as a reference for the calculation of V_{cl} in the other wells. However, since clay volumes from thin sections are also available, the exact values of the V_{cl} parameters are finally selected by calibration with the clay volumes obtained from point counting in thin sections.

For wells 7122/2-1, 7120/1-2, 7120/10-2 well and for 7120/2-2 S1-Lower, the match of V_{cl} with the volumes from thin sections was reached using very similar computing parameters as for the reference claystone interval. However, for the upper zone of well 7120/2-2, V_{cl} computing parameters had to be modified from those of the reference interval in order to reach a good fit between V_{cl} and core data and between V_{cl-GR} and V_{cl-N} .

9.1.2. Porosity parameters

- Wet clay density and neutron values

The wet clay density and neutron values are the same as the values of the clay point estimated in the calculation of V_{cl} from the neutron-density crossplot.

- Clay Porosity

The porosity of the clay or the density of the dry clay are ideally taken from X-ray diffraction (XRD) and scanning electron microscope (SEM) but since XRD and SEM studies are not included in this project, one of these values has to be assumed. For this project, a value of around 20% for the clay porosity is assumed based on

bibliographic information (Rider and Kennedy, 2011). This is the typical porosity value for clay after compaction; however, it should be handled with caution because it can vary depending on the degree of compaction.

- Mineral inputs for the mineral models and true mineral densities

The simplification of the petrographic results in order to select the mineral inputs to use in the models is a very important step in the calculation of the variable matrix density and thus, the final porosity. Since only three minerals can be selected, the computed matrix density will most probably not be exactly the same as the real rock matrix density. With this in mind, the main objective to reach when choosing the mineral inputs is to honor the rock matrix density as better as possible. This is done by choosing the most representative minerals. Since the density of the mineral is what is important for the calculations, minerals with similar densities might be also grouped (e.g. quartz and feldspar)

Based on the results from the petrographic analysis, it is decided to choose the same mineral inputs for the four reservoirs. Three mineral groups are chosen based on the similarity of their densities (table 9). Even though the volume of heavy minerals measured in thin section is comparatively lower than of the quartz, feldspar and clay, they need to be included as in the mineral models due to their high densities, which might affect considerably the matrix density.

Quartz (quartz + feldspar)	Average density= 2,65 g/cc
Heavy minerals (the heavy mineral assemblage)	High densities (uncertain)
Wet Clay [Values taken from the results of the clay point in Vcl analysis]	Average density= 2,62 g/cc (for wells 7122/2-1, 7120/1-2, 7120/10-2 and 7120/2-2 S1-Lower) Average density= 2,60 g/cc (for well 7120/2-2 S1-Upper)

Table 9 – True mineral densities for the calculation of RHOMA

The precise density of the heavy minerals group is uncertain because a quantitative study of heavy minerals was not available yet in the research by (Matthews et al.,

2015). Since the volumes of each mineral are unknown, the density of the heavy mineral assemblage cannot be precisely calculated. In spite of this, an approximation can be calculated based on the experiment of Pyles et al. (2013). This experiment documents that mineral fractionation in a turbidite system depends on several factors, being one of them the minerals shape (see chapter 2). Angular minerals tend to deposit towards distal depositional environments while rounded minerals tend to do it closer to the distributary channel, in proximal environments. This assumption is supported by the results from thin sections which show a higher amount of muscovite and biotite in the distal parts of the fan (*figure 13E*).

The calculation of the approximate density of the heavy mineral assemblage is explained in four steps. First, the total of heavy minerals in *table 6* is divided in two groups according to their shape, in order to distinguish between those heavy minerals that might be deposited towards distal environments of deposition from those deposited closer to proximal environments. The first group is formed by biotite and muscovite which are considered to have angular shapes due to their mineral cleavage. The second one is formed by the rest of heavy minerals, considered as rounded minerals. Second, the average density is calculated for each group. Third, taking into account the volumetric results from the shape experiment (Pyles et al., 2013)(*figure 8*), the average volumes for both mineral groups in proximal and distal environments are assumed to be the followings (*table 10*):

	Volume of Muscovite + Biotite (Group 1 - angular minerals)	Volume of rest of HM (Group 2 - rounded minerals)
PROXIMAL	60%	40%
DISTAL	80%	20%

Table 10 – Volumes of the two heavy minerals groups for distal and proximal areas (Pyles et al., 2013).

Finally, considering the average density and average volume of each group, a final density for the heavy mineral assemblage is calculated for proximal and distal environments. These densities are then taken as values of reference when calculating the mineral volumes, taking into account the environment of deposition that was interpreted for each well zone in section 3.2. A summary with the reference

values for the heavy mineral assemblage for each well and environment is given in *table 11*.

- Mineral models end members

The proposed mineral model, based on the results from the petrographic analysis and on data from well 2-1, was tested in the cored intervals of wells 1-2 and 2-2 with successful results. Only small changes in the end members were needed in order to reach a good fit between the computed curves, (Vmi, RHOMA, PHIE, PHIT) and core data. These slight variations between the models could be related to the small differences in the heavy mineral assemblage between proximal and distal environments and between wells (*table 11*). In well 7120/10-2, due to the absence of sonic log, the mineral model could not be tested and neither the minerals volumes calculated. Nevertheless, the model might probably work fine for this well also since the petrographic analysis shows for this reservoir a very similar mineralogy to the other three. The heavy mineral assemblage (which is unknown at the moment for this well) or the type of clay of this reservoir would have to be very different in order to modify the proposed mineral model.

PROXIMAL ENVIRONMENTS Assumption: Volume HM – Group 1: 60% // Volume HM- Group 2 : 40%					
WELL	HM Assemblage (Group 1)	Average Density (g/cc)	HM Assemblage (Group 2)	Average Density (g/cc)	Total Average Density (g/cc)
2-1	mosc	2,82	trm, rt, apa, pyr, zr	4,026	3,30
1-2	mosc, biot	2,905	apa,chl,sp,zr	3,575	3,17
2-2	mosc, biot	2,905	gar, chl, sp, zr	3,8525	3,28
DISTAL ENVIRONMENTS Assumption: Volume HM – Group 1: 80% // Volume HM- Group 2 : 20%					
WELL	HM Assemblage (Group 1)	Average Density (g/cc)	HM Assemblage (Group 2)	Average Density (g/cc)	Total Average Density (g/cc)
2-1	Mosc	2,82	trm, rt, apa, pyr, zr	4,026	3,06
1-2	mosc, biot	2,905	apa,chl,sp,zr	3,575	3,04
2-2	mosc, biot	2,905	gar, chl, sp, zr	3,8525	3,09

Table 11 – Tables with the reference values for the heavy minerals assemblage densities to use in the calculation of RHOMA. Slight variations in density occurs between wells and environment of deposition

9.1.3. Water saturation parameters

A clean water bearing sand interval was identified in all the analyzed well sections and therefore, water resistivity could be calculated using both the Picket Plot and Apparent Water Resistivity ($R_{wApp} = R_t/F$), from the Interactive Plot in IP. From the Picket Plot “m” and “a” values could be estimated as well for the clean sands. Although this way of estimating the cementation and tortuosity factors is not very precise, the resulting values are very similar from the reference values given in general literature (table 12), given this support to the numbers obtained from the Picket Plot. Finally, since no SCAL measurements are available, the saturation exponent is assumed to be equal to 2, which is the most common value according to experience (Rider and Kennedy, 2011). It is important to mention that these bibliography values are all applicable to sandstones, not shales. Furthermore, the 100% saturation line in the Picket Plot was adjusted to water bearing sands. Thus, there is no control of the cementation factor, the tortuosity factor and the saturation exponent for the shale intervals.

Rock type	“a”	“n”	“m”
Ideal clean sandstone	1	2	2
Typical unconsolidated sandstone	0,62	2	2,15
Typical consolidated sandstone	0,81	2	2
Practical experience	1	2	1,75-4

Table 12 – Cementation factor, saturation exponent and tortuosity factor values for some common sandstones and practical experience (values taken from Rider and Kennedy (2011))

9.2. RESULTS

The CPI for each well zone showing the results from the petrophysical evaluation are shown in *Appendix 2* together with the core data used for calibration.

9.2.1. Volume of clay

The resultant Vcl logs for wells 7122/2-1, 7120/10-2, and 7120/2-2 show a good fit with the mineral volumes calculated from point counting in thin sections.

In well 7120/1-2, when the Vcl computing parameters from the reference claystone interval in well 7122/2-1 are used, a mismatching between the resulting Vcl log and the volume of clay obtained from thin sections is observed (figure 16A). Nevertheless, if this Vcl curve is used as input for the computation of RHOMA and PHIE/PHIT, a good fit is reached between these computed logs and core data. Therefore, it is believed that the mismatching observed for well 7120/1-2 is not related to the Vcl computing parameters assumed for this well. The problem might be related to the minimum bed resolution of the logging tools, which is “the thinnest bed for which a logging tool is able to make a true measurement” (Rider and Kennedy, 2011). This means that if a bed is thinner than a tool’s minimum resolution, the log response for this bed will be only a percentage of its true value. The rocks observed in cores of well 7120/1-2 consist of intercalation of sands and shales forming centimetric beds which are in most cases thinner than the minimum resolution of the logs used to calculate Vcl (GR, NPHI, RHOB and DT). On the contrary, thin sections are very punctual measurements that provide, in general, very precise results that will not fit with the partial log-measurements of the Vcl.

9.2.2. Porosity

The calculated porosity logs show acceptable results when compared with lab measurements. Core-porosity values lie in between PHIE and PHIT. It is not clear if core porosity values should theoretically match with PHIE or with PHIT, but in practice they generally lie within the middle of these two curves (Lehne, 2015), which is what is observed from results. In order to reach these results, the clay porosity was reduced to 15% from the reference value in Rider and Kennedy (2011) because 20% resulted in too high total porosity when compared with core porosities. Regarding the porosity results from the point counting analysis in thin sections; only

well 7120/2-2 shows a noticeable mismatching in one of the measurements (figure 16B). When the rocks are very fine grained, as it is the case for several intervals in this well, the point counting technic becomes very challenging for the identification of porosity, especially when thin section are not impregnated with blue epoxy. Because of this, this punctual measurement is considered to be wrong. For the rest of the wells the porosity results from thin section analysis are very close to PHIE, giving consistency to the log calculations.

RHOMA also shows a good fit with grain density values for all the wells.

The Vmi obtained from the mineral models present an acceptable fit in wells 7122/2-1 and 7120/2-2 when compared with the results form point counting. However, for well 7120/1-2, if the core porosity and grain density data want to be honored when calculating PHIE and RHOMA, it is not possible to get a good match between Vmi and the thin sections measurements (figure 16A). The reason of the mismatching was already explained in previous section. It is not a problem with the mineral model but with the minimum resolution of the logs and the very precise measurements of thin sections, which makes improbable the matching of Vcl and Vmi with the resulting volumes from the point counting analysis for this lithofacies (LF5). The reason why RHOMA and PHIE/PHIT show a good fit with core data and Vcl exhibits a mismatching at the same time, is a matter of the different resolution of each type of measurement. The resolution of lab-porosity and grain density measurements is lower than of thin sections. Therefore, lab measurements are more approximated to the partial log readings than thin section measurements.

In well 7120/10-2, due to the absence of sonic log, the mineral model could not be built and neither mineral volumes calculated. Nevertheless, the grain density values, which are all very close to 2,68 g/cc as well as the analysis of the core, suggest clean and homogeneous sandstones for this cored interval, composed mostly by quartz and few clay. Therefore, a constant matrix density of 2,68 g/cc is assumed for the calculation of porosity. This assumption results in a good fit for the part of the core that corresponds

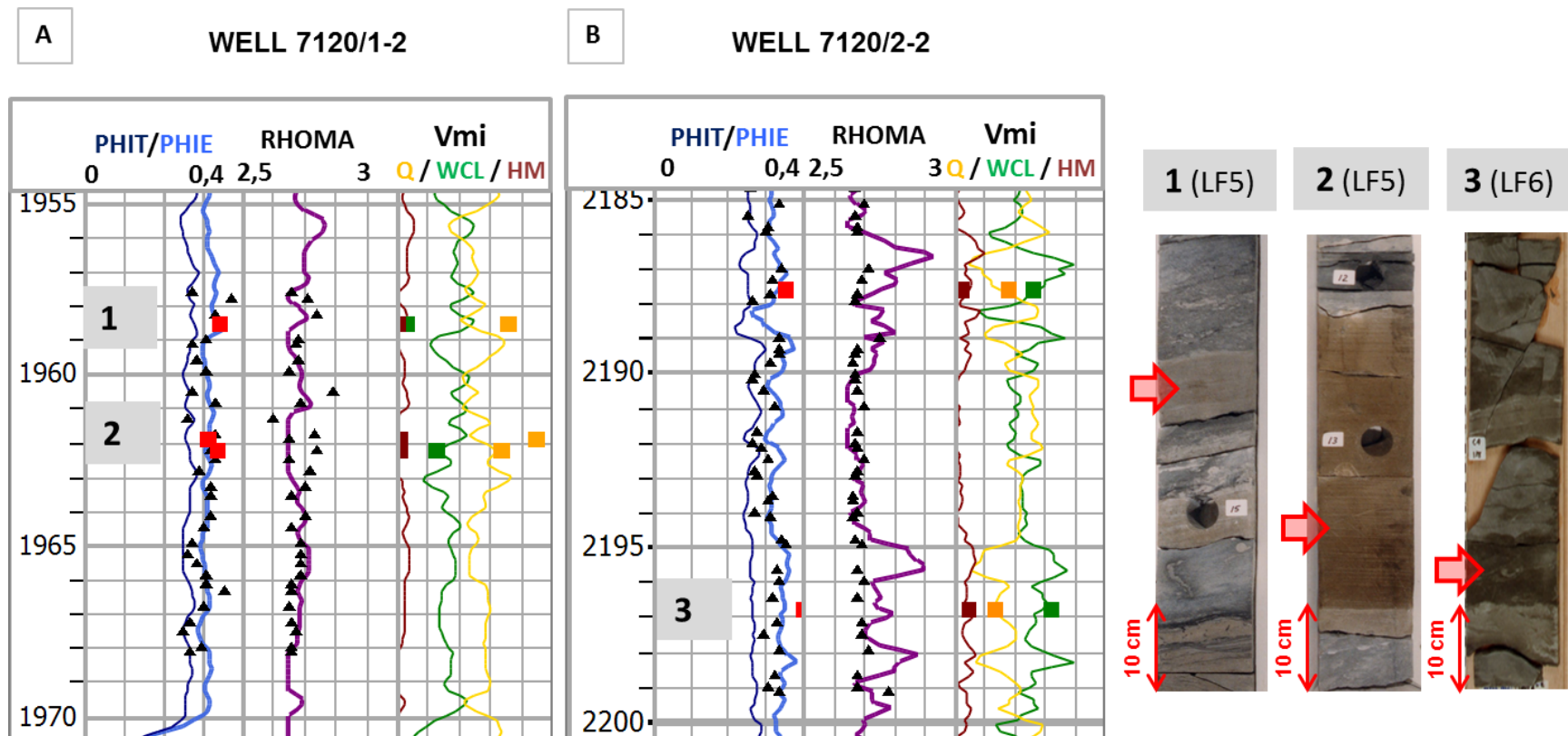


Figure 16– Mismatching between computed curves and lab-measurements from point counting. A) (1,2) Mismatching affecting the computed mineral volume curves, due to the minimum bed resolution of the logs that cannot resolve the thin layering of the rock (LF5) in well 7120/1-2..
 B) (3) Mismatching affecting the computed porosity due to the very fine grain size of the rock (LF6) in well 7120/2-2.

with LF4. However, in the last part of the core which corresponds with LF5, the log-porosity shows lower values than expected from core data. This is probably due to the more complexity of LF5 compared to LF4 which cannot be represented with a constant matrix density.

9.2.3. Mineral model

In general, the results of the mineral model shows for all the wells higher volumes of clay and heavy minerals in the reservoir zones corresponding with distal environments, while proximal environments show quite clean sands with few heavy minerals. The only exception is well 7122/2-1, that shows clay and heavy minerals in the intervals corresponding with the conglomerates. In the lower zone of well 7120/2-1, the mineral model was tested but due to the absence of core data, the model could not be calibrated. The resulting volumes from the application of the model to this reservoir are in accordance with the results obtained in the wells where the model was calibrated. An increase in the heavy mineral volume together with an increase in clay is observed as well as clean sandstones with few heavy minerals. This is an example of how mineral volumes can be calculated without core data for calibration by assuming a mineral model from an analogue reservoir.

9.2.4. Water saturation

The results from the computation of the water saturation confirms that these wells are mostly water bearing. Only for wells 7120/1-2 and 7120/2-2 some oil is observed filling these sandstones.

In well 7120/1-2, water saturation varies from 57% to 38% in the interval 1945 to 1953 meters. This interval coincides with the production test done in this well which proved movable oil (*table 3*). Although for the rest of the well an average saturation of 65% is calculated, it is unclear what this saturation represents. When looking at S1-Upper, one could think that it represents oil shows, but the fact that S1-Lower shows the same average saturation value only within the shaly intervals, suggests better a possible problem with Indonesia Equation. There is not control on “a”, “m” and “n” factors for the shaly intervals and this might result in the instability on the equation for V_{cl} values higher than 0,3.

In well 7120/2-2 an average value of 52% water saturation is calculated in a one and a half meter sandstone at 2483 meters depth. Some residual saturations are observed as well that can be related with oil shows. The problematic observed in well 7120/1-2 with Indonesia Equation does not occur in this well. The reason for this is unclear. A deeper study of the computing parameters for the calculation of water saturation would be necessary for its clarification.

9.2.5. Permeability

The crossplot between core porosity and core permeability shows quite scattered data. However, a general trend can be established upon core data of the four study wells with a quite good R2 coefficient (*figure 17A*). R2 is an important measure in permeability calculation which estimates how well the regression line represents the data and how certain one can be in making predictions from it.

Apart from this general trend, the classification of the data upon lithofacies shows that each lithofacies seems to follow a specific permeability-porosity trend (*figure 17B*), which means that there is an important textural control on the trends (since lithofacies are defined according to textural parameters). *Table 13* shows the equations of the regression lines that have been used to compute the permeability log, based on the different lithofacies. It is observed that all the equations except the correspondent to T3 have R2 coefficients higher than 0,45 which is good for these type of permeability analysis. T3 gives less confident results with an R2 of only 0,3.

The computation of permeability is done using the trends based on lithofacies and not the general trend because all these trends exhibit higher R2 (or very similar in the case of T1) than the general trend, except for T3. Therefore, the confidence in the results is higher if using these trends.

TREND NAME	LITHOFACIES	EQUATION	R ²
TGENERAL	(All the core data)	$PORC = 0,115721 * e^{0,179427 * \text{Log}(KLHC)}$	0,47
T1 (Orange)	LF1, LF2	$\text{Log}(KLHC) = 0,329553 + 12,8933 * PORC$	0,45
T2 (Blue)	LF3	$\text{Log}(KLHC) = -1,26137 + 19,9734 * PORC$	0,70
T3 (Red)	LF4	$\text{Log}(KLHC) = -3,76955 + 32,8211 * PORC$	0,32

T4 (Green)	LF5	$\text{Log(KLHC)} = -2,60206 + 23,7862 * \text{PORC}$	0,61
T5 (Pink)	LF4 (well 7120/2-2)	$\text{Log(KLHC)} = -3,912 + 22,4205 * \text{PORC}$	0,98
T6(Purple)	LF6	$\text{Log(KLHC)} = -2,44667 + 11,7573 * \text{PORC}$	0,64

Table 13 – Equations representing the porosity-permeability trends

Grain size, sorting and amount of depositional matrix are the main parameters defining texture. The way these parameters affects porosity-permeability trends is summarized in the following statements (Cade et al., 1994; Weibel et al., 2012):

- Grain size affects permeability but not porosity.
- An increase in grain size results in an increase in permeability.
- Sorting affects mostly porosity.
- An increase in sorting results in an increase in porosity.
- The amount of depositional matrix affects both permeability and porosity.
- An increase in depositional matrix results in a decrease in permeability and porosity.

Figure 18 summarizes these statements and explains the porosity-permeability trends observed in Knurr Formation based on the textural parameters observed in cores and thin sections. The effect of the average grain size in the trends is very well documented in this figure, with T1 showing the highest permeability for any equal porosity value followed by T2, T3, T4 and T5-T6, listed in descending order of permeability. T3 presents a very steep slope indicating that this facies has big variations in permeability for small porosity changes. This is explained by the nature of LF4 which is organized in finning-upwards units, with big changes in grain size from base to top (from coarse to fine). The deviation of T2 towards the right respect T1 and T3 is explained by the better sorting of LF3. The fact that the data representing LF5 is not localized in a defined area, like it happens with LF2, LF3 and LF4, can be explained by the heterogeneity of this lithofacies. LF5 presents differences in grain sizes due to its structure in finning-upwards units (as for LF4 but with a less pronounced grain size variation) and also an increase in clay content towards the top of these units. This results in big variations of porosity and permeability within a single facies. The data representing T5 and T6 present quite

low permeability due to the fine grain size of LF6, however porosity do not change much from the data in trends T3 and T4. A possible explanation for this might be the moldic porosity that was observed in the rocks of well 7120/2-2. This type secondary porosity would increase the overall porosity of the rock without increasing the permeability because the pores are not connected between each other.

The relation between carbonate cement and the trend lines is difficult to document because this cement occurs only in some specific intervals and therefore there is not enough data to really see its effect.

The computed permeability log show in general a good fit between Kh and core data in all the wells. Only in well 7120/10-2 the log-permeability gives comparably lower values than the permeability from lab measurements in the interval corresponding to LF5. This is probably an effect of the poor matching that also exists in this same interval for log-porosity and core data, giving the log-porosity also lower values than expected from core data.

9.2.6. Net to gross

Three reservoir properties are analyzed to decide the cutoff to calculate the net to gross (*figure 19*). For shallow wells like the ones in this study, it would be expected Vcl to be the property controlling the net sand. However, since this area has experienced uplift, it can notice that it is actually permeability and porosity the main controlling properties. Taking this into account, a cutoff of $KH > 0.05$ is selected, based on the common practice in the Norwegian Continental Shelf. This values is extrapolated to the effective porosity giving a final cutoff value of $PHIE > 0.09$.

The difference between depositional environments is very notable in the net to gross results. Zone S1-Lower, representing more proximal environments, shows remarkably higher net to gross values than S1-Upper, representing more distal areas. Well 7120/2-2 is an exception with low values for both zones. This is because both zones in this well represent distal environments. In well 7122/2-1, the environment changes within zone S1-Lower from a proximal to a distal environment, presenting in both cases high net to gross values. This is due to the sand-rich nature of the turbidite system drilled by this well. Sand-rich fans present generally high net to gross values across the whole system (Richards and Bowman, 1998).

9.2.7. Summary of results

Table 14A summarizes the average values of the calculated reservoir properties for each of the depositional environment identified in the studied wells and furthermore an estimation of the reservoir quality. Reservoir quality (RQ) can be qualitatively evaluated by multiplying net to gross (N/G) by effective porosity, so the higher the product the better the reservoir quality (Lehne, 2015). In order to get a more understandable number for the result of this product, the following scale from 0 to 100 has been built:

- $N/G * \Phi_E = 1 * 0,2 = 0,2 \rightarrow RQ=100$ (considering that the highest average porosity value for the reservoirs under study is 0,195).
- $N/G * \Phi_E = 0 \rightarrow RQ=0$

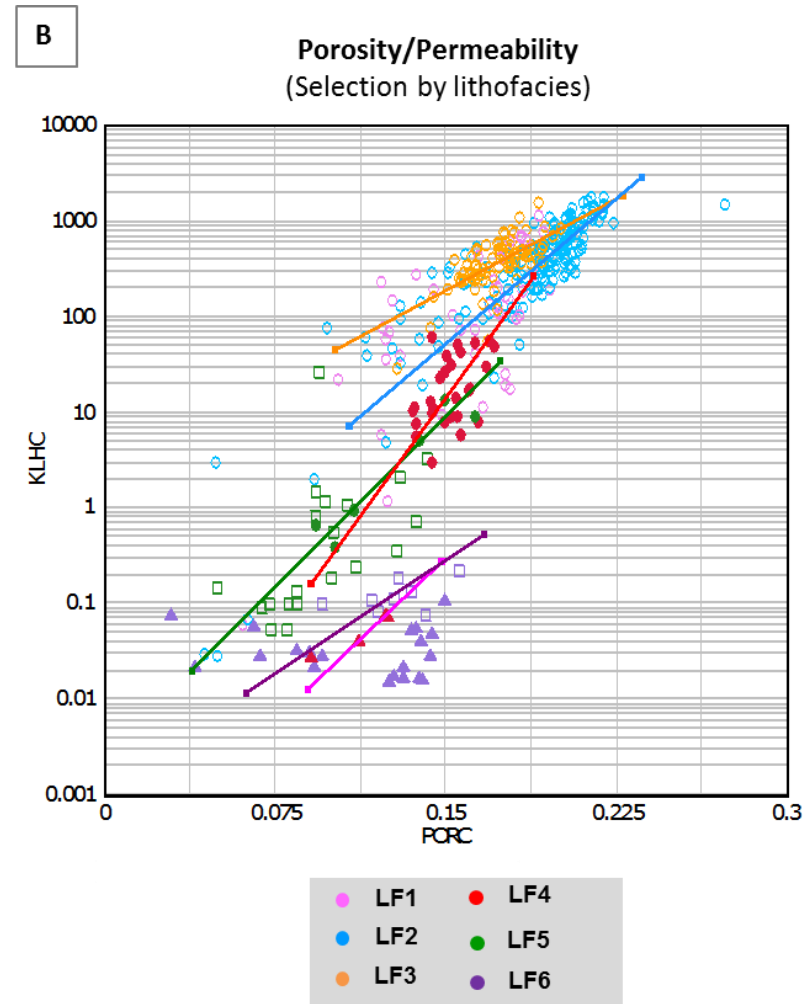
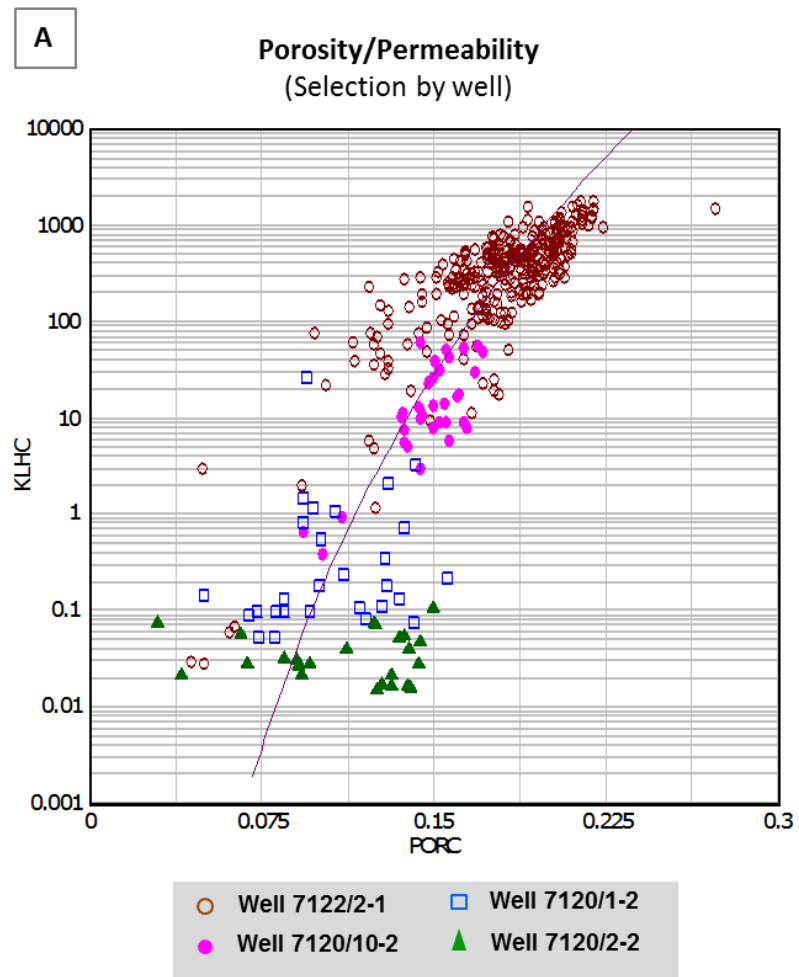


Figure 17– A) Porosity-permeability crossplots with data grouped by well, showing the general trend based on an exponential function. B) Porosity-permeability crossplots with data grouped by lithofacies, showing each lithofacies trend which are based on linear functions.

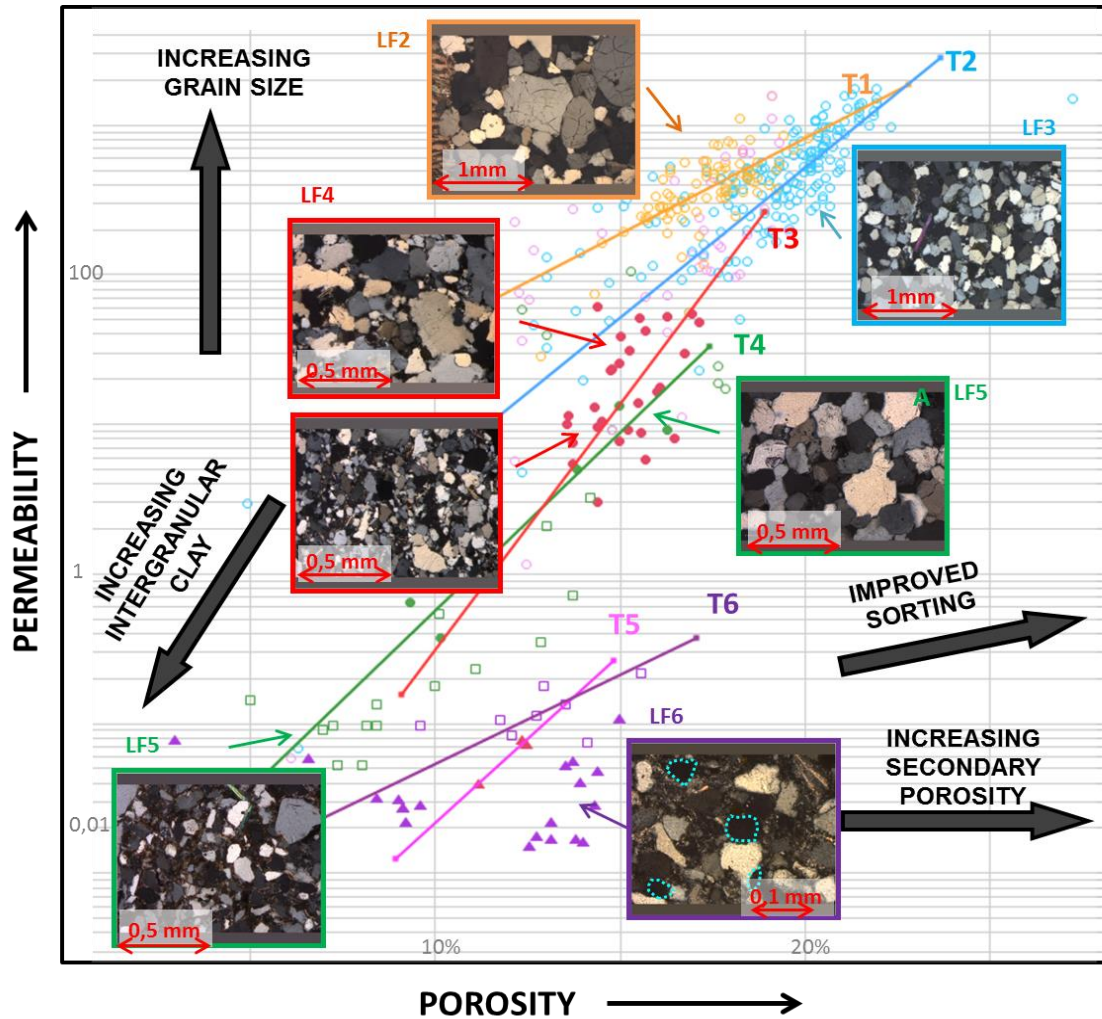


Figure 18– Explicative diagram of the effect that texture has on the porosity-permeability trends based on lithofacies. Examples of thin sections representing each lithofacies are included for further clarification. For those lithofacies that exhibit important textural variations, two photos are included.

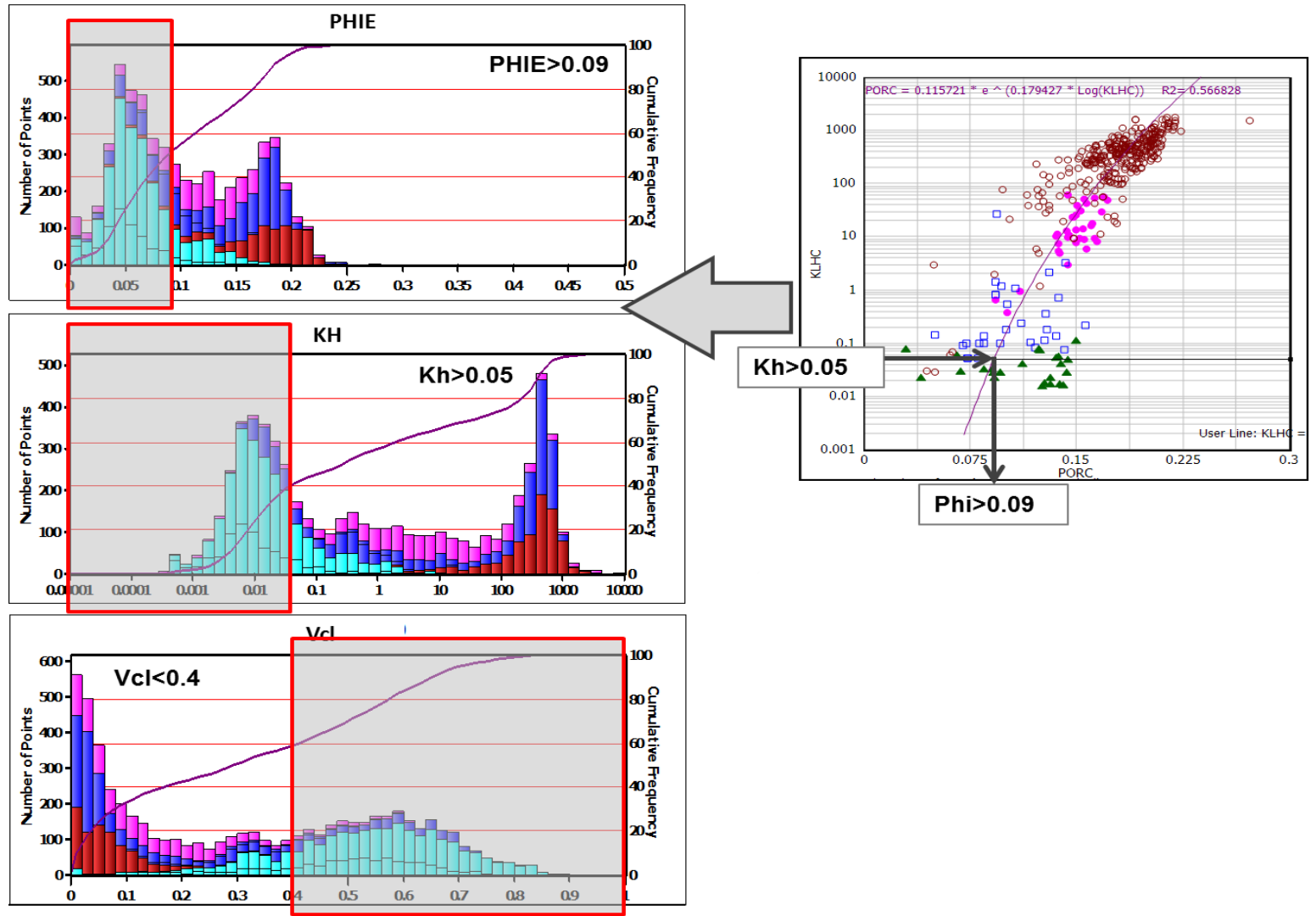


Figure 19– Analysis of Vcl, PHIE and KH histograms in order to find the best cutoff for the calculation of the net to gross.

A REAL VALUES – RESERVOIRS AT PRESENT DEPTHS

WELL	SECTION	TYPE OF SYSTEM	ENVIRONMENT	DEPTH (base reservoir)	NET SAND	NET/GROSS	AVERAGE PHIE	AVERAGE KH	PHI*N/G
7122/2-1	Lower	Sand rich	Proximal Fan	1953 m	48,79 m	0,965	0,171	459 mD	0,165 (83)
	Lower	Sand rich	Middle Fan	1900 m	56,09 m	0,984	0,195	618 mD	0,192 (96)
7120/1-2	Lower	Mixed	Proximal Fan	2137 m	141,46 m	0,982	0,162	336 mD	0,159 (79)
	Upper	Mixed	Distal Fan	1983 m	24,61 m	0,3	0,105	52 mD	0,032 (15)
7120/2-2	Lower	Mixed	Distal Fan	2503 m	6,88 m	0,065	0,11	0,8 mD	0,007 (3)
	Upper	Mixed	Distal Fan	2393 m	8 m	0,037	0,107	0,9 mD	0,004 (2)
7120/10-2	Lower	Mixed	Middle Fan	2260 m	130,78 m	0,84	0,15	190 mD	0,126 (63)

B HYPOTHETICAL VALUES – RESERVOIRS SHIFTED TO REFERENCE DEPTH (1900 m):

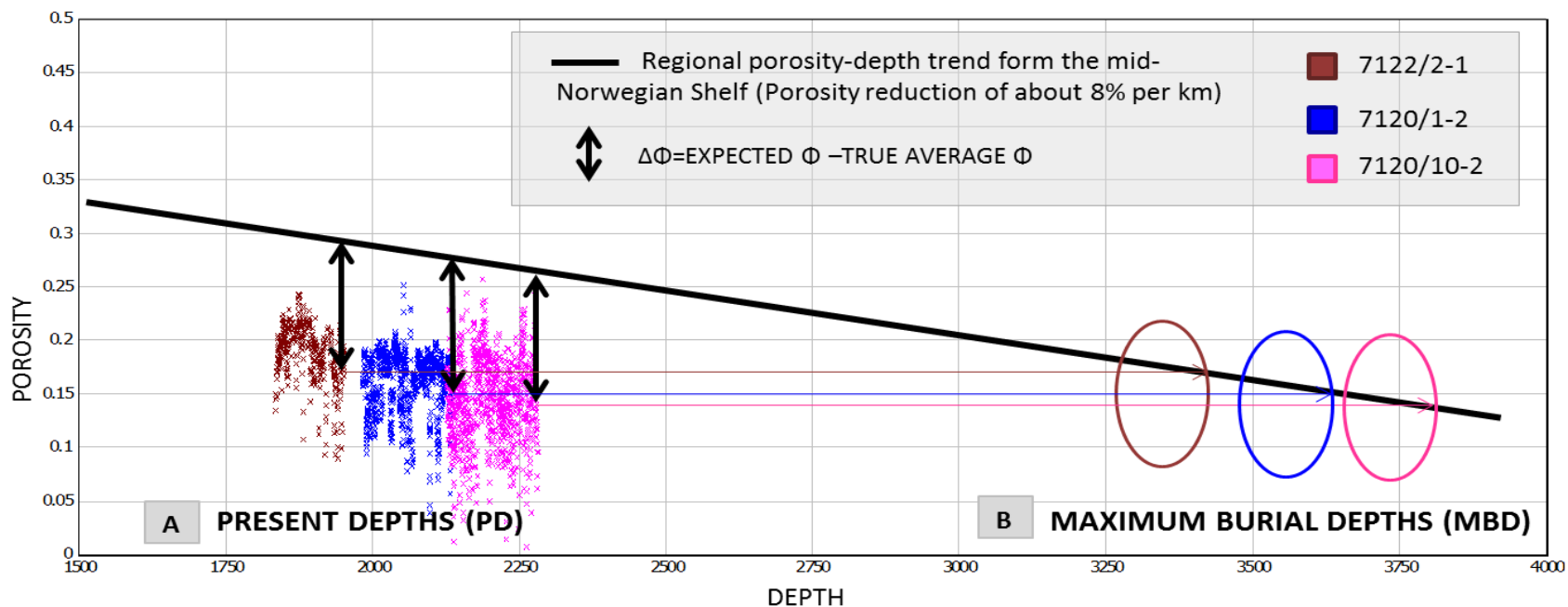
WELL	SECTION	TYPE OF SYSTEM	ENVIRONMENT	DEPTH (reference)	SHIFT	NET SAND	NET/GROSS	AVERAGE PHIE	AVERAGE KH	PHI*N/G
7122/2-1	Lower	Sand rich	Proximal Fan	1900	53	49,24 m	0,971	0,174	456 mD	0,169 (85)
	Lower	Sand rich	Middle Fan	1900	0	56,09 m	0,984	0,195	618 mD	0,192 (96)
7120/1-2	Lower	Mixed	Proximal Fan	1900	237	143,29 m	0,995	0,18	332 mD	0,176 (89)
	Upper	Mixed	Middle Fan	1900	83	38,02 m	0,47	0,106	34 mD	0,049 (24)
7120/2-2	Lower	Mixed	Distal Fan	1900	66	11,81 m	0,055	0,105	0,56 mD	0,006 (3)
	Upper	Mixed	Distal Fan	1900	-44	6,32 m	0,06	0,106	0,91 mD	0,006 (3)
7120/10-2	Lower	Mixed	Middle Fan	1900	360	144,34 m	0,927	0,172	172 mD	0,159 (80)

Table 14 – A) Computed reservoir properties average values. B) Reservoir properties average values after shifting the reservoirs to a reference depth of 1900 meters and applying a correcting in porosity based on the mid-Norwegian Shelf porosity-depth trend (8% decrease in porosity per kilometer). An estimation of the reservoir quality for both cases is given in the last column. In brackets and bold numbers is the reservoir quality product (PHIE*N/G) reconverted to a scale of 100%.

10. FINAL INTERPRETATIONS

10.1. ESTIMATION OF UPLIFT

Reservoir quality decreases with increasing burial depth due to diagenesis but it does not recover itself with uplift. Because of this, it is important to know when uplift has affected a reservoir in order to make predictions of its reservoir quality. Henriksen et al. (2011) documents the uplift affecting the Barents Sea during the Cenozoic. This article shows how porosity data from Barents Sea sandstones fit with the mid-Norwegian Shelf porosity-depth trend (based on sandstones from the Haltenbanken area) when these sandstones are corrected to their maximum burial depth prior to uplift. This trend indicates a porosity reduction of the 8% per kilometer. When the same regional trend is plotted with data from the clean sandstones (e.g. $V_{cl} < 0.4$) of the study wells, one can realize how uplift has affected Hammerfest Basin (*figure 20*) (well 7120/2-2 and the upper zone of well 7120/1-2 are not plotted because they do not have enough clean sandstones). The reservoirs present less porosity than it would be expected at their current depths. An estimation of the maximum burial depth of these reservoirs, prior to uplift, can be calculated considering the sandstones average porosity nowadays and their expected porosity according to the mid-Norwegian Shelf trend. The results from this estimation generally agree with the net erosion map made by Henriksen et al. (2011) for the Greater Barents Sea, which shows a net erosion of around 1500 meters for the flanks of Hammerfest Basin (*figure 21*). From the same article, the uplift of well 7120/2-2 can be estimated to be ~1000 meters. This value attracts the attention when is compared with the uplift value of 1500 meters calculated in this study for well 7120/1-2. With this results, it seems that, prior to uplift, well 7120/2-2 was shallower than well 7120/1-2 (maximum burial depth of 3300 meters compared to 3637 meters for both wells respectively), which is the opposite as what is seen today for these reservoirs. These results would support the previously mentioned interpretation by Sandvik (2014), indicating a shallow environment for the upper zone of well 7120/2-2.



WELL	ZONE	ENVIRONMENT	PD (Base of reservoir)	TRUE AVERAGE Φ	EXPECTED Φ	$\Delta\Phi$	UPLIFT (U)	MBD (Base of reservoir)
						$[\Delta\Phi = \text{EXPECTED } \Phi - \text{TRUE AVERAGE } \Phi]$	$[\text{UPLIFT} = \Delta\Phi / 8]$	$[\text{MBD} = \text{PD} + \text{U}]$
7122/2-1	Lower	Proximal Fan	1953 m	18,1%	30,0%	11,9%	1487,5 m	3440,5 m
7120/1-2	Lower	Proximal Fan	2137 m	16,2%	28,2%	12,0%	1500 m	3637 m
7120/10-2	Lower	Middle Fan	2282 m	15,1%	27,3%	12,2%	1525 m	3807 m

Figure 20 – A) Porosity VS. Depth for clean sandstones ($V_{cl} > 0,04$) of wells 7122/2-1, 7120/1-2 and 7120/10-2 with a trend line from the mid-Norwegian Shelf inserted for comparison. B) Estimated maximum burial depths (MBD) for the same three reservoirs prior to uplift. The steps follow for the calculations with the final estimated values are shown in the table under figure.

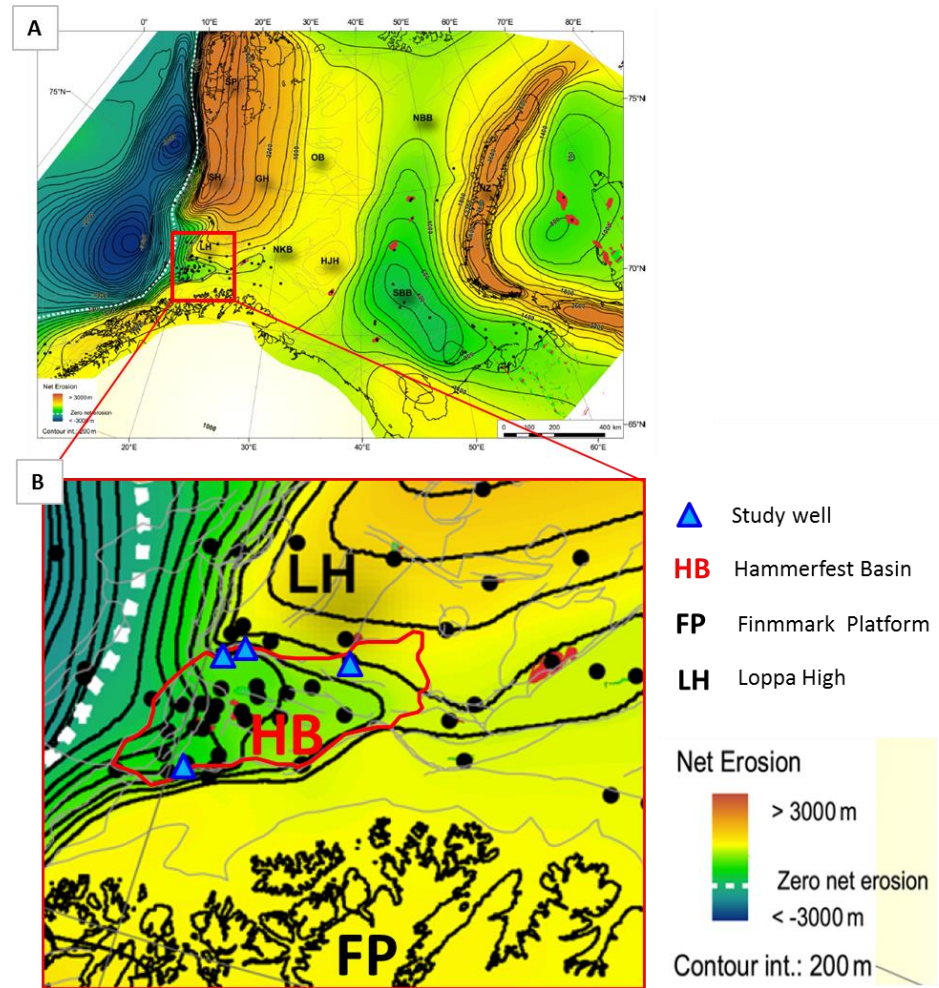


Figure 21– Net erosion regional map for the Greater Barents Sea (A) showing in detail the Hammerfest Basin and the wells under study (B). An uplift over 1500 meters can be estimated from this map for the study wells

10.2. RESERVOIR QUALITY

Taking into account the results from the petrophysical evaluations (table 13A) together with the results of the environmental analysis, it is clear that reservoir quality, apart from being dependent in burial depth, depends on the different depositional environments. In one hand it can be observed for the sand rich fan system that both proximal and middle areas show very good reservoir qualities. This agrees with the results from Richards and Bowman (1998), that indicates high and constant average sand-shale ratios across the whole turbidite fan for sand rich systems. However, in this particular turbidite system, reservoir quality even increases towards the middle fan which is most probably related to the presence of conglomerates in the very proximal part of this system deposited by debris flows. The porosity of these conglomerates is noticeable lower than of the proximal sandstones, decreasing in this way the total reservoir quality in the proximal depositional environment. In the other hand, the reservoir quality of the sand-mud rich systems is noticeably lower than of the sand rich system, and furthermore, it exhibits a remarkably decrease from proximal to middle areas.

However, these values of reservoir quality are affected by differences in burial depth between the reservoirs. Therefore, they do not show the real variations of reservoir quality with depositional environment within a single system. This problem is approach by calculating the hypothetical porosity and net to gross that each well's depositional environment would have if they all had been deposited at a same hypothetical depth. The reservoirs are shifted to this hypothetical depth and the new porosities and net to gross are calculated based on the mid-Norwegian Shelf porosity-depth trend (8% decrease in porosity per kilometer). The depth selected as a reference for the calculation is irrelevant since the main objective is to understand the variations of reservoir quality between different environments, eliminating the effect of depth, and not to know their actual reservoir quality values at this depth. What is important for this calculation is that the relative depths between the reservoirs are the same as before uplift. Thereby, the shift applied in the calculation will represent the difference in porosity and net to gross due to burial depth, so that it can be subtracted.

Wells, 2-1, 1-2 and 10-2 meet this requirement because they have all experienced very similar uplift (~1500 meters). Well 2-2, however, has experienced less uplift and therefore its depth has to be corrected to keep the same relative depth with the other wells as before uplift (*figure 22*). The final results of this correction are shown in *table 13B* for all the wells. With this approach the variation in the reservoir quality within a single turbidite fan and between sand-rich and sand-mud rich systems are analyzed (*figure 23A-B*).

The new results do not show big differences for the sand rich system, since the selected reference depth for the shifting was within this reservoir. The reservoir quality for this system is good from proximal to middle areas. Nevertheless, considering the results of the mud-sand rich systems, changes in the reservoir quality values can be observed. A decrease in reservoir quality from proximal to distal areas is still observed, however, it seems that this decrease is in fact, more restricted to the middle fan, corresponding with the turbidite fan depositional lobes. In the proximal fan and in the proximal part of the depositional lobes, reservoir quality is actually very similar to that of the sand rich system.

10.3. STUDY OF ANALOGUES

As it has been documented in the petrophysical evaluation section, the calculation of porosity and permeability is based on the definition of several computing parameters and relationships which were calibrated with core data (Appendix1). When cores are not available, these computing parameters and relationships are associated with a big uncertainty. In order to reduce this uncertainty it is necessary to use reference values for the computing parameters based on core-calibrated analogues. In the southwestern Barents Sea, many wells drilled through the Lower Cretaceous do not have core data within this stratigraphic unit. Because of this, any petrophysical evaluation involving these wells should be based on analogues in the area.

The four turbidite systems analyzed in this study are proposed as analogues for any future petrophysical evaluation of the Lower Cretaceous sandstone wedges involving wells without core data. However, one has to keep in mind that these wedges have

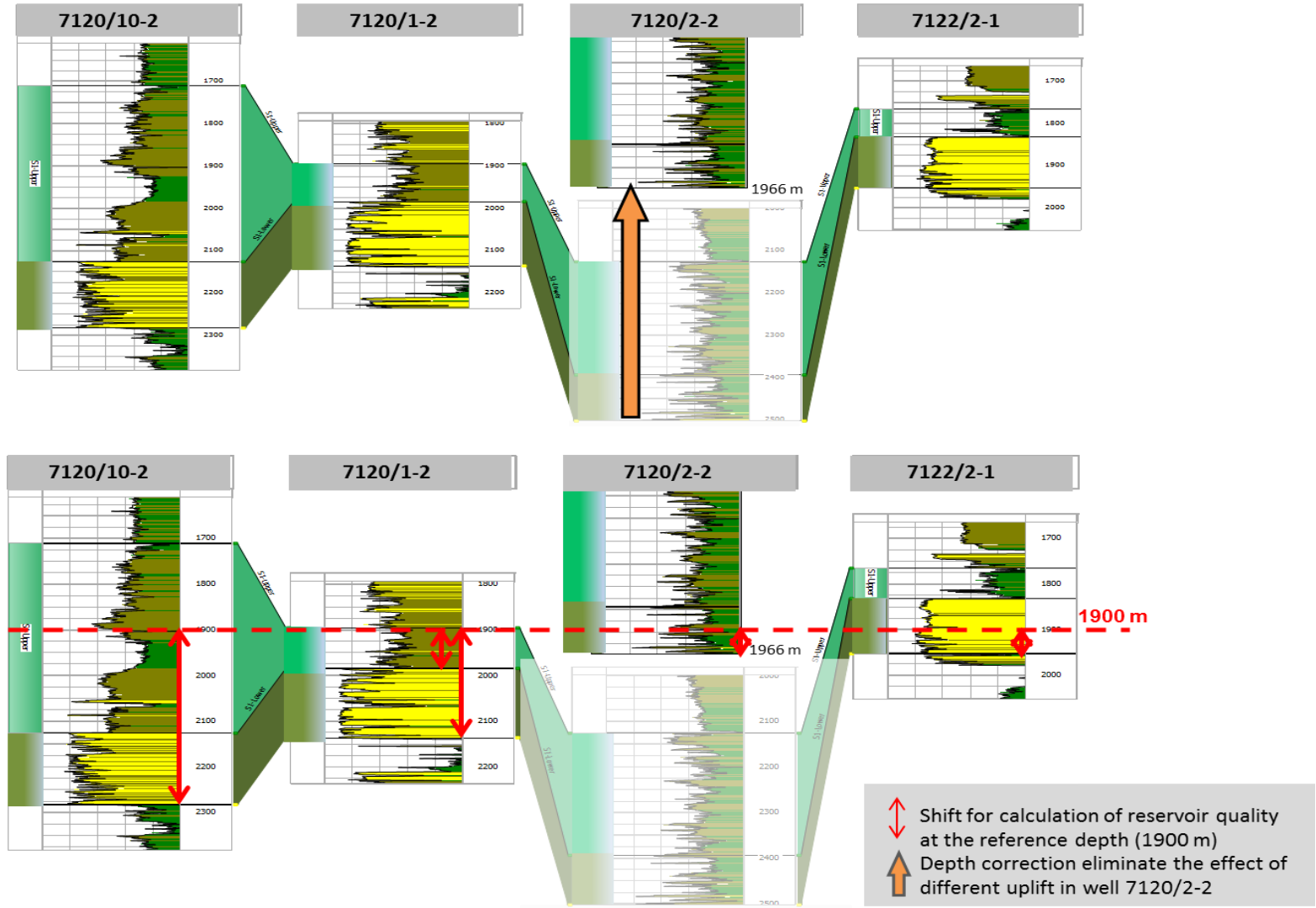


Figure 22– Sketch showing the depth correction applied to the different reservoir zones.

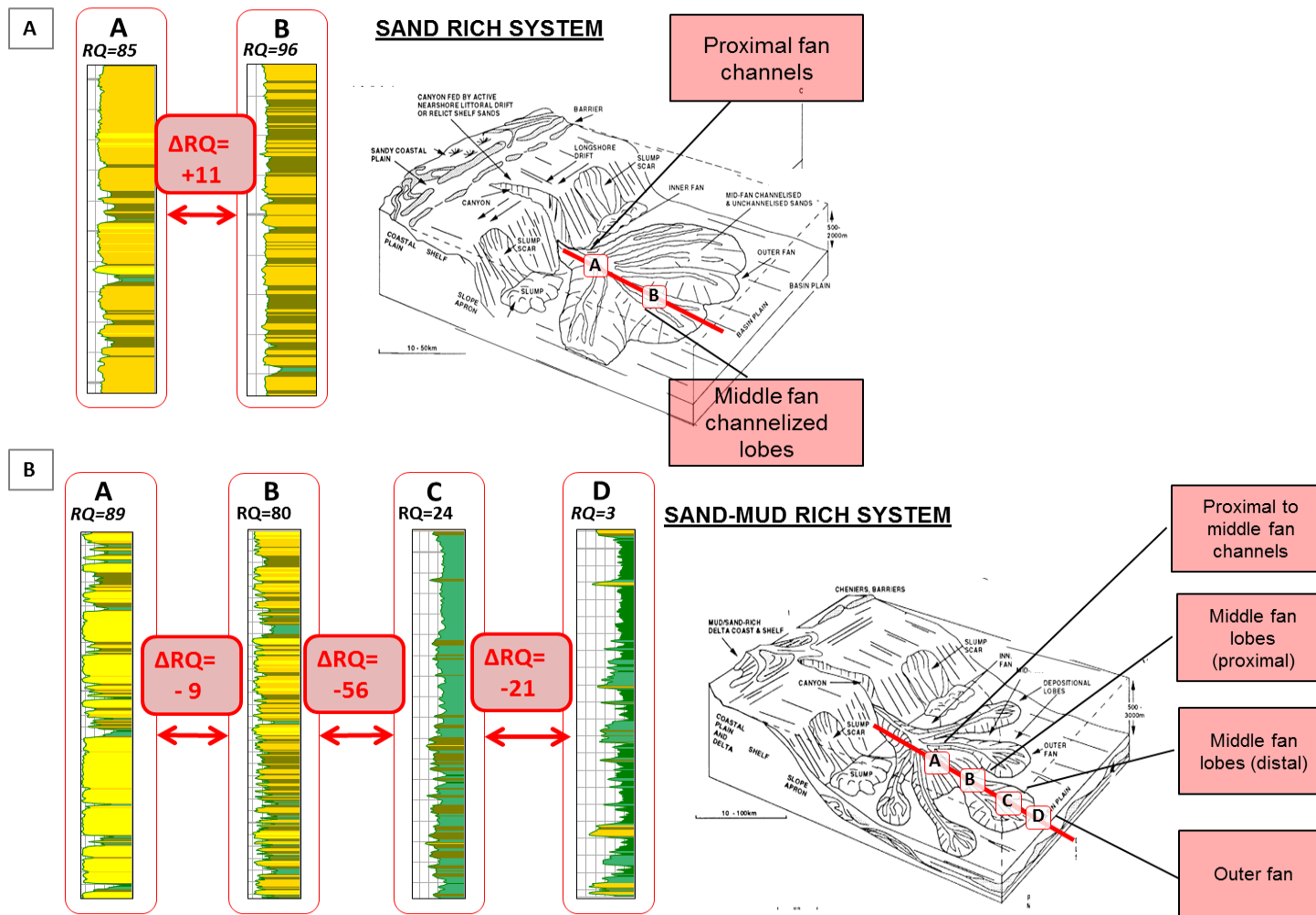


Figure 23– Sketch showing the relative variations of reservoir quality (ΔRQ) between different environments in a sand rich system (A) and a mud-sand rich system (B). The hypothetical reservoir quality values (RQ) for a reference depth of 1900 metros are also shown for comparison of values between the sand-rich system and the mud/sand-rich system

different source areas. Source area affects, among other factors, the reservoir mineralogy and rock texture, factors that are reflected in some of the computing parameters and relationships that are used to calculate porosity and permeability. The Vcl computing parameters give an idea of the possible type of clay in the system, the mineral models represent the broad reservoir mineralogy and finally, porosity-permeability trends reflect rock texture. Hence, the fact that these turbidite systems are source from different areas could have an effect on the computing parameters and/or on the porosity-permeability trends. This has to be analyzed in order to be able to establish these turbidite systems as possible analogues in the southwestern Barents Sea.

Three different source areas are considered in the analysis: east of Loppa High represented by well 7122/2-1, west of Loppa High represented by wells 7120/1-2 and 7120/2-2 and west of Finnmark Platform with represented by 7120/10-2 (*figure 1*). The computing parameters for which calibration was possible (clay line, clay point, mineral inputs for the mineral models and porosity-permeability trends), are compared for the four turbidite systems (see *Appendix 1* for computing parameters values):

- 1) The Vcl parameters show similar results in the four reservoirs suggesting that all the source areas are feeding the turbidite fans with similar type of clay. Thus, the same computing parameters can be used independently of the source area. The only exception is the upper zone of well 7120/2-2, with Vcl parameters slightly different than from the other wells. This could be probably related to the shallower environment that is proposed for this well zone by Sandvik (2014). Differences in the diagenetic processes occurring between shallow marine and deep marine environments could result in modifications in the original type of clay.
- 2) The same mineral model was proven to work fine for wells 7122/2-1, 7120/1-2 and 7120/2-2. This suggests that possible differences in mineralogy of the source areas are not significant enough to affect the proposed mineral model. This model could not be tested in well 7120/10-2 due to the absence of the sonic log. However, the results from the petrographic analysis suggest the same group of minerals to be used as inputs for the mineral model, thus, most probably this model would be successful in this well too.

3) Porosity-permeability trends showed a direct correlation with rock texture and therefore, with depositional environment. In this respect, a difference in source area was observed in the environmental analysis. The reservoir in well 7122/2-1, sourced from the east of the Loppa High, is interpreted as a sand-rich system, while the reservoirs sourced from the west area of both Loppa High and Finnmark Platform, wells 7120/2-1, 7120/2-2 and 7120/10-2, are interpreted as mixed sand-mud rich systems. With these results it is suggested that porosity-permeability trends from the sand-rich system should be used in permeability calculations for wedges sourced from the eastern part of Loppa High. Trends from the mixed sand-mud rich systems should be used for the western area of Hammerfest Basin.

A table with the computed parameters for the calculation of porosity and permeability is included in Appendix 1 so that they can be used as values of reference for future petrophysical evaluations of the Lower Cretaceous sandstone wedges when core data is not available.

11. CONCLUSIONS

- 1) Two different types of turbidite systems might be expected in Hammerfest Basin:
 - Sand rich systems, distributed along the northwestern flank of the basin and sourced from the west of Loppa High.
 - Sand-mud rich systems, distributed along the northeastern and southeastern flanks and sourced from the east of Loppa High and Finnmark Platform.
- 2) Each of these systems exhibits its own characteristic lithofacies and correlative log facies which are variable for each depositional environment within the system.
- 3) Reservoir quality is directly related to the type of turbidite system and to the depositional environments within the system. Overall, it can be suggested that sand-rich fans have good reservoir quality along the whole system while in mud/sand-rich systems it decreases towards the distal areas and more remarkably within the depositional lobes. Mud/sand-rich fans present good reservoir quality in the proximal fan and beginning of middle fan, with values similar to those of the sand-rich systems, and it decreases until almost values of zero in the distal areas.
- 4) Computing parameters for the calculation of V_{cl} and $PHIE/PHIT$ resulted, after calibration, in similar values for all reservoirs, independently of their source area. This suggests that source area does not affect the calculations of V_{cl} and $PHIE/PHIT$.
- 5) Taking into account conclusion number 3, future petrophysical evaluations of the Lower Cretaceous sandstone wedges for which core data are not available, might use the core-calibrated computing parameters of the four studied systems as analogues for the calculations of V_{cl} and $PHIE/PHIT$, regardless of the source area of the turbidite system under consideration.

- 6) The porosity-permeability trends defined in this project might also be used as analogues for the calculation of permeability. However, in this case, because trends are based on lithofacies, source area as well as depositional environment should be considered.

- 7) The study of the porosity-depth trends suggests an average uplift of 1500 meters for wells 7122/2-1, 7120/1-2 and 7120/10-2 which is general accordance with the values calculated by Henriksen et al. (2011).

12. FUTURE WORK

Due to the time constraint for this master thesis, some of the planned studies could finally not be carried out. First of all, a complete petrophysical evaluation would imply to perform a detail uncertainty analysis. This is especially important in areas where core data is limited, like this one. Together with the uncertainty analysis, a sensitivity analysis should be done in order to understand which parameters are affecting the most to the calculation of the final reservoir properties.

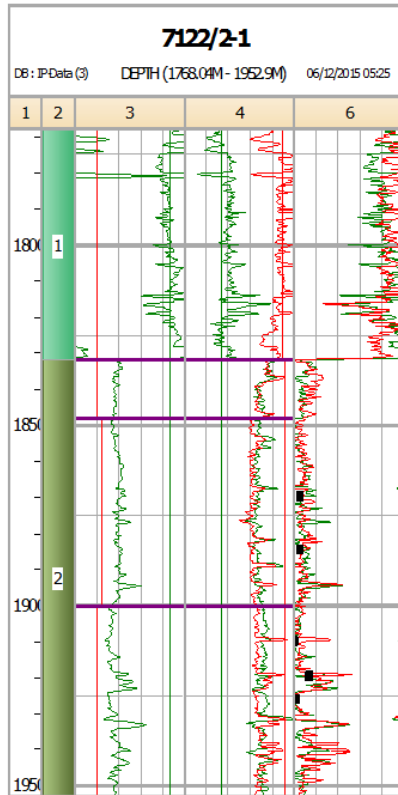
A petrographic study in more detail, with a quantitative analysis of the heavy mineral assemblage for each well, would probably help to highlight possible mineralogical differences between the wells that could affect the mineral models.

Finally, it would be very interesting to test the proposed computing parameters in a different well with no core data available to see how effective the reservoirs in this study are as analogues for other turbidite systems..

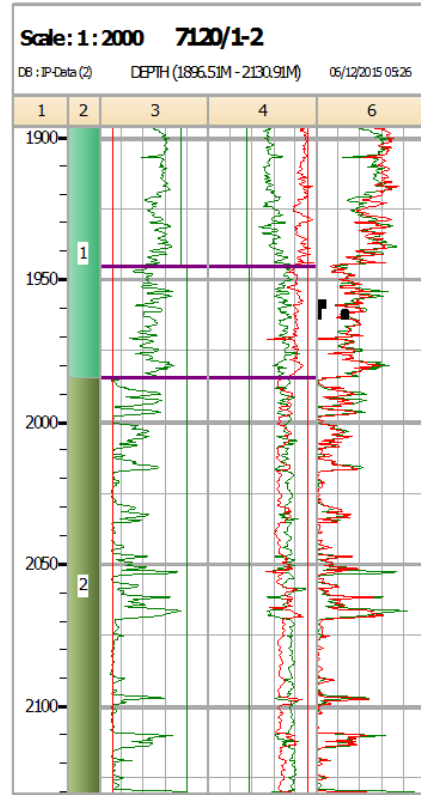
APENDIX 1

Description of the computing parameters for the calculation of V_{cl} , PHIE/PHIT and S_w . To use as analogue values in future petrophysical studies.

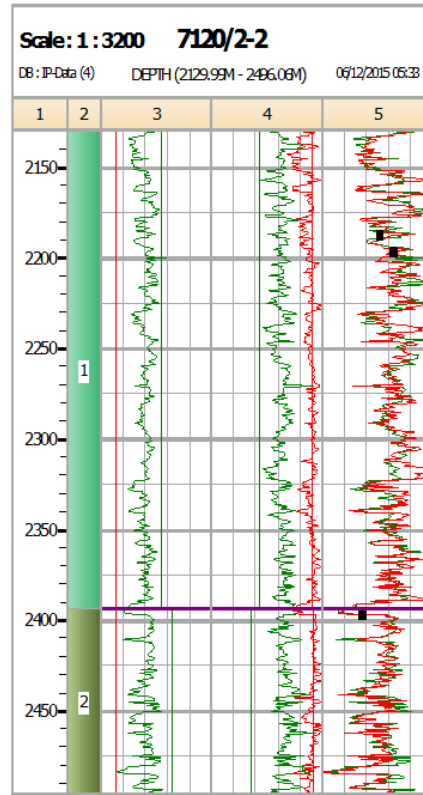
Vci COMPUTING PARAMTERS (CALIBRATED)



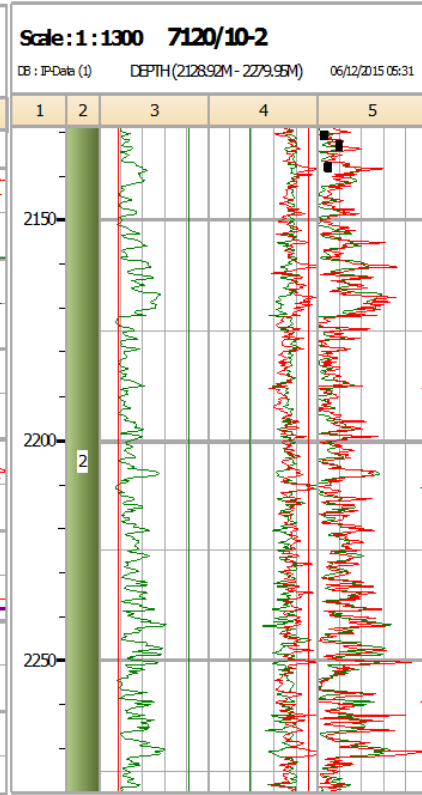
Grmin: 32
Grmax: 130
CP_N:0,40
CP_D:2 618



Grmin: 17
Grmax: 121
CP_N:0,39
CP_D:2 618



S1-Lower	S1-Upper
Grmin: 33	Grmin: 33
Grmax: 162	Grmax: 139
CP_N:0,39	CP_N:0,34
CP_D:2 62	CP_D:2 603



Grmin: 27
Grmax: 123
CP_N:0,39
CP_D:2 618

TRUE MINERAL DENSITIES (*CALIBRATED*)

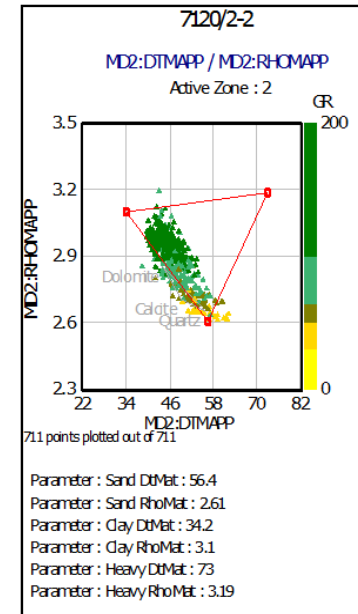
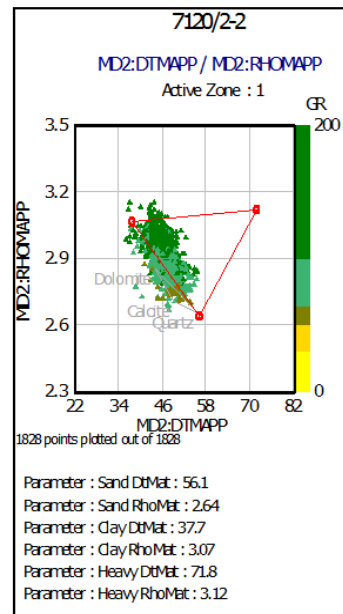
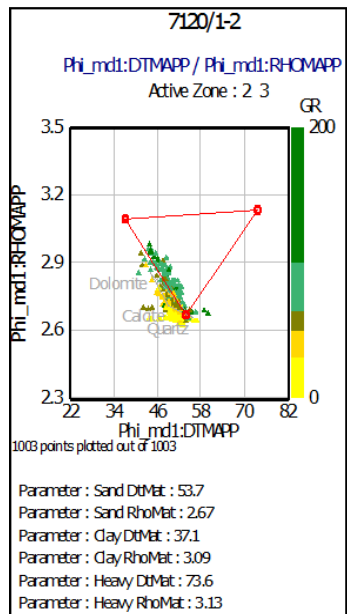
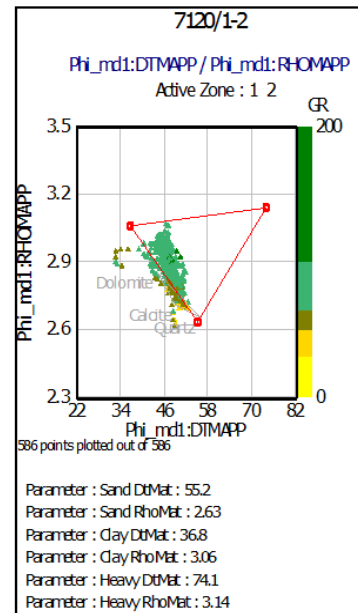
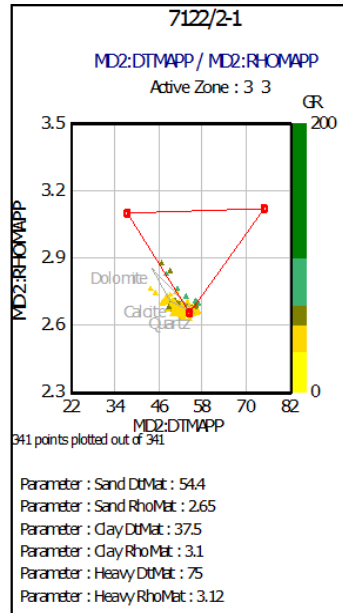
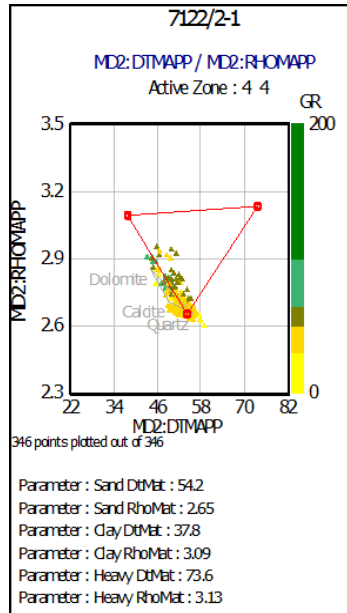
Heavy mineral assemblage

PROXIMAL ENVIRONMENTS					
WELL	HM Assemblage (Group 1)	Average Density (g/cc)	HM Assemblage (Group 2)	Average Density (g/cc)	Total Average Density (g/cc)
2-1	mosc	2,82	trm, rt, apa, pyr, zr	4,026	3,30
1-2	mosc, biot	2,905	apa,chl,sp,zr	3,575	3,17
2-2	mosc, biot	2,905	gar, chl, sp, zr	3,8525	3,28

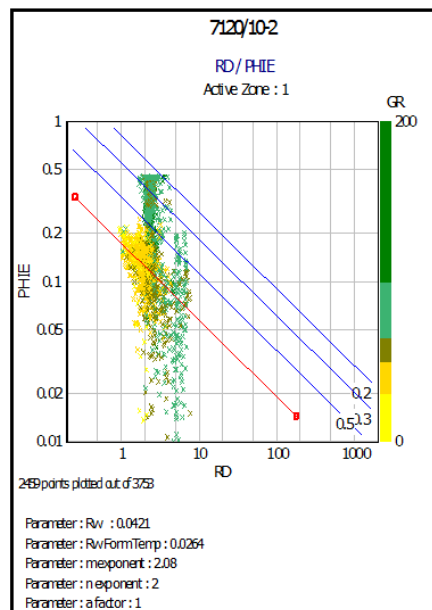
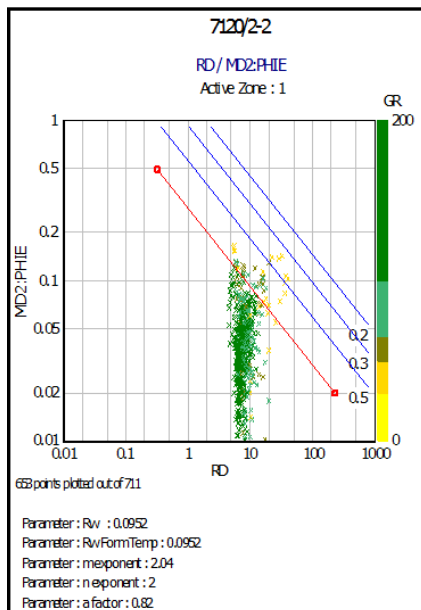
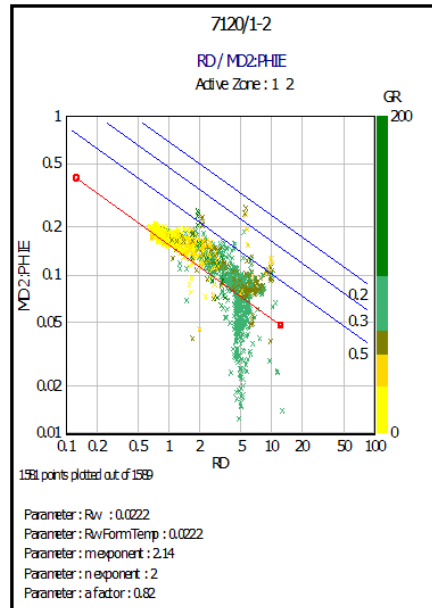
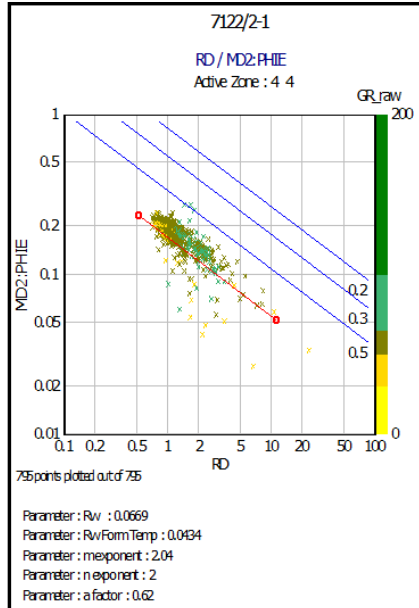
DISTAL ENVIRONMENTS					
WELL	HM Assemblage (Group 1)	Average Density (g/cc)	HM Assemblage (Group 2)	Average Density (g/cc)	Total Average Density (g/cc)
2-1	mosc	2,82	trm, rt, apa, pyr, zr	4,026	3,06
1-2	mosc, biot	2,905	apa,chl,sp,zr	3,575	3,04
2-2	mosc, biot	2,905	gar, chl, sp, zr	3,8525	3,09

Quartz + Feldspar	Average density= 2,65 g/cc
Wet Clay	Average density= 2,62 g/cc (for wells 7122/2-1, 7120/1-2, 7120/10-2 and 7120/2-2 S1-Lower) Average density= 2,60 g/cc (for well 7120/2-2 S1-Upper)

MINERAL MODELS PARAMTERS (CALIBRATED)



WATER SATURATION PARAMETERS (NO CALIBRATED)



APENDIX 2

CPI for each zone and each well showing the results from the petrophysical evaluation.

CPI Legend:

- Raw logs: C, GR, GR-S, NPHI, RHOB, DT, RD
- Computed curves: PHIT, PHIE, RHOMA, KH, Vmi, Vcl, SW, N.
- ▲ Lab measurements of porosity, grain density and horizontal permeability (corrected for overburden)
- Porosity volumes from point counting
- Clay volumes from point counting
- Quartz volumes from point counting
- Heavy minerals volumes from point counting

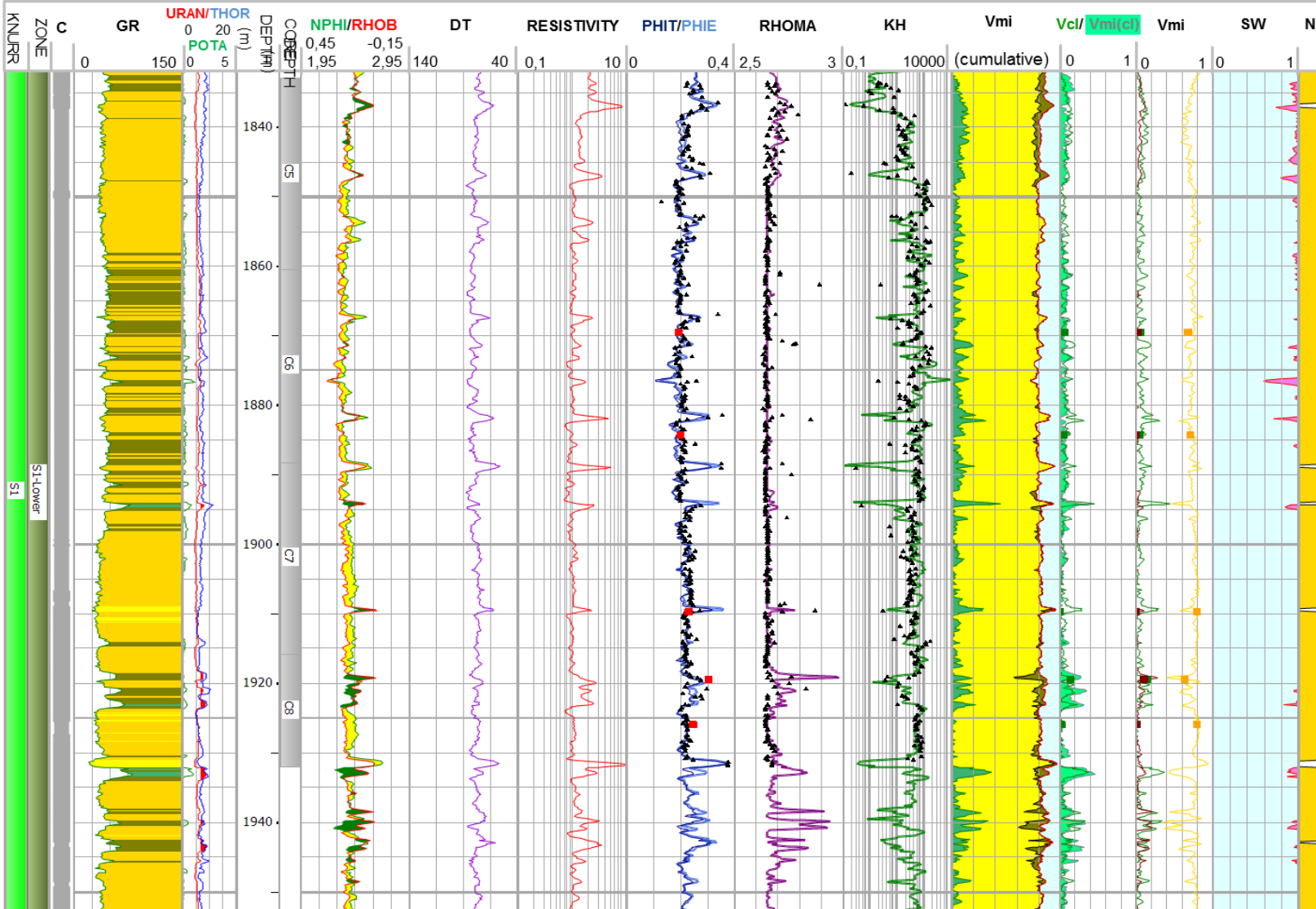
Scale : 1 : 600

7122/2-1

DB : IP-Data (3)

DEPTH (1832.05M - 1952.9M)

06/11/2015 22:13



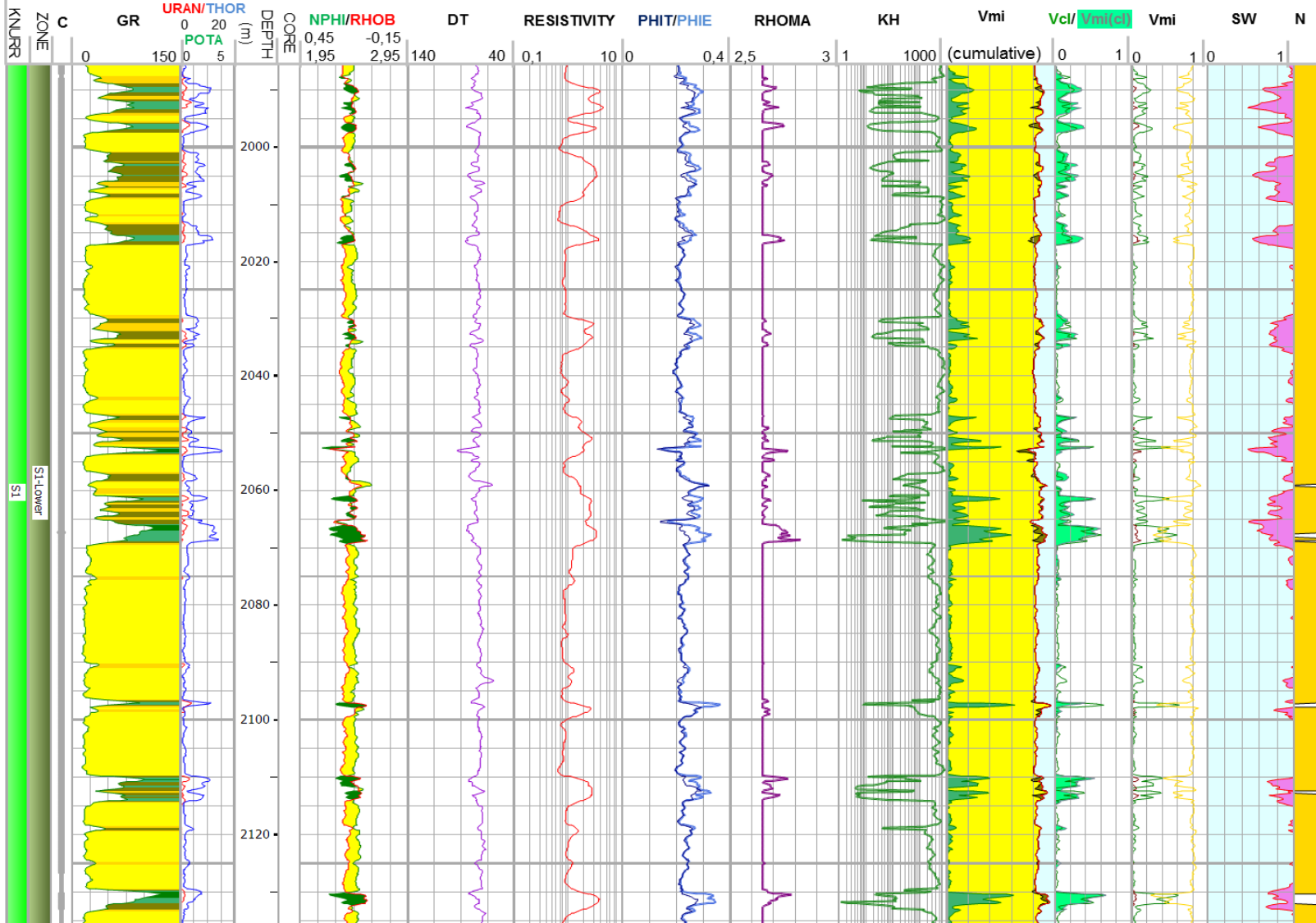
Scale : 1 : 700

7120/1-2

DB : IP-Data (2)

DEPTH (1985.06M - 2135.93M)

06/11/2015 23:40



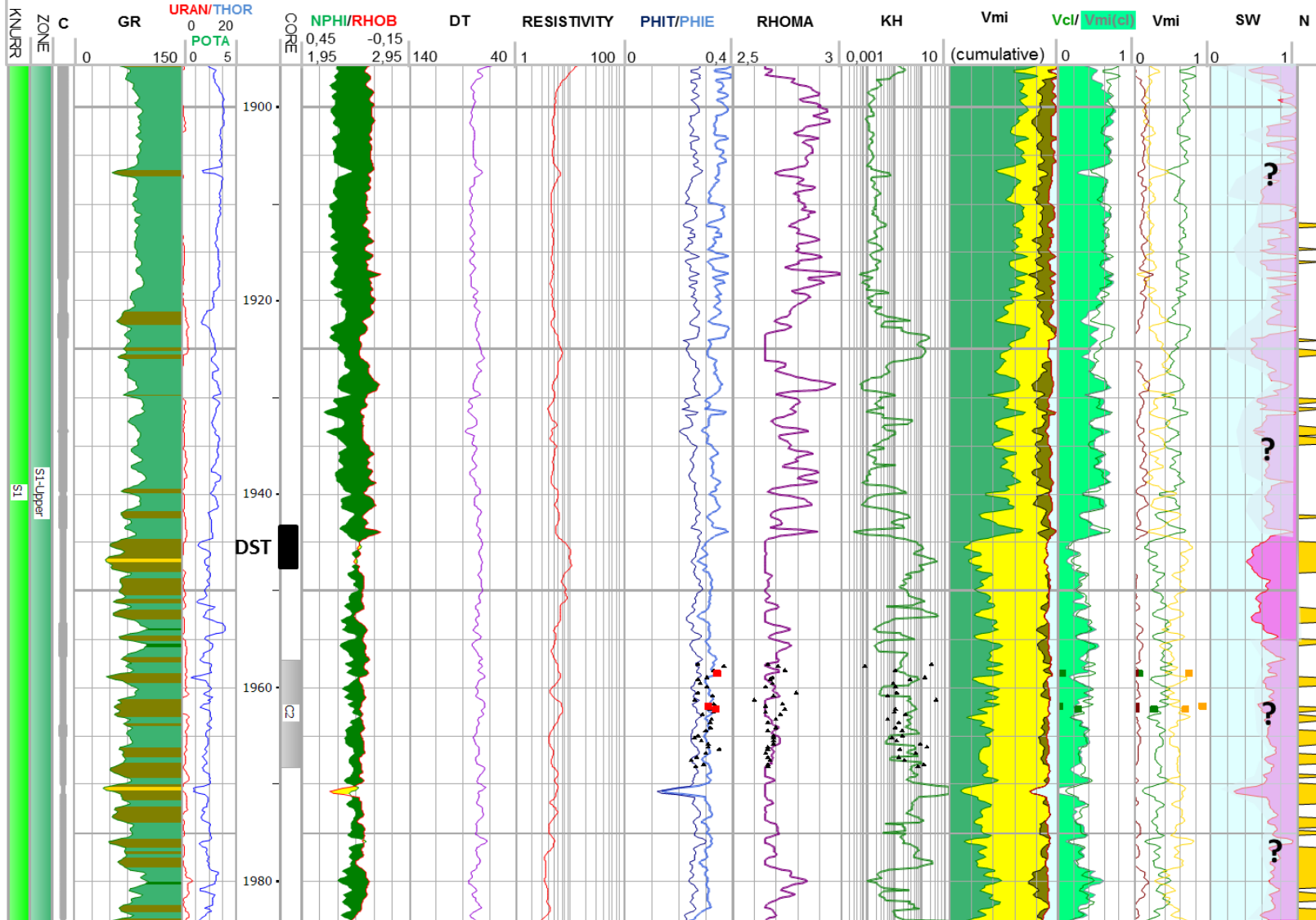
Scale : 1 : 400

7120/1-2

DB : IP-Data (2)

DEPTH (1895.75M - 1984.14M)

06/11/2015 23:42



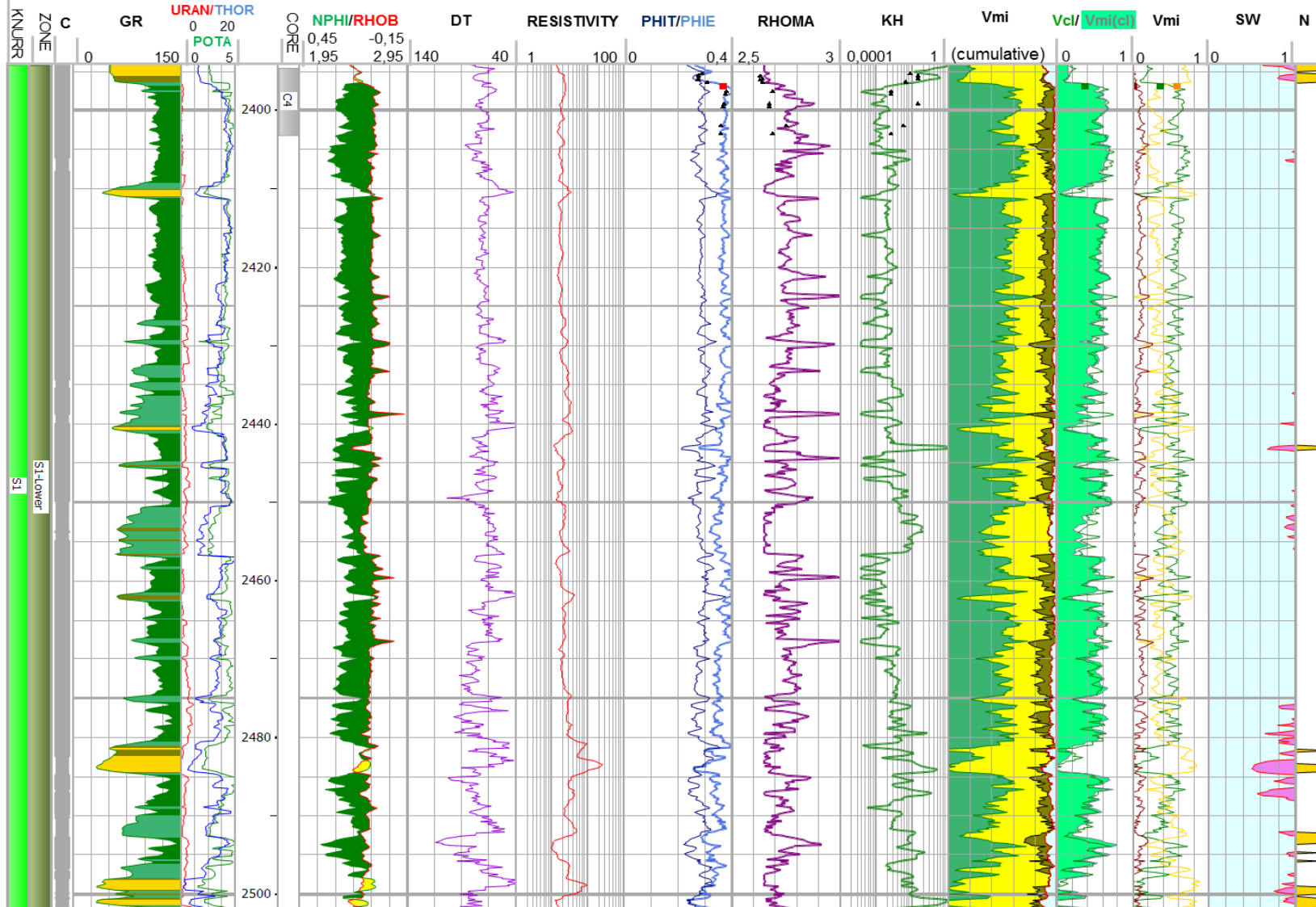
Scale : 1 : 500

7120/2-2

DB : IP-Data (4)

DEPTH (2394.25M - 2501.85M)

06/11/2015 23:45



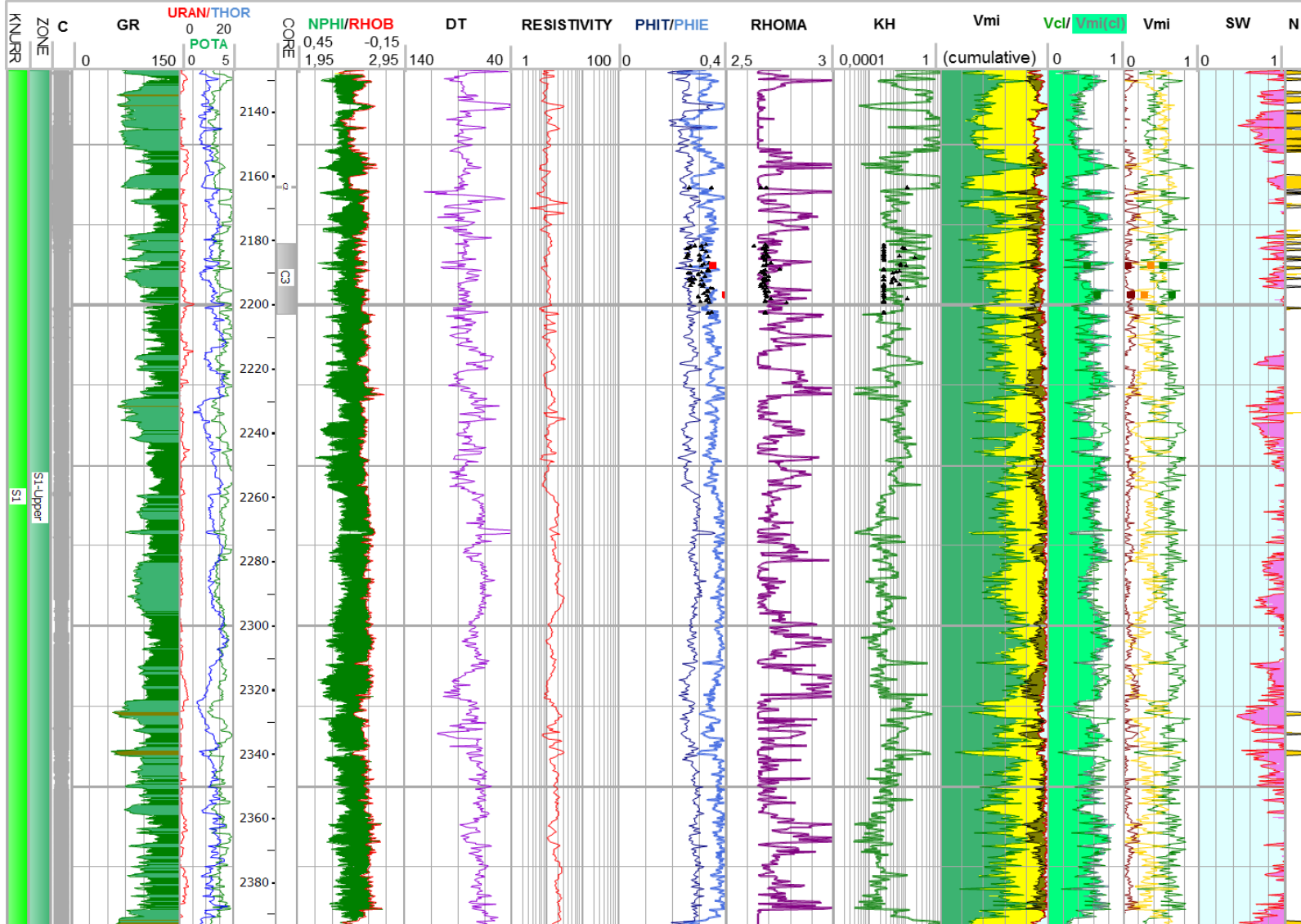
Scale : 1 : 1200

7120/2-2

DB : IP-Data (4)

DEPTH (2126.94M - 2393.34M)

06/11/2015 23:46



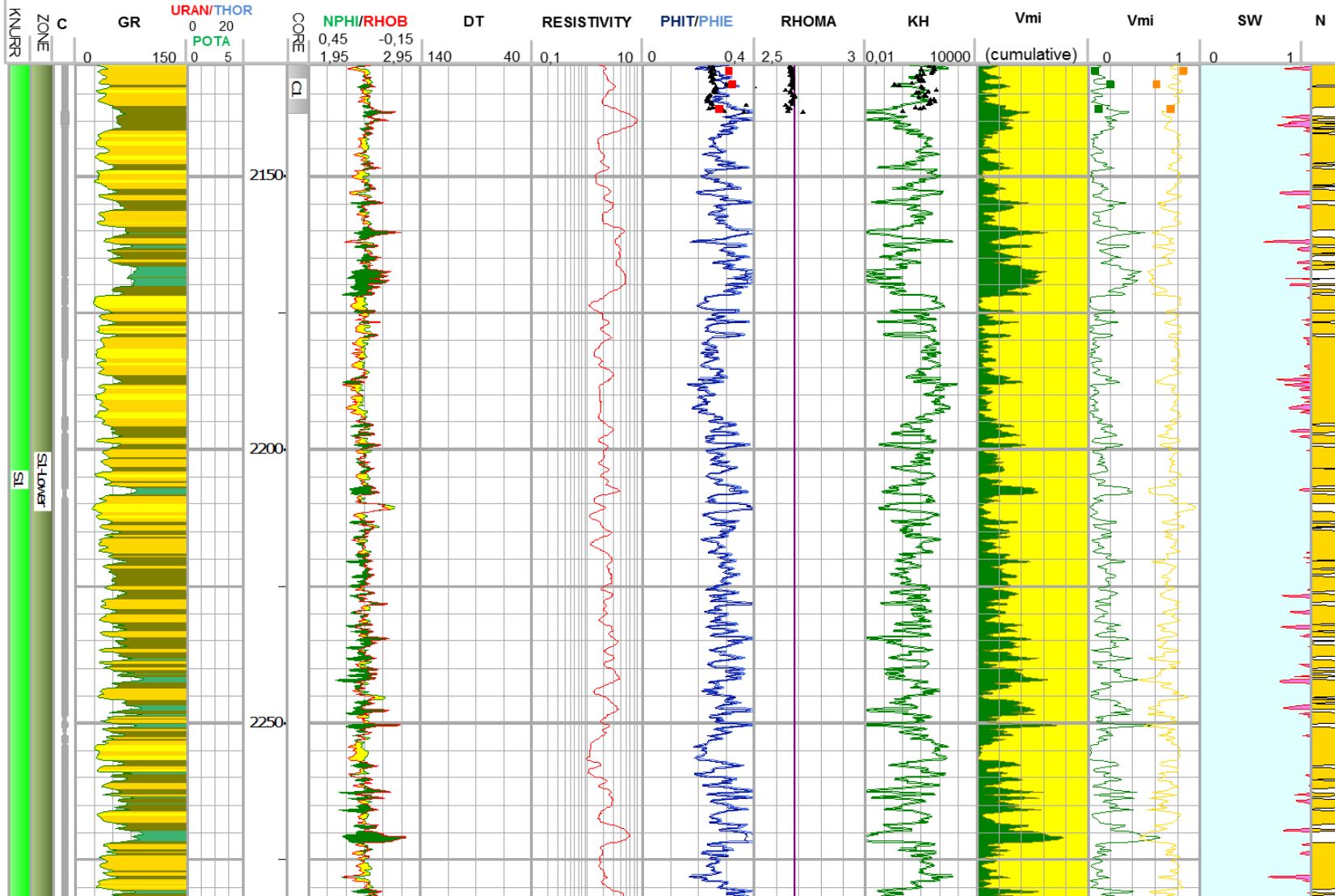
Scale: 1: 800

7120/10-2

DB: IP-Data (1)

DEPTH (2129.69M - 2281.93M)

13.06.2015 21:47



GLOSSARY

C – Caliper

GR - Gamma Ray

Kh - Permeability (Horizontal)–

KHL - Core Permeability

KHLC (=Kcore) - Core Permeability (with overburden correction)

N - Net sand

PHIE - Porosity (Effective)

PHIT – Porosity

PORC (=PHIcore) - Core Porosity (with overburden correction)

PORO - Core Porosity

K-Sp – Potassium Spectral Gamma Ray

RD - Resistivity

RHOB - Density

RHOMA - Matrix density

RHOMAPP - Apparent matrix density

DT – Sonic

Th-Sp – Thorium Spectral Gamma Ray

U-Sp – Uranium Spectral Gamma Ray

Vmi - Mineral volumes

Vcl - Volume of clay

REFERENCES

- Cade, C. A., I. J. Evans, and S. L. Bryant, 1994, Analysis of permeability controls: a new approach: *Clay Minerals*, v. 29, p. 491-501.
- Dalland, A., D. Worsley, and K. Ofstad, 1988, A lithostratigraphic scheme for the Mesozoic and Cenozoic succession offshore mid- and northern Norway: *Norwegian Petroleum Directorate Bulletin*, v. 4, p. 65.
- Dore, A. G., 1995, Barents Sea geology, petroleum resources and commercial potential: *Arctic*, v. 48, p. 207-221.
- Døssing, A., H. R. Jackson, J. Matzka, I. Einarsson, T. M. Rasmussen, A. V. Olesen, and J. M. Brozena, 2013, On the origin of the Amerasia Basin and the High Arctic Large Igneous Province-Results of new aeromagnetic data: *Earth and Planetary Science Letters*, v. 363, p. 219-230.
- Faleide, J. I., K. Bjorlykke, and R. H. Gabrielsen, 2010, Geology of the norwegian continental shelf, *Petroleum Geoscience: From Sedimentary Environments to Rock Physics*, Springer Berlin Heidelberg, p. 467-499.
- Faleide, J. I., S. T. Gudlaugsson, and G. Jacquart, 1984, Evolution of the western Barents Sea: *Marine and Petroleum Geology*, v. 1, p. 123-128, IN1-IN4, 129-136, IN5-IN8, 137-150.
- Faleide, J. I., E. Våagnes, and S. T. Gudlaugsson, 1993, Late Mesozoic-Cenozoic evolution of the south-western Barents Sea in a regional rift-shear tectonic setting: *Marine and Petroleum Geology*, v. 10, p. 186-214.
- Fjeld, T. L., 2014, *Seismic Characterization of Lower Cretaceous clastic wedges in the Tromsø Basin*, The University of Stavanger, Stavanger.
- Gabrielsen, R. H., 1984, Long-lived fault zones and their influence on the tectonic development of the southwestern Barents Sea: *Journal of the Geological Society*, v. 141, p. 651-662.
- Gabrielsen, R. H., R. B. Færseth, L. N. Jensen, and F. Riis, 1990, Structural elements of the Norwegian Continental Shelf. Part I: The Barents Sea Region: *Norwegian Petroleum Directorate Bulletin*

v. 6, p. 1–33.

Hearst, J. R., P. H. Nelson, and F. L. Paillett, 2000, Well logging for physical properties, 483 p.

Henriksen, E., H. M. Bjørnseth, T. K. Hals, T. Heide, T. Kiryukhina, O. S. Kløvjan, G. B. Larssen, A. E. Ryseth, K. Rønning, K. Sollid, and A. Stoupakova, 2011, Chapter 17: Uplift and erosion of the greater Barents Sea: Impact on prospectivity and petroleum systems, Geological Society Memoir, p. 271-281.

Lehne, K. A., 2015.

Marin, D., A. Escalona, A. Kayukova, A. Stoupakova, and A. Suslova, 2014, Characterization of Lower Cretaceous seismic clinoforms in the SW Barents Sea: Implication to sand prone bodies prediction.

Matthews, N., U. Zimmermann, E. Mostafa, C. Ruud, L. Støle, T. J. Lapen, and R. Andreasen, 2015, Provenance data from Mesozoic rock successions in the Hammerfest basin, University of Stavanger, University of Houston.

Normark, W. R., D. J. W. Piper, and G. R. Hess, 1979, Distributary channels, sand lobes, and mesotopography of Navy Submarine Fan, California borderland, with applications to ancient fan sediments: *Sedimentology*, v. 26, p. 749-774.

NPD, 2015.

Pettijohn, F. P., P. E. Potter, and R. Siever, 1973, *Sand and sandstones*: New York, Heidelberg, Berlin Springer-Verlag 618 p.

Poupon, A., and J. Leveaux, 1971, Evaluation of water saturation in shaly formations: SPWLA 12th Annual Logging Symposium.

Pyles, D. R., K. M. Straub, and J. G. Stammer, 2013, Spatial variations in the composition of turbidites due to hydrodynamic fractionation: *Geophysical Research Letters* v. 40, p. 3919-3923.

Richards, M., and M. Bowman, 1998, Submarine fans and related depositional systems II: Variability in reservoir architecture and wireline log character: *Marine and Petroleum Geology*, v. 15, p. 821-839.

- Rider, M., and M. Kennedy, 2011, *The Geological interpretation of well logs: Scotland*, Rider-French Consulting Ltd., 431 p.
- Riis, F., V. J., and M. Sand, 1986, Tectonic development of the western margin of the Barents Sea and adjacent areas., *Future Petroleum Provinces of the World*, v. 40, AAPG Memoir p. 661-665.
- Roduit, N., 2015, *JMicroVision: Image analysis toolbox for measuring and quantifying components of high-definition images*.
- Sandvik, S. E., 2014, *Description and comparison of Lower Cretaceous deposits from Svalbard and the southern Loppa High*, University of Bergen, University Centre in Svalbard,, 135 p.
- Schlumberger, 1997, *Log interpretation charts*, Schlumberger.
- Seldal, J., 2005, Lower Cretaceous: The next target for oil exploration in the Barents Sea?, *Petroleum Geology Conference Proceedings*, p. 231-240.
- Senergy Software, 2011, *Interactive Petrophysics*
- Smelror, M., O. V. Petrov, G. B. Larsen, and S. e. Werner, 2009, *Atlas—Geological History of the Barents Sea*, Trondheim, Geological Survey of Norway, p. 135.
- Walker, R. G., 1976, Turbidites and associated coarse clastic deposits *Journal of the Geological Association of Canada*, v. 3, p. 25-36.
- Weibel, R., L. Kristensen, M. Olivarius, M. L. Hjuler, A. Mathiesen, and L. H. Nielsen, 2012, Investigating deviations from overall porosity–permeability trends: PROCEEDINGS, Thirty-Sixth Workshop on Geothermal Reservoir Engineering.
- Worsley, D., 2008, The post-Caledonian development of Svalbard and the western Barents Sea: *Polar Research*, v. 27, p. 298-317.

